This is to certify that the

dissertation entitled

Position Feedback Estimation Procedure In A large scale Musculoskeletal System via extended Linearization

presented by

YASIN Y. DHAHER

has been accepted towards fulfillment
of the requirements for

PH.D degree in Mechanics

Major professor

Date 12-9-96

POSITION FEEDBACK ESTIMATION PROCEDURE IN A LARGE SCALE MUSCULOSKELETAL SYSTEM VIA EXTENDED LINEARIZATION

By

Yasin Yousef Dhaher

A DISSERTATION

Submitted to
Michigan State University
in partial fulfillment of the requirements
for the degree of

DOCTOR OF PHILOSOPHY

Department of Materials Science and Mechanics

1996

ABSTRACT

Position Feedback Estimation
Procedure in a Large Scale
Musculoskeletal System
Via Extended Linearization

By

Yasin Y. Dhaher

Synthetic studies of human cybernetics have been the focus of intensive studies in the past decade. Considered a branch of motor control, sensory feedback, modulated by sensory information, responds to changes in system states. The nature of the feedback adaptability is considered to be fundamental to the functional coordination in human motion activity.

This study proposes an approach to compute the position feedback in an arbitrary human activity. Pivotal to the method is the idea that any human activity can be characterized by an input/output mathematical model where the system inputs and outputs are the muscular activity and the motion nominal trajectories, respectively. This model includes both the human dynamics and control elements, and therefore is a closed loop system. The parameters needed for the closed loop model are obtained using the predictive error parametric identification method. To describe human dynamics, an anthropomorphic musculoskeletal model is proposed that includes the same number of inputs and outputs measured in the identification of the closed loop system. Since the

anthropomorphic model is free of any feedback components, it is defined as the open loop system. The open loop model is nonlinear, thus an extended linearization method was used. The linearization procedure reduced the nonlinear model to a family of linearized systems parametrized by the same set of measured operating points used in the estimation of the closed loop system. A key step in the procedure is to represent both the estimated closed loop system and the proposed open loop model in the same state space representation. The block observer form was utilized as the standard state space realization of the closed and open loop systems.

Once the open and closed loop systems are available, the feedback gain estimation is obtained by finding the feedback gain matrix that when combined with the proposed open loop model resembles the estimated closed loop structure. An explicit solution of the feedback gain matrix and a detailed discussion of the methods to validate the solution are included. The proposed method is demonstrated for the movement of squatting. Quantitative results of the positional feedback gains are presented. Results of agonist/ antagonist position feedback synergy in the muscles included in the model are also shown. A brief discussion on the use of the estimation method proposed is given in the areas of predictive orthopaedic surgeries and neurological deficiencies.

Acknowledgments

I take this opportunity to show my appreciation to the following people whose contributions made the completion of the thesis possible

To my major professor, Dr. Robert Soutas-Little, for his continued support and encouragement.

To Dr. Hasan Khalil, for sharing his expertise in the development of the control theory part of the present work.

To my committee members: Dr. Gary Cloud, Dr. Joseph Vorro, and Dr. Robert Hubbard.

To Stefanie Bonin, Patricia Soutas Little, LeAnn Slicer and all my peers (past and present) at BEL.

Table of Contents

List of Tables

List of Figures

CHAPTER ONE

INTRODUCTION

1.1 Why Study the Feedback Problem?

The complexity of the human body requires an advanced control system. This control system continuously manipulates and processes sensory information relayed by local and global sensory components. In this manner, sensory feedback is considered as the principal component in movement organization and control in humans. Stability, precision, and hierarchical control of movements are considered to be the major products of the sensory system. Since general human activity involves large motions, the nature of a feedback system is self-tuning. Responding to positions, velocities, and forces, the feedback system reschedules its sensory information to obtain the three products as defined above. The relationships between physical quantities (position, velocities, forces. etc.) and the electrical signals produced by the sensory system are known as feedback gains.

Classical approaches used to compute these feedback gains, such as the state-feedback analyses, fail to address the adaptability of such gain values. State-feedback methods, for example, are useful in the study of human activities that exhibit linear dynamics such as postural control. It is also important to note that the state-feedback analysis depends on the assumed values of the closed loop eigenvalues. The sign and the magnitudes of these eigenvalues are always chosen to maintain a stable closed loop

system. Unfortunately, classical methods give no physical justification for the choice of these values.

Since complex motions, for example, rising from a chair, are mathematically represented in terms of nonlinear dynamics, a self-tuning feedback control structure is required to accommodate the large changes in system configurations. Thus, the current constant feedback studies fail to represent the muscular synergies of the agonist and antagonist actuators controlling the activity.

The development of a method to compute the feedback gains that deals with the nonlinear dynamics of the open loop system as well as the actual dynamic behavior of the closed loop system, provides significant challenges in the field of human cybernetics. This type of analysis has not been published in the literature. The proposed procedure to compute the feedback gains depends on the actual open and closed loop systems. Fundamental to the method is the construction of input / output mathematical models for both the closed and the open loop systems. The open loop structure is obtained using theories in musculoskeletal modeling. The nonlinear form of the musculoskeletal model is converted to a family of parameterizeparameterized set of linear systems using extended linearization approach. System identification theory is used to construct an input / output closed loop mathematical model from data measured on a live subject.

The computation of feedback gains are important to areas of the closed loop control design of the functional electrical stimulation systems (Stanic and Trnkoczya, 1974; Kralj *et al.*, 1980; Crago and Chizeck, 1986; Khogh and Zajac, 1989, I;II). Applications of the feedback analyses are essential to understanding the sensory components' contribution to the stability, precision and control of the human motion (Brain, 1989; Iqbal and

Hemami, 1993; Kuo, 1995). The application of computing the feedback gains to the field of predictive orthopaedic surgeries would prove to be beneficial in future research.

1.2 Background, Modeling, Identification and Control

In the following discussion, the literature on concepts used in the development of the theory of this thesis will be presented. To follow the development of the theoretical model, the discussion starts with an overview on the theory of system identification and its application to the field of biodynamics. Next, a detailed presentation of basic research and ideas concerning modeling of musculoskeletal structures are given. Lastly, the theories and research on human control system are discussed.

The dynamics of a system can be described by a mathematical model that relates its inputs and outputs. The inputs and outputs are a set of time sequences that represent the external variables acting on the system, as well as the observable responses of that system. In general, the system can be investigated either theoretically or experimentally. The theoretical analysis of a process is based on the use of a set of physical balance equations and the understanding of the phenomenological laws. Experimental analysis treats the system as a black-box with a mathematical structure that consists of a set of elements to be estimated through the use of any of the available identification routines (Ljung, 1987; Zhang *et al*, 1990). The sequential input/output relation that describes the process dynamics is defined as the transfer function represented in terms of a backward shift operator (q) as used in control theory (Strejc, 1981). In the multi-inputs multi-outputs (MIMO) case, the transfer function will not be a single function, but a matrix that in general takes the form

$$H(q) = \begin{bmatrix} h_{11}(q) & h_{12}(q) & \dots & h_{1m}(q) \\ h_{21}(q) & h_{22}(q) & \dots & h_{2m}(q) \\ \dots & \dots & \dots & \dots \\ h_{p1}(q) & h_{p2}(q) & \dots & h_{pm}(q) \end{bmatrix}$$

where $h_{ij}(q)$ are in general rational functions of q. The input/output relation can then be written as follows

$$Y(q) = H(q) \cdot U(q)$$

Where $Y(q)$ and $U(q)$ are the output and input vectors, respectively. The problem of finding the coefficients of the functions $h_{ij}(q)$ from measured input and output data is commonly known as transfer function identification (Soderstrom *et al.*, 1989). The identification of the transfer matrix can be done using either parametric or non-parametric identification procedures (Jenkins *et al.*, 1969; Soderstorm, 1984; Ljung, 1986). In the non-parametric identification method, the identification is carried out without employing a set of parameter vectors in search for the best description, hence the name non-parametric (Jenkins *et al.*, 1969). Unlike non-parametric identification, parametric identification methods do not depend on test signals to identify a model. A selected model is chosen and is characterized by a set of parameters. The best set of parameters to minimize a selected criterion is obtained by an estimation process. The prediction error method is one of the most commonly used parametric identification procedures. The search process in the prediction error method is based on the least square method of linear regression where the parameter vectors are found such that the sum of the squares of the output prediction errors are small (Lawson and Hanson, 1974; Ljung, 1986). The choice of the parameters is highly dependent on the model chosen. Models are usually selected

from a wide range of already established models (Soderstorm, 1984). The Autoregressive (ARX) and the Autoregressive Moving Average (ARXMA) models are among the commonly used system structures (Ljung, 1986).

Treating the electromyographic myosignals as system inputs and the joint or segmental angles as system outputs, the human musculoskeletal system transfer function can be modeled and identified. Zhang *et al.*, (1990) considered the modeling and identification of human knee joint dynamics. Eight myosignals representing eight muscles crossing the knee joint were considered as the system inputs. Data for the six degrees of freedom of the knee joint were selected as the system outputs. Several methods were then tested to carry out the identification procedure of a proposed linear, (ARX), and nonlinear model. The results obtained using the prediction error method for both the linear and nonlinear models were comparable. Other identification methods, like the instrumental variable method and the non-parametric identification method, were also used to study human postural global control (Ishida and Miyazaki, 1987; Johansson and Magnusson, 1991).

Modeling and identification of human structures are important to understand the synthesis and control of the musculoskeletal system. Identification, for example, can be useful in areas such as the restoration of functional tasks to paralyzed muscle-limb systems by means of the functional electrical stimulation (FES) (Franklen *et al.*, 1995; Franklen *et al.*, 1995). Franklen *et al.* (1995) examined a system which consisted of the quadriceps electrically stimulated using surface electrodes. A parametric model was then derived to adequately represent the active component of the muscle that would be used to enhance the control performance of the electrically stimulated paralyzed limbs.

Theoretical mechanical models of the segmental human musculoskeletal body appear

frequently in the literature (Nubar and Contini, 1961; Beckett and Chang, 1968; Kane and Scher, 1970; Krogman and Johnston, 1970; Von Gierke, 1971; Chao and Rim, 1973; Hatze, 1973; Seirge and Arvikar, 1973; Hatze, 1976; and others). The first analytical model that defines human dynamics was introduced by Fisher in 1906. Fisher developed a set of equations of motion of an n-links model using Lagrangian dynamics.

Before the introduction of methods and the development of an analytical dynamic model, some of the difficulties that are inherent characteristics of the musculoskeletal system will be explored. Owing to the complexity of the human musculoskeletal system, (144 joints, including the minor joints, and approximately 750 muscles) assumptions should be made to reduce the number of joints and muscles that are to be included in the model. The inclusion of all the six degrees of freedom of each joint in a model results in about 850 degrees of freedom to represent the whole system dynamics. Clearly, the inclusion of about 850 degrees of freedom combined with about 750 muscles results in an overly complicated system. Hence, simplifications have to be introduced in the process of modeling the skeletal system. The question is: How many muscles and joints and degrees of freedom of each joint should be included in the model? Decisions are usually made depending on the type of activity considered in the study. For example, in the case of squatting, the dominant motion of all the joints is in the sagittal plane; and, in the absence of pathology, a one degree of freedom model of the included joints may be adequate (Hemami, 1978; Hatze, 1981; Huoston and Passarello, 1982).

The other major component of the musculoskeletal model is the muscle that acts as the actuator for force generation to drive the skeletal system. Two main issues are important when considering muscles in a model; the muscle architecture; the moment arm about the

joint that the muscle spans. Although Fisher's work is considered to be the foundation of studies of human mechanics, his work was insufficient to explain the generalized forces in the Lagrange's formulation. Since the moment arm is fundamentally one of the components in the computation of the generalized forces, Hatze (1965) was the first to introduce a transformation based method through which the moment arm of a muscle about a joint can be represented in terms of that joint's angle, provided that the muscle origin and insertion data are known. The method developed by Hatze was modified by a more recent work presented by Gordon *et al.* (1986). In both the early work of Hatze and the most recent work by Gorden *et al.*, the anthropometric data of the muscle origin and insertion are of most importance. Thus, many cadaver based studies, focusing on obtaining muscle origin and insertion points were done (Alexander and Vernon, 1975; Brand and Crowninshield, 1982; White *et al.*, 1989; Seirg and Arviker, 1989; Komistek *et al.*, 1994; and others).

Inclusion of a muscle model in the analysis of human dynamics is significant since different muscle models affect the prediction of muscle forces, hence joint moments and generalized forces. Mathematical modeling of muscles has been the subject of research on both the molecular (see Needham (1971) for a review) and macroscopic (Carlson, 1957; Green, 1969; Crowe, 1970; Pierrynowski and Morrison, 1985) levels. Macroscopically, muscles with tendons are divided into two major parts, the muscle tendon and the muscle belly. The tendon, a collagenous tissue structure, has been shown to exhibit a nonlinear viscoelastic behavior (Fung, 1967; Haut and Little, 1972; Soong and Huang, 1973; Jhonson *et al.*, 1992). The muscle belly consists of many individual muscle fibers held together by connective tissue (fascia). This fascia is called the epimysin. Another type

of fascia is the perimysin. The perimysin is a fascia that penetrates the muscle belly separating muscle fibers into groups called fasciculi. Each fasciculus consists of a number of muscle fibers wrapped with another connective tissue known as the endomysin. Collectively, the epimysin, perimysin, and endomysin act as passive elements that are structurally located parallel to the muscle fibers, hence the name parallel elements. D.K. Hill (1968) showed that most of the tension observed when stretching a resting muscle comes from the parallel elements. Based on quick release tests, Soong and Huang (1973) showed that a constitutive equation of the muscle parallel element takes a nonlinear exponential form. The presence of muscle series elements was theorized to exist based on experiments formed by Hill A. V. (1938; 1950; 1953); Wilkie (1956); Sonnenblick (1964); and others. Unlike the parallel element, the muscle series element exhibits elastic behavior that is activation dependent. Functionally, the series element is responsible for the transmission of tension to the end points of the muscle fiber when stimulation takes place (Hatze, 1975). To model a constitutive equation of the series elastic element, Pierrynowski and Morrison, 1985, developed a model using experimental data from earlier research done by Bahler (1967); Bahler and Fales (1968); and Close (1972). More details on the muscle series element are found in the comprehensive study of Ehema and Huijing (1990).

The only force-generating activation dependent muscle element is the muscle contractile element. Structurally, the contractile element represents a set of cascaded building blocks known as sarcomeres. Sarcomere shortening develops due to the sliding (cross-bridging) of its major components, actin and myosin filaments. The contractile force produced by a muscle fiber is equal to the sum of all cross-bridges in one half-sarcomere of a

fiber. The functional contribution of the contractile element to the muscle machine is its force-velocity relation. A.V. Hill (1938) was one of the first to propose an experimentally based model relating the contractile element force with its shortening velocity. A rectangular hyperbolic relation was developed and is known as Hill's model. Other models were also developed to characterize the actin/myosin bridge force generation and contraction. All of the studies discussed so far suffered from the inability to explain the stretching behavior of the muscle model (Pringle, 1960). To account for the lengthening of muscle fibers, Sugi (1972) modified Hill's model based on his experimental observation of the muscle fiber force generation in the presence of stretching. He observed that, with the increasing stretching velocities, the force at first rises above the isometric value but then levels off. Most recently, Hatze (1990) provided a comprehensive discussion on the physical and experimental complications in modeling the contractile element force-velocity relation.

One may wonder if all the elements of the muscle should be included in the model and how complex the mathematical model of every element should be. To answer these questions the model chosen should pass the following test: can the model predict the muscle force generated in both muscle's lengthening and shortening phases. It should also be noted that increased complexity of the muscle model will subsequently increase the computational time for analysis of the complete human system dynamic synthesis. Thus, the dynamics synthesis computational time is also a factor that affects the choice of the muscle model. Winters and Stark (1987) provided a good summary of the effect of the muscle model selection on the amount of information gained or lost in the process of human dynamic studies. A non-dimensional generalized model that may be used in computer

simulation was first introduced by Zajac *et al.* (1986). This model is dependent on the muscle static properties, tendon slack length, muscle maximum isometric force, and other factors. Details on the development of this model are given in the review by Zajac (1989).

Once skeletal and muscle models are chosen, the derivation of the musculoskeletal dynamic equations is commonly done by Lagrangian dynamics (Goldstein, 1959; Maros and Orlanda, 1971; Leu and Hemati, 1986; Vukobrtatovic *et al.*, 1990), Euler-Newton's (Chace and Bayazitolque, 1971; Wittenburg, 1977), Hamiltonian (Vane and Sitchin, 1970; Hagedorn, 1979), and others. Lieh *et al.* (1990) provided an informative review of the existing multi-body dynamics formulation techniques and their application to biomechanical systems.

The dynamics of human movement is controlled by inputs from sensory systems, or triggered by sensory signals or some internal desire to produce a movement. The two systems interact in a way so that rhythmic movement is monitored and continually commanded for reinforcement and accuracy (Herman *et al.* 1976). Relevant to the present work, the sensory feedback mechanism is two parts, a local feedback component defined as a spinal segmental loop, and a global feedback component that is modulated through a higher level of the central nervous system (CNS) as defined in Brooks (1989). The main local and global feedback structures in the musculoskeletal system are the joint sensors (Boyd and Roberts, 1953; Williams, 1981; Johansson and Magnusson, 1991), proprioceptive sensors in the joint capsules, tendons, skin and muscles (Houk *et al.*, 1970; Agarwal *et al.*, 1970; Boyd, 1980; Johansson and Magnusson, 1990), vestibular (Nashner, 1971; Horak *et al.*, 1990; Barker, 1991), and visual (Reichardt and Paggio, 1979; Rei-

chardt, 1980; Barker, 1991) systems. Both joint and proprioceptive sensors consists of receptors in joints and muscle tissues. These sensors detect the relative position, motion and forces at the joints and in the muscle tendons (Magnus, 1926; Grigg and Greenspan, 1977; Hasan, 1983). Attempts were made to model and describe the general transfer function of these sensors (Grigg and Greenspan, 1977; Diener and Dichgans, 1988). However, a complete model of the joint and proprioceptive sensors that can be used for the analysis of human dynamic structure does not yet exist (Williams, 1981; Hemami, 1985). On the other hand, both the visual and vestibular systems were studied intensively and reported in the literature. The vestibular system provides both the positional and the dynamic information needed to stabilize the system (Young, 1970; Nashner, 1973; Magnusson, 1986). The vestibular system responds to dynamic stimulation, (linear and angular acceleration), through its sensory organs in the semicircular canals. However, the positional information that the vestibular system provides is due to the interconnections and integration of information provided by the visual system. For example, the vestibular system provides postural stability and updates the system with spatial awareness by providing an eye tracking system such that a visual contact is maintained during head movement. Functional models were developed to simulate the vestibular systems and their contribution to postural stability (Young, 1970; Nashner, 1973). Awareness of position is mainly attributed to the visual system. The visual feedback provides the system with information concerning the relative position between a body and external references (Lehman and Stark, 1983).

A large number of analytical studies have been conducted to model and study the effects of sensory mechanisms on human postural control and stability. Nashner (1971,

1972) developed a model of the postural balance in a rigid body of one degree of freedom about the ankle joint. The focus of this study was the investigation of postural control strategies and their relation to the proposed model. Later models, similar to those hypothesized by Camana *et al.* (1977) and Golliday and Hemami (1976) were proposed to represent both the velocity and the position feedback sensory modalities in a biped postural model. He *et al.* (1991) developed a complex model where they included the feedback pathways that represents the upper motor neurons to account for both the vestibular and visual systems. They also included other sensory modalities intrinsic and extrinsic to the muscle. Utilizing optimal control theory, they investigated the relationship of the selection of the input and states weighting matrices on the effect of the sensory components proposed in the postural stability problem. Iqbal and Hemami (1993) explored a conceptual feedback model of the proprioceptive sensory systems and studied the effect of the model on the sway stability in a four link model.

An alternative approach to the micro-modeling of the sensory components is the black-box approach. Analytically, the black-box method lumps all sensory feedback mechanisms of the same nature in one element. Further decomposition of the estimated or computed elements is then made to account for the different modalities (Hemami and Golliday, 1977; Hemami and Jaswa, 1978; Brain, 1989; Kuo, 1995).

The control of a human activity is the most challenging issue to be resolved. About fourty years after the first modeling attempt done by Fisher, Bernstein in 1947 investigated the global control of human dynamics. He suggested that the overall control of the musculoskeletal system consists of six components: 1. actuator (muscle), 2. sensor (receptor) that senses information from both the skeletal and the muscular systems, 3. a

programing device (CNS) which describes the necessary value of controlling parameters to the system, 4. discriminator which gives the difference between the desired and actual control parameter, 5. a coder system that decodes the signals from the discriminator and sends them to the regulator (controller) through a feedback loop, and finally, 6. the controller that controls the actuator function. A conceptual illustration of Bernstein's interpretation of the human motion control is shown in Figure 1.1.

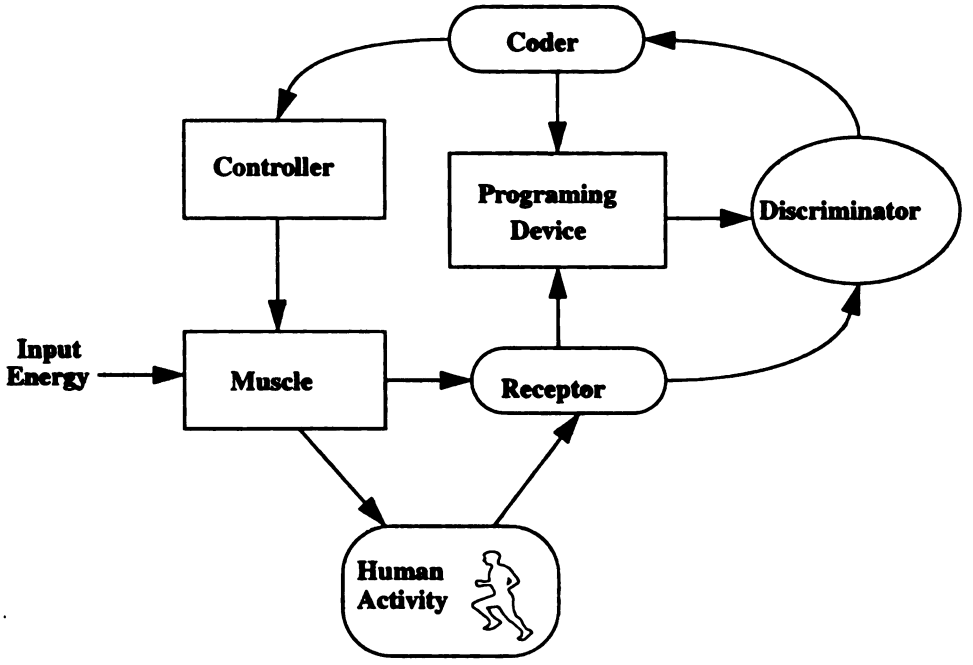

Figure 1.1 Conceptual representation of the human global control as proposed by Bernstein, 1947.

However, the criterion by which the controller (regulator) makes up the control signals was not clearly identified. Theoretical studies were then developed to give more understanding of the form by which the control procedure defined by Bernstein is carried out. Optimal control (Chow and Jacobson, 1971; Hatze, 1976; Khang and Zajac, 1989; Pandy *et al.*, 1990; Kuo, 1995), parametric optimization (Pandy *et al.*, 1992; 1995), constant state feedback (Zheng and Hemami, 1984 ; Brian, 1989), force feedback (Whit-

ney, 1977; Raibert and Graig, 1981), nonlinear feedback (Hemami and Camana, 1976), and Lyapunov stability (Hemami and Cvetkovic, 1977; Takeyaki and Arimoto, 1981; Iqbal and Hemami, 1993) theories were used to define the control procedure in the human structural control.

The basic question of the optimal control theory is to find a control input that minimizes a predefined performance criterion with and without terminal conditions (Owens, 1981). In general, the solution of the optimal control problem leads to the solution of a two point boundary value nonlinear problem defined by a set of equations known as the Reccati equations (Owens, 1981). The size and the degree of the nonlinearity of the Reccati equations depends on both the number of degrees of freedom included and the number of input signals introduced in the system. The coefficient matrices in the Reccati equations are defined in term of input and output weighting matrices. He (1991) proposed different forms of these matrices to account for different control strategies in the postural sway problem. He assumed that for the linear postural system, the muscle excitations are independent, hence the input weighting matrix was chosen to be diagonal. On the other hand, the state weighting matrix was determined by the control strategies simulated. It is interesting to note that both the form and values of the matrices are of no physical significance.

An alternative method of solving the optimal control problem is to convert the problem to a parametric optimization problem (Sirisena and Tan, 1974; Goh and Teo, 1988; Nagurka, 1990). Nagurka and Yen (1990) showed that by expanding the generalized coordinates of the system in terms of Fourier series, the optimal control problem reduces to finding the coefficients of the series expansion that would minimize a given objective

function. At every iteration, the inverse-dynamic equations are solved for the set of the control inputs, hence the name inverse parametric optimization method. The iterations continue until a minimum value of the objective function is reached (Gill and Murray, 1981). The major disadvantage of this method is that it can not cope with optimal control problems that are Bang-Bang where the control input takes its limiting values and switches between these values at given time intervals (Nagurka and Yen, 1990; Pandy *et al.*, 1992). Unlike the indirect method, in the direct parametric optimization procedure described by Goh and Teo (1988), the system direct dynamic equations are solved for every iteration seeking a minimal value of the objective function. The procedure starts by parametrizing the input controls in terms of nodal points and then the system dynamic equations are solved at discreet points in time. At every point, the objective function is evaluated and compared with its previous value. Pandy *et al.* (1992, 1995) and Tashman *et al.* (1995) applied the direct optimization method to a large-scale musculoskeletal model. The direct method involves a large CPU time usage in the processes of reaching an optimal solution. A detailed discussion of the CPU implications of the direct optimization method is given by Ziegler *et al.* (1992). In both theories, optimal control and parametric optimization, a set of control inputs are the main outcome of the analysis and they are not constructed to compute any form of feedback structure that may represent the internal feedback of the system. Studies involving the computation of the feedback structure found in the literature, including the ones mentioned above, only deal with an activity that exhibits a linear dynamic model, as in the case of the postural control problem.

1.3 Overview of the Thesis

Approaches to compute the position feedback gains in fields of human dynamics and

robotics involve either the use of optimal control theories or the state feedback analysis. In general, the optimal control problem reduces to the solution of a set of nonlinear first order differential equations representing the necessary optimal conditions. Unfortunately, closed form solutions of these equations are hard to obtain due to the mixed boundary conditions on the states and co-states equations. Therefore, numerical solutions are found by applying forward integration to the state equations and backward integration to the co-state equations. Numerical solutions are time-consuming, thus they are not robust enough in cases where the feedback structure is self-tuning. It is also well known that the complexity of the optimal control problem increases with highly nonlinear system dynamics, as in the case of a large scale human activity. The state feedback analysis, on the other hand, is generally based on the assumptions made over the closed loop eigenvalues or characteristic equation. Since robots are man-made structures, the closed loop eigenvalues are usually chosen to meet certain performance requirements. However, in human activities, less is known about these eigenvalues, beyond the fact that they are stable.

This study describes an alternate approach for computing the position feedback gains in a large scale human activity. Pivotal to the method is the idea that any human activity can be characterized by an input/output mathematical model where the system inputs and outputs are the muscular activity and the nominal motion trajectories, respectively. Since the input/output data are measured from a human subject, the model represents both human dynamics and control, hence is defined as the closed loop system. The identification of such a model from input/output data is obtained by using parametric identification methods. The estimation procedure and issues related to the input and output data are discussed in Section 2.1.

To describe the human dynamic model, an anthropomorphic skeletal model that includes the same number of inputs and outputs used in the identification of the closed loop model is proposed. Implications, such as the number of degrees of freedom that best define the activity under study, discussed in the previous section should also be addressed in the modeling of the skeletal structure. A detailed development of the skeletal model is found in Sections 2.2.1 and 2.2.3. This model is generally nonlinear, thus a linearization procedure is invoked. Utilizing the extended linearization method proposed in the literature, see Rugh (1984), the nonlinear dynamic equations of the skeletal model are represented in terms of a family of linear systems parameterizeparameterized in terms of the structure input/output operating points. The dynamic system's nominal output data are those measured and used in the identification of the closed loop system. However, since the inputs of the skeletal dynamic system are the muscle forces, the system's nominal input data are not available for measurements. Analytical methods are used instead. Section 2.2.2 discusses an analytical method to compute the nominal muscle force based on a muscle mechanics model given in the literature concerning the relationship of the muscle force trajectories and the corresponding muscle activation curves. Both the computed and measured input/output data together with the dynamic model are combined and manipulated to form the family of linearized equations given in Section 2.2.3. Since the anthropomorphic model is free of any feedback components, it is defined as the open loop system.

The next step in the analysis is to estimate the position feedback gain matrix from the available closed and open loop models. A key point in the procedure is to represent both the open and close loop structures in the same state space model. The block observer state

space model is used as the standard structure for the analysis of this thesis. The computation of the feedback gain matrix is based on the following question: what would the feedback matrix be such that when combined with the open loop model it resembles the closed loop structure? The procedure and condition of good estimation are given in Section 2.3.

Finally, in Chapter 3, the utility of the proposed method is demonstrated by applying it to the squat activity. Also in that chapter are qualitative results of the feedback coefficients and results of agonist/antagonist synergies of the muscles included in the model are shown.

CHAPTER TWO

THEORETICAL DEVELOPMENT

This chapter presents a quantitative method to predict the position feedback for a given human activity. The method is based on two major structures, the open and closed loop systems. As stated in the previous chapter, the proposed procedure starts by noting that for given inputs (muscular activity) and outputs (joint's or segmental angles), a mathematical model that defines the input/output relation can be identified. Since this model is a representation of the particular activity of a live subject, it will include both the subject dynamics and control thus defined as the closed loop structure. In the present work, a parametric estimation procedure was utilized to estimate the closed loop model. The estimation procedure used is presented in Section 2.1.

The next step in the analysis is to propose an anthropomorphic skeletal model that best represents the activity under study and also includes the same number of inputs and outputs used in the estimation of the closed loop system. Since the proposed model is free of any form of feedback, it is defined as the open loop model. A detailed discussion of the development and modeling of the open loop model is given in Section 2.2. The resulting open loop model (skeletal linkage model) is generally a nonlinear model, so an extended linearization method is invoked. The linearization procedure described in Section 2.2.3 uses the framework introduced by Rugh (1984) and is based on the idea that the nonlinear open loop system can be replaced by a family of linearized systems parameterizeparame-

terized by a set of joint (segment) motions and nominal muscle forces data (operating points). The nominal motion data are commonly measured using either photogrammetric techniques or goniometers. On the other hand, a noninvasive nominal muscle force measuring technique does not exist. Thus, alternate analytical methods are used to compute the nominal muscle forces during a given activity. Among these procedures is the method of static optimization (Seireg and Arivkar, 1973; Penrod et al., 1974; Crowninsheld and Brand, 1981). Crowninshied and Brand used the static optimization theory by utilizing a nonlinear performance criterion based on muscle endurance. One of the disadvantages of using the optimization method is the large computational time needed to compute these forces. However, Crowninshied and Brand found that the muscle nominal force computed was in agreement with the linear envelope of its electrical activity (Winter et al., 1980). Consistent results were also found recently by Yamaguchi (1990). Thus, in the present work, the physiological model developed by Gordon et al., (1986) is used to evaluate muscle nominal forces computed from measured muscle activities. The proposed method is dependent on the understanding of a muscle phenomenological model used, thus a detailed discussion of modeling a muscle architecture is given in Section 2.2.2. Finally, Section 2.3 presents the position feedback estimation procedure used when both the open and closed loop systems are mathematically defined.

2.1 Identification of the Closed Loop System

The terms "closed" and "open" loop systems will be used frequently in this work. The closed loop system is defined as the actual dynamics of the human neuromusculoskeletal system characterized by a set of experimentally obtained myosignals and segmental angles. The dynamic activity observed is a product of not only the pure rigid body dynam-

ics but also includes the neurological system feedback and control. The open loop system is defined as a mathematical model that consists of a set of articulated rigid bodies connected by joints.

The goal of the present study is to construct a position feedback structure that, when combined with a proposed open loop mathematical model, resembles an experimentally developed closed loop structure. The computation of such a feedback structure depends on the existence of a high quality closed loop model of the dynamics and control. The main purpose of system identification theory is to develop a mathematical model that defines the physical system from input/output experimental data. Various identification algorithms, such as least squares, maximum likelihood, instrumental variable method, cross correlation, and stochastic approximation have been applied successfully to the parametric identification problem. Experimentally, the input/output data are available only at discrete points in time t_0, t_1, t_2, . . . These instances of time can be arranged as integral multiple of some basic unit t_s, say 0 t_s, 1 t_s, 2 t_s. . . In which case t_s is often known as the sampling period and the instants of time are defined in terms of a time parameter k, where k takes the values 0, 1, 2, 3, . . . The sequential input/output (I/O) relations that describe the process dynamics are known as difference equations. A typical single-input single-output (SISO) n^{th} order difference equation takes the form (Streje, 1981)

$$a_n \cdot y(k-n) + a_{n-1} \cdot y(k-(1-n)) + \ldots + y(k) =$$

$$b_o \cdot u(k) + b_1 \cdot u(k-1) + \ldots + b_n \cdot u(k-n) + e(k) \qquad (2.1.1)$$

where $y(k)$ is the output (generalized coordinates), $u(k)$ is the input (activations), and

$e(k)$ is the error associated with either the model or the experimental data. A delay operator q, is defined such that

$$(q^{-1})^n \cdot u(k) = u(k-n) \qquad n = 1, 2, \ldots \tag{2.1.2}$$

The delay operator q has the same role in discrete systems that the Laplace transform has in continous systems. For example, the q-transform of Equation (2.1.1) leads to an algebraic equation in terms of the delay operator q. The resulting relation is known as the transfer function between the input and the output. Invoking the delay transform of Equations (2.1.2) on Equation (2.1.1) gives

$$a_n \cdot q^{-n} \cdot y(q) + a_{n-1} \cdot q^{-(n-1)} \cdot y(q) + \ldots + y(q) =$$

$$b_o \cdot u(q) + b_1 \cdot q^{-1} \cdot u(q) + \ldots + b_n \cdot u(q) + e(q) \tag{2.1.3}$$

or

$$(a_n \cdot q^{-n} + a_{n-1} \cdot q^{-(n-1)} + \ldots + 1) \cdot y(q) =$$

$$(b_o + b_1 \cdot q^{-1} + \ldots + b_n \cdot q^{-n}) u(q) + e(q) \tag{2.1.4}$$

In the multi-input multi-output (MIMO) case, Equation (2.1.4) can be written as

$$A(q) \cdot Y(q) = B(q) \cdot U(q) + E(q) \tag{2.1.5}$$

where $Y(q) \in R^r$ is the output vector, $U(q) \in R^m$ is the input vector, $A(q)$ and $B(q)$ are polynomial matrices of q with the appropriate dimensions. In Equation (2.1.4), $A(q)$ and $B(q)$ were (1x1) matrices where

$$A(q) = a_n \cdot q^{-n} + a_{n-1} \cdot q^{-(n-1)} + \ldots + 1 \tag{2.1.6}$$

$$B(q) = b_o + b_1 \cdot q^{-1} + \ldots + b_n \cdot q^{-n} \tag{2.1.7}$$

For the multi-variable model of Equation (2.1.5), $A(q)$ and $B(q)$ generally take the following form

$$A(q) = A_n \cdot q^{-n} + A_{n-1} \cdot q^{-(n-1)} + \ldots + I_r \tag{2.1.8}$$

$$B(q) = B_o + B_1 \cdot q^{-1} + \ldots + B_n \cdot q^{-n} \tag{2.1.9}$$

where A_i and B_i are constant matrices of appropriate dimensions and I_r is an r x r identity matrix. It will become apparent in the following sections that, for the purpose of the present study, the order of the difference Equation (2.1.5), n takes the value 2. The model developed and described above is commonly called a Discrete Autoregressive (DARX) (MIMO) (I/O)-model (Isermann, 1989).

The identification process is the process of finding the appropriate coefficient matrices of Equations (2.1.8) and (2.1.9), $A_1, A_2, \ldots, B_o, B_1, \ldots,$ that will satisfy a certain criterion. The prediction error method is used in this study, as it is able to deal with the parametric identification of MIMO systems. The predictive error method is one of the least square based algorithms that has been used successfully in the parametric identification of problems that involve the parametric estimation in a large scale musculoskeletal systems (Zhang *et al*, . 1990; Franklen *et al.*, 1995). A detailed study of the method appears in the work of Ljung (1986).

Rewriting Equation (2.1.5) in its equivalent difference equations the following is obtained

$$A_n \cdot Y(k-n) + A_{n-1} \cdot Y(k-n+1) + \ldots + Y(k) =$$

$$B_o \cdot U(k) + B_1 \cdot U(k-1) + \ldots + B_n \cdot U(k-n) + E(k) \qquad (2.1.10)$$

Define R as

$$R = \left[A_1, A_2 \ldots, B_o, B_1 \ldots\right] \qquad (2.1.11)$$

Then Equation (2.1.10) can be rewritten in the following form

$$Y(k) = R^t \cdot \Psi(k) + E(k) \qquad (2.1.12)$$

where

$$\Psi(k) = \left[-Y^t(k-1) \ , -Y^t(k-2) \ \ldots \ U^t(k) \ , U^t(k-1) \ \ldots\right]^t \qquad (2.1.13)$$

and

$$Y(k-i) = \left[y_1(k-i) \ , y_2(k-i) \ \ldots \ y_p(k-i)\right]^t \qquad i = 1,2\ldots n \quad (2.1.14)$$

The form given in Equation (2.1.12) is known as the regression equation. The next step in the estimation procedure is to solve Equation (2.1.12) for the parameter matrix R. A complete study of the available methods developed to accurately compute R from Equation (2.1.12) is presented in Ljung (1989). Based on the predictive error method, the estimation of R involves an iterative checking scheme where the difference between the actual output and predicted output is examined for a minimum value. The study of the convergence and precision of the method is available in the system identification literature (Isermann, 1989; Ljung, 1986; Soderstrom and Stocia, 1989; etc).

The block diagram shown in Figure 2.1. illustrates the general concept of the identification procedure proposed here for the closed loop system. The availability of the experimental data at discrete points in time is represented on Figure 2.1.1. In this study, the closed loop inputs are considered to be the muscle activations and the outputs are the sys-

tem measured generalized coordinates. A comprehensive discussion on the nature of the system inputs is given in this section, while the system outputs are discussed in detail in Chapter 3.

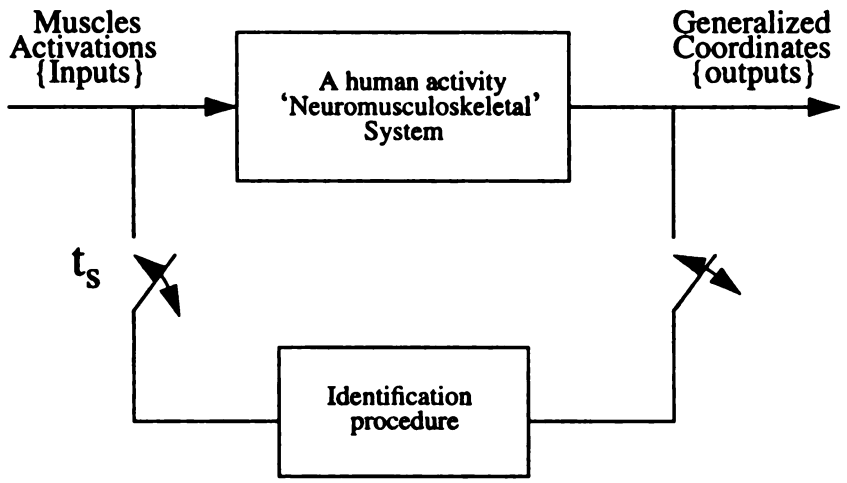

Figure 2.1.1 Schematic illustration of the identification procedure defined in the present study, where t_s is the sampling period.

For the purpose of the current study, the inputs were the myosignals. The muscle force generation process can be generally divided into two major mechanisms, muscle activation and muscle contraction. The later will be discussed in detail in the following sections. Muscle activation is defined by the electrochemical process that takes place upon the arrival of action potentials (AP) at the neuromuscular junction at the terminal arbor. Ebashi and Endo (1968) stated that the activation dynamics of a muscle are best described by the concentration of the Ca^{++} ions in the intera-filamentary space where the activation state is defined by the relative amount of Ca^{++} ions bound to the troponin (Ebashi and Endo, 1968; Hatze, 1980; Pierrynowski and Morrison, 1985; Shipping and Zahalak, 1988). If the maximum number of potential interactive sites on the actin fila-

ments are exposed by the action of the calcium, then the activation is said to be maximum and takes a value of one. The muscle initial activation is defined as the minimum potential interactive sites that are present while the muscle is at rest. Hatze (1977) proposed a second order lumped system that represents the hypothesis first proposed by Ebashi and Endo (1968) and later was found to be consistent with the microscopic model developed by Shipping and Zahalak (1988). Their model considered the action potential signal as the system input (myoelectrical signal). Levine and Zajac (1984) developed a first order bilinear contraction dynamic model as an activation model simpler than that developed by Hatze (1980). The general form of the bilinear model as described in Zajac (1989) is

$$\frac{d}{dt}a(t) = -\left[\frac{1}{\tau}\cdot(\beta+(1-\beta)\cdot u(t))\right]\cdot a(t)+\frac{1}{\tau}\cdot u(t) \qquad (2.1.15)$$

where $u(t)$ is the input neural electromyosignal, $a(t)$ is the muscle activation, τ is the activation process time constant, and β is a constant parameter defined as the ratio of the muscle activation time constant over the muscle relaxation time constant, $0 < \beta < 1$. Burker *et al.* (1973) experimentally found that the activation time constant is the same for the three types of muscle fibers, slow twitch, fast twitch and fast twitch fatigable fibers. They estimated the activation time constant to be approximately 0.003 seconds. Typical values of β ranges from 1/3 to 1/2 depending on the type of the muscle fiber (Close, 1972; Altringham and Jhunson, 1982). As a demonstration, Equation (2.1.15) was simulated with an input that represented a typical electromyographic (EMG) signal shown in Figure 2.1.2A. As shown in Figure 2.1.2B, the output of the bilinear model of Equation (2.1.15) basically rectifies and modulates the raw EMG signal. Hence, in this study an equivalent signal processing approach, that obtains the same outcome as that of the bilinear model, was used. The experimental EMG signal was processed by first filtering and

then rectifying and modulating. A band-pass Butterworth filter of 5Hz and 200Hz cut-off frequencies was used to filter the EMG. Then a full wave rectifier accompanied with a low-pass Butterworth filter, 8Hz cut-off frequency, was used to obtain the corresponding muscle activation curve. The result of the procedure is then considered to be the system input used in the identification procedure presented earlier in this section. This signal processing procedure is shown to be equivalent to the output of the model of Equation (2.1.15), see Figure 2.1.2B, and was recommended by Shiavi *et al.*, 1985; Zajac, 1989; Winter, 1990; Zhang, 1990 and others as an alternative to solving and simulating Equation (2.1.15).

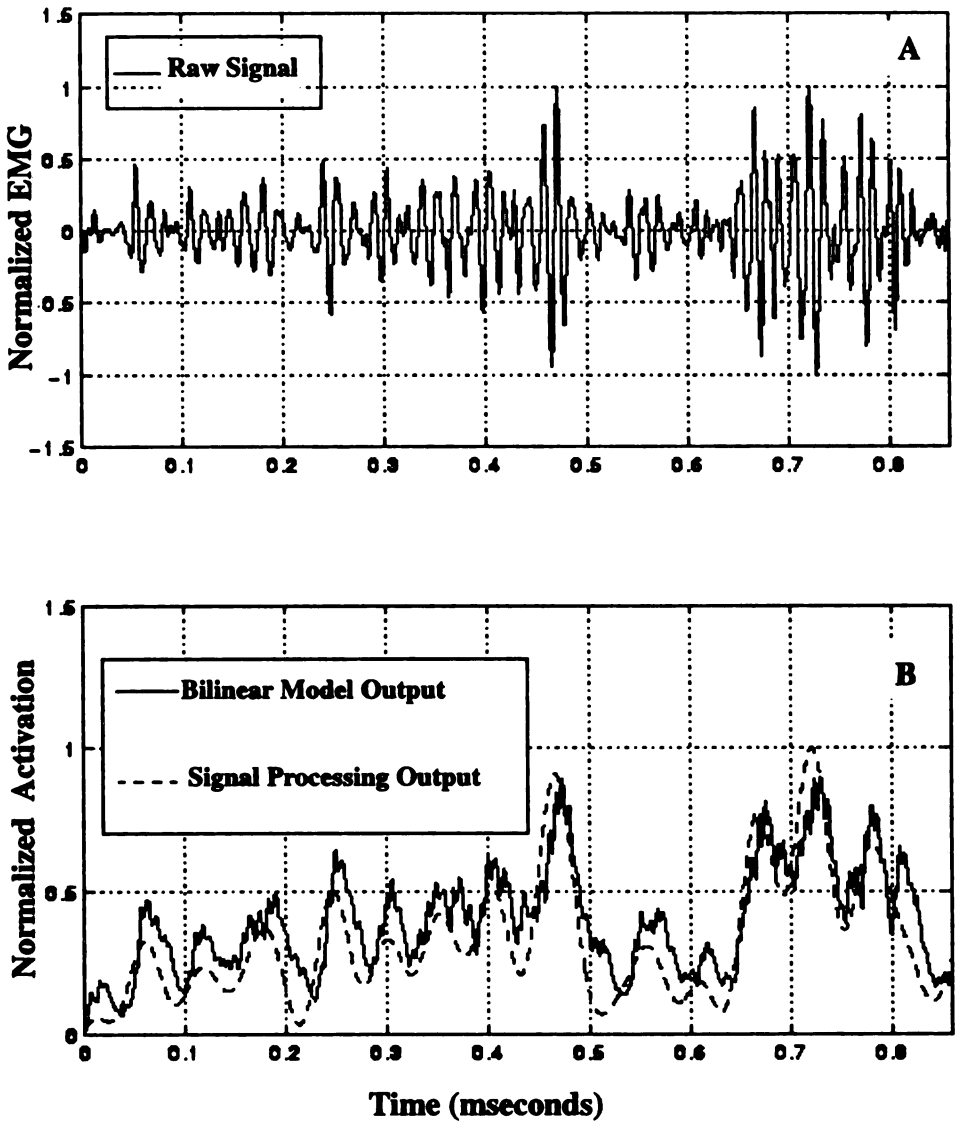

Figure 2.1.2A. A typical electromyographic signal.
Figure 2.1.2B. A comparison between the output of the bilinear model of Zajac, 1989 and the signal processing method used in the present study.

2.2 Modeling of The Open Loop System

The open loop system, as defined in the previous section, consists of a system of articulated rigid bodies. The choice of the number of muscle forces and the degrees of freedom of the rigid bodies or the joints, is dictated by the number of inputs and outputs observed in the identification procedure presented in Section 2.1. For example, if the knee joint is modeled with six degrees of freedom, then all the six quantities should be available for measurement. Muscles in musculoskeletal structures can be modeled as either moment generators or sub-systems (Hatze, 1980). Including muscles as sub-systems will only increase the number of the states and equivalently increase the order of the system. However, the conceptual implementation of the proposed position feedback estimation procedure will not change. In this study, muscles are modeled as moment generators. In the next sub-section, a brief representation of the muscle moment arm computation is presented. Then a complete discussion on muscle modeling and architecture is presented in Section 2.2.2. Finally, the rigid body skeletal system mechanical modeling is presented in Section 2.2.3.

2.2.1. Musculotendon Moment Arm Computation

To illustrate the computation of a muscle moment arm, consider the sketch shown in Figure 2.2.1. In the sketch shown, $\vec{r}_o$ and $\vec{r}_I$ represent the vectors to the origin and insertion points with respect to their body segment coordinate systems, respectively. Yamaguchi *et al.* (1990), provided tabulated values of $\vec{r}_o$ and $\vec{r}_I$ for a large number of human muscles from experimental studies on cadavers. Generally, a muscle may span more than one joint and overlap more than one body segment (the hamstrings, for example). There-

fore, Figu

where n is

resent the

Mus

Tendo

Figu

I

fore, Figure 2.2.1 illustrates a general muscle spanning (m) joints and (n) body segments, where n is equal to ($m+1$). In Figure 2.2.1 the coordinates (X_j, Y_j, Z_j), $j = 1, 2, \ldots n$, represent the n segmental coordinates of the n body segments the muscle spans

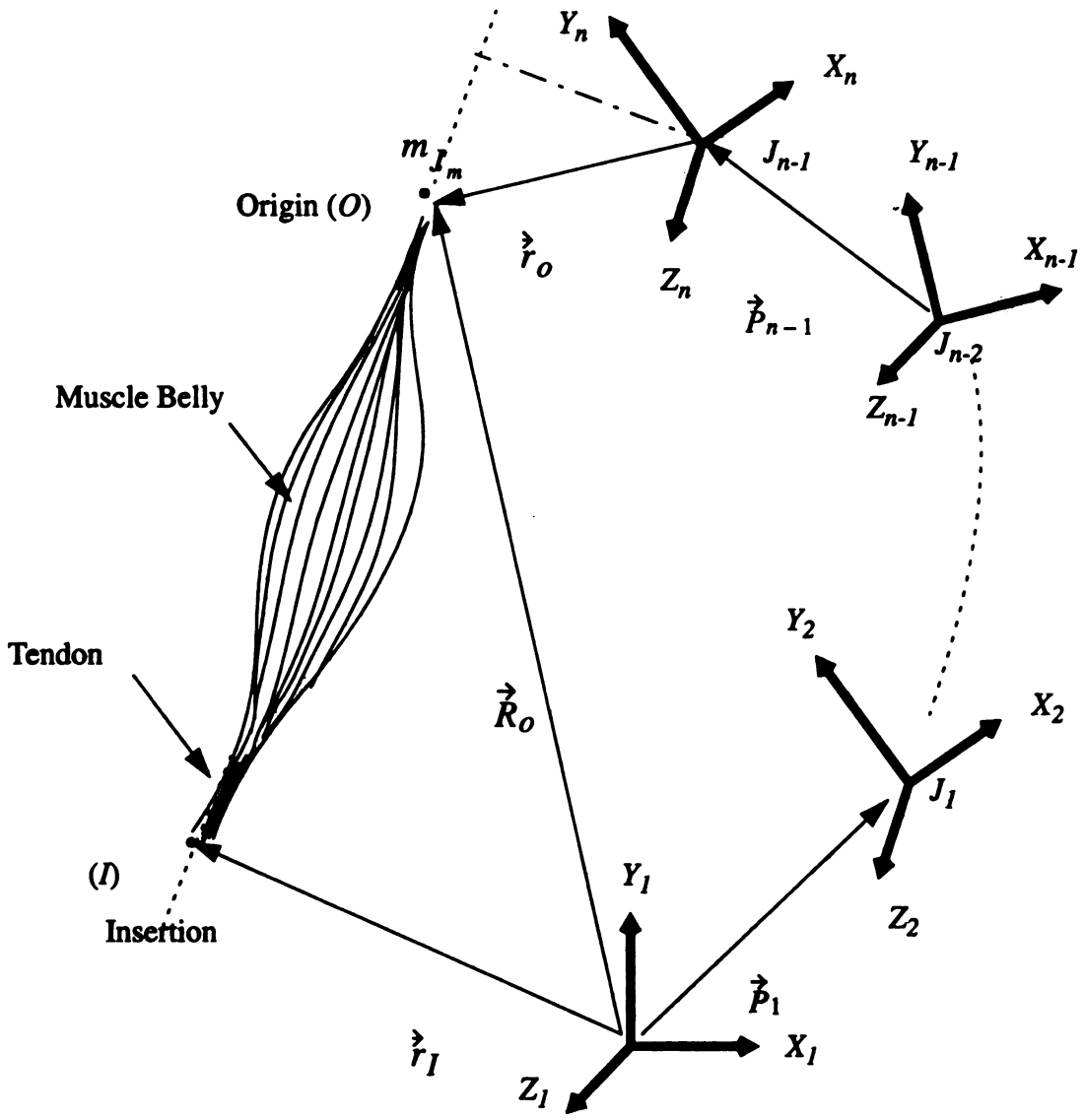

Figure 2.2.1 Schematic sketch of an m-articular muscle used for muscle moment arm and length calculations.

It can be easily shown that the position vector of the origin point with respect to the

insertion point coordinate system (X_I, Y_I, Z_I) is given in its matrix form as

$$R_o = \prod_{j=1}^{m} T_j \cdot r_o + \sum_{j=1}^{m} \left\{ \prod_{i=1}^{j} T_{j-1} \cdot P_j \right\} \tag{2.2.1}$$

where T_j is the transformation matrix of (X_{j+1}, Y_{j+1}, Z_{j+1}) coordinates to (X_j, Y_j, Z_j) coordinates and represents the rotational degrees of freedom of j^{th} joint, J_j, P_j is the position vector of the (X_{j+1}, Y_{j+1}, Z_{j+1}) coordinate system with respect to the (X_j, Y_j, Z_j) coordinate system defined in the (X_j, Y_j, Z_j) coordinates and represented in its matrix form, and T_0 is an identity transformation matrix. In general, P_j is not function of time unless the joint is said to have translational degrees of freedom. In that case, P_j is taken to be a variable function of time that represents some fixed value and defines the structural distance between the consecutive joints, and the translational $J_j{}^{th}$ joint degrees of freedom. Once the position vector of the origin point R_o is computed, the insertion to origin position vector is given as

$$\overrightarrow{R_{o/I}} = \vec{R}_o - \vec{r}_I \tag{2.2.2}$$

In cases where the muscle may have more than one insertion or origin points, (for example the tibialis anterior muscle), effective origin or insertion points are introduced, (see Gordon *et al.*, 1986; Hoy *et al.*, 1990) and the formulation above holds true.

The moment arm of the muscle can be computed from Equation (2.2.2) above using the fact that the muscle moment arm is always perpendicular to the line of action of the muscle force as shown in Figure 2.2.1. Thus, the moment arm of the muscle about for example, the m^{th} joint J_m, is given as

$$m_{J_m} = \left| \left(\overrightarrow{\prod_{j=1}^{m} T_j \cdot r_o} \right) \times \overrightarrow{R_{o/I}} \right| / \left| \overrightarrow{R_{o/I}} \right| \tag{2.2.3}$$

It should be obvious from Equation (2.2.3) that the muscle moment arm is a function of system degrees of freedom through both $\overrightarrow{R_{o/I}}$ and T_j's. This dependency adds another complexity to the musculoskeletal system through the introduction of coupling in the dynamic equations as will be shown in later sections. It can be easily shown that the moment of the muscle, $\overrightarrow{\tau_{J_m}}$, about the J_m joint shown in Figure 2.2.1 is given as

$$\overrightarrow{\tau_{J_m}} = \underbrace{\left(\overrightarrow{\prod_{j=1}^{m} T_j \cdot r_o} \right)}_{\substack{moment\ arm \\ vector}} \times \underbrace{\left(p \left(\frac{\overrightarrow{R_{o/I}}}{\left| \overrightarrow{R_{o/I}} \right|} \right) \right)}_{\substack{muscle\ force \\ vector}} \tag{2.2.4}$$

where p is the muscle force computed from a proposed muscle model (see the next section for details).

Finally, both the muscle moment and moment arms computed using Equations (2.2.3 and 2.2.4) may also be used in cases where the joint exhibits translational degrees of freedom. In these cases, the origin point position vector $\vec{r}_o$ will consists of two parts. The first represents the anthropomorphic origin point location, obtained from the literature, and the second component characterizes the translation motion of the joint. However, to use Equations (2.2.3 and 2.2.4), the vector $\vec{r}_o$ should be represented in the $(X_{n-1}, Y_{n-1}, Z_{n-1})$ coordinate system shown in Figure 2.2.1.

2.2.2. Muscle Modeling and Architecture

As proposed in Gordon *et al.*, (1986), the mechanics of muscles are divided into two major components, 1. the activation and 2. the contraction mechanics. Activation dynamics is proposed by the work Zajac (1989) to be parametrically independent of the system states (velocities and positions). A detailed discussion of the EMG-to-activation process and its equivalent signal processing procedure used here was given in Section 2.1. Utilizing the output of the activation dynamics as the input to the muscle contraction process, Zajac (1989) presented a comprehensive development of a non-dimensional muscle model based on an earlier work done by Gordon *et al.* (1986). The output of the model was the muscle force detected at the tendon.

The lumped muscle model proposed by Gordon *et al.* (1986) shown in Figure 2.2.2, satisfies four criteria to be suitable for computer simulative studies. The first criteria is the low order of the mathematical model. Secondly, the model is developed based on muscular architecture. The third is the model was non-dimensionalized with respect to muscle and tendon mechanical (static) properties. Last, and most important, the muscle model output, muscle force, should be consistent with the computed nominal muscle force obtained using optimization techniques. Static properties of muscle fibers, such as muscle optimal length, optimal muscle force, and tendon slack length, have been intensively studied. Yamaguchi *et al.* (1990) surveyed these studies and provided a tabulated summary of their results for a wide number of human muscles. As has been defined in Chapter 1, the lumped muscle architecture can be divided into two major components, active and passive elements. The passive element includes both the muscle belly passive element and the tendon spring-like element. The active element represents the actin/myosin

cross-bridges that are the sight of the activation input (Hatze, 1973).

A typical musculotendon architecture is shown in Figure 2.2.2. In the model shown, PE is the muscle parallel element, SE is the muscle series element, T is the tendon, and CE is the muscle active element. The α–angle shown is the muscle pennation angle.

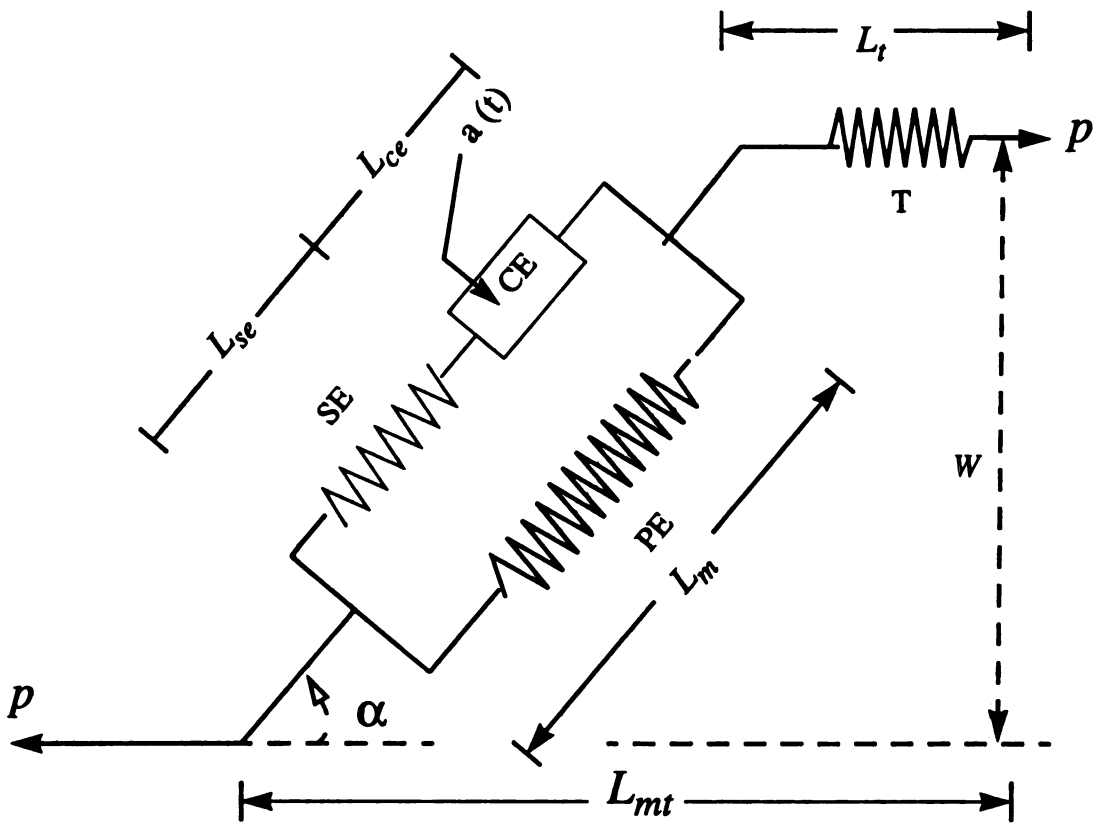

Figure 2.2.2. Schematic sketch of the muscle architectural model developed in Gordon *et al.*, 1986.

The muscle parallel element is defined as the activation independent elastic component of the muscle belly. This element has nonlinear exponential properties as shown by Fung (1967) and Haut and Little (1972). An experimentally based constitutive equation of the parallel element was developed in Fung (1967) that takes the form

$$p_{pe} = c_1 \cdot p_o \cdot e^{(c_2 \cdot (L_m - (c_3 \cdot L_o))/(c_3 \cdot L_o))} \tag{2.2.5}$$

where p_o and L_o are muscle optimal force and length, L_m is muscle fiber length, p_{pe} is muscle parallel element force, and c_1, c_2, c_3 are model constants found to be 0.05461, 4.0, and 1.0, respectively. It should be clear that the muscle parallel element will produce no force for muscle lengths less than the slack length of the muscle. The muscle series element (SE) is an activation dependent elastic element that was first observed by the work done by A.H. Hill (1938).

The significance of the series element arises in cases of transient force loading such as heel strike in running or the takeoff stage in vertical jumping (Winters and Starks, 1987). Based on a set of quick release experimental tests, Pierrynowski and Morrison (1985) developed a series element compliance equation that took the form

$$L_{se}/L_o = 0.5 + (A \cdot x + B \cdot x^2 + C \cdot x^3) \tag{2.2.6}$$

where

A = 0.2118

B = -0.2265

C = 0.0844

$x = p_{se} / p_o$

and L_{se} and p_{se} are the series element length and force, respectively.

The constitutive equation for the activation dependent element of the muscle, the contractile element (CE), was first proposed by the work of A.H. Hill (1938; 1950) in the form of a force velocity hyperbolic equation. This equation relates the contractile element

contraction (shortening, $L_m < L_o$) velocity to the force generated through the element. To account for the lengthening ($L_m > L_o$), Audu and Davy (1985), constructed a bihyperbolic equation that can be expressed as

$$v_{ce} = \begin{cases} -b_1 \cdot (1 - p_{ce}/p_{iso})/(b_2 + p_{ce}/p_{iso}) & p_{ce}/p_{iso} \le 1 \\ \quad shortening & \\ -b_3 \cdot (1 - p_{ce}/p_{iso})/(1.33 - p_{ce}/p_{iso}) & p_{ce}/p_{iso} > 1 \\ \quad lengthening & \end{cases} \tag{2.2.7}$$

where p_{ce} is the contractile element force, b_1, b_2, and b_3 are model constants that takes different values for different muscles. A. H. Hill (1938) noted that the maximum contraction velocity in the contractile element V_m occurs when the muscle is at rest and from Equation (2.2.7), the ratio of b_1/b_2 is equal to V_m. The maximum shortening velocity is found to be dependent on the muscle optimal (slack) length, L_o, and is taken to be $10\ L_o$ sec^{-1} (Zajac, 1989). In Equation (2.2.6), the constant b_3 was introduced to insure smooth matching at the point where the two curves, shortening and lengthening, meet. Values of the different constants in Equation (2.2.7) are tabulated in Audu and Davy (1985), for selected lower extremities muscles. The isometric muscle force, p_{iso}, appearing in the velocity-force relation given above is taken from the isometric tension-length curve first observed by Gordon *et al.* (1966). By investigating the relation between the isometric force in frog striated muscle at maximum activation, Gordon *et al.* (1966), found that the maximum isometric muscle occurs at the muscle optimal (slack) length and vanishes at above 180 percent and below 58 percent of the muscle slack length. Partial activation of the muscle will then logically produce less force. Hatze (1977) and later

Winters and Starks (1985) suggested that the muscle isometric force-length relation at partial activation is only a scaled version of the relation at full activation provided that the other characteristics are preserved. Therefore, Hatze (1977) fitted experimental isometric force-tension data of a fully and partial activated muscle fibers and developed a force-length relationship at any activation level. Thus the relationship takes the following form

$$\frac{p_{iso}}{p_o} = \left\{\left(a_1 + a_2 \cdot e^{\left(a_3 \cdot \left(\frac{L_m}{L_o} - 1\right)\right)}\right) \cdot \sin\left(a_4 \cdot \left(\frac{L_m}{L_o} - a_5\right)\right)\right\} \cdot a(t) \qquad (2.2.8)$$

where

$$a_1 = 0.32$$

$$a_2 = 0.71$$

$$a_3 = -1.112$$

$$a_4 = 3.722$$

$$a_5 = 0.656$$

p_o is the muscle optimal (maximum) isometric force, and $a(t)$ is the muscle activation. Finally, the tendon elasticity is assumed to exhibit the same exponential form that the muscle parallel element exhibits.

A full mathematical description of the lumped model shown in Figure 2.2.2 is given in Appendix A and takes the general form

$$\dot{p} = f(L_{mt}, V_{mt}, p, a(t)) \qquad (2.2.9)$$

where $\dot{p} = \frac{dp}{dt}$, L_{mt} and V_{mt} are the musculotendon length and velocity, respectively.

To avoid the complexity and the nonlinearity of the lumped muscle model discussed above, Khang and Zajac (1989 I, II) developed a linearization procedure through which a linear model of the form

$$\dot{p} = -c \cdot p(t) + c \cdot p_o \cdot a(t) \tag{2.2.10}$$

was constructed. The constant (c) appearing in Equation (2.2.10) above was determined by the rate of tension of the muscle. To determine the rate (c), Equation (2.2.9) was simulated using the muscle and tendon static properties assuming that musculotendon length and velocity were constant at maximum activation ($a(t)=1$). To illustrate the computation, Equation (2.2.8) was simulated for the rectus femoris and the hamstring muscles. The simulation starts with the computation of the musculotendon length, L_{mt}. The muscle was modeled as a straight line connecting the origin and insertion points. The musculotendon length can be easily computed from Equation (2.2.2) as follows

$$L_{mt} = \left|\overrightarrow{R_{o/I}}\right| \tag{2.2.11}$$

A graphical display of the simulation result of Equation (2.2.9) appears in Figure 2.2.3 below. Keep in mind that the linear model of Equation (2.2.10) is a first order mathematical model with a time constant of $1/c$. Thus, the time constant of the force development in the rectus femoris muscle, for example, is the time it takes the muscle force to reach 63.21 percent of the steady state value, see Figure 2.2.3.

This new linearization procedure used in the present work was adopted for two reasons. The first is based on the nature of the model developed, where every variable

(L_{mt}, V_{mt}, p, $a(t)$) explicitly defined in the model is an implicit function of either the system states (angles and velocities through the computation of the musculotendon length, see Equation 2.2.11) and/or the other explicit variables appearing in the model. These interdependencies make the Jacobian based linearization procedure hard to perform in this case. The second reason depends on the way the force model is used in the context of the present study. The form given in Equation (2.2.10) will not be used in its present form but a sequential transform of the equation instead is used. Also the assumption is made that the muscle force rate of development from one value to another is constant over the sampling time period (*1/1000* of a second.).

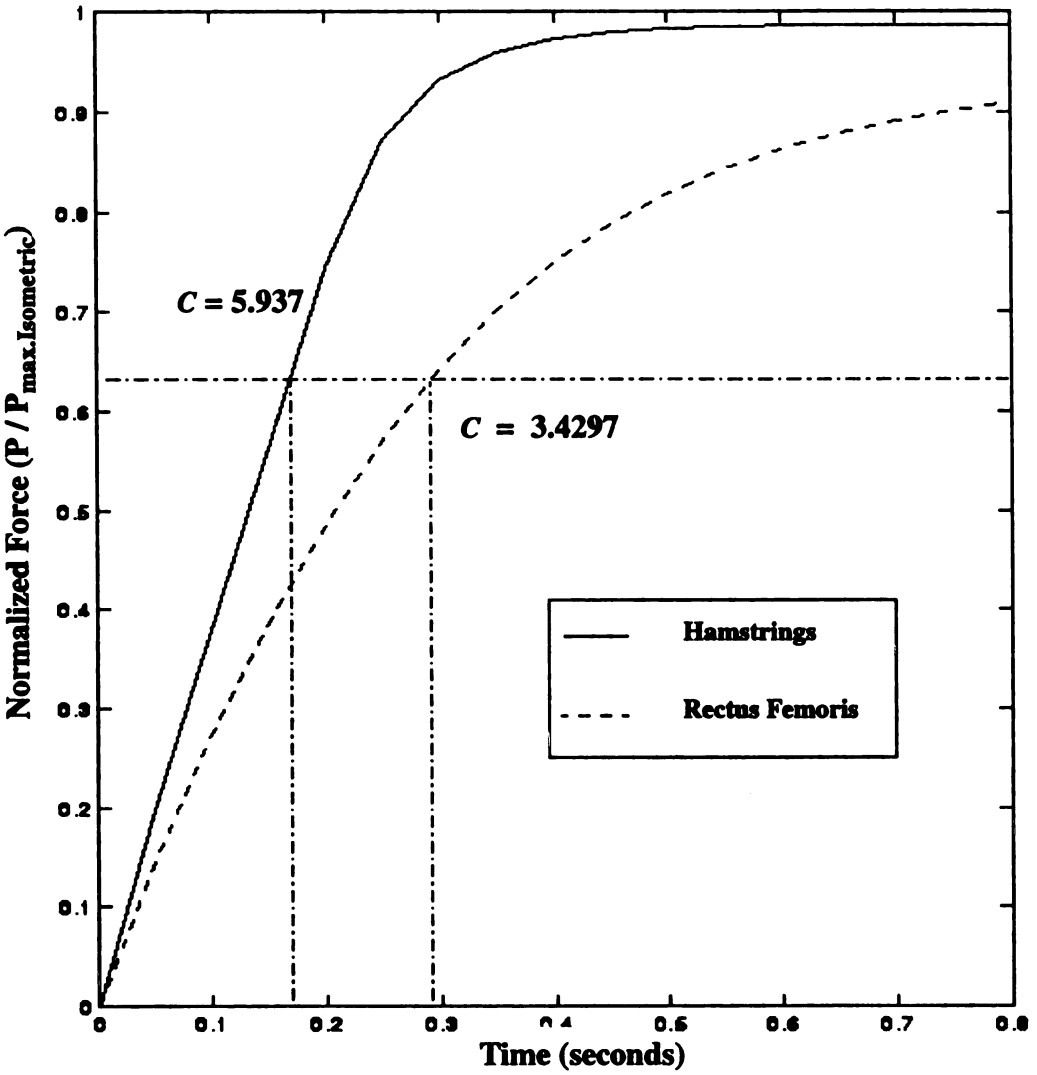

Figure 2.2.3. Simulation display of the muscle nonlinear contraction dynamics of the rectus femoris and hamstring muscles. The rate of tension defined in equation (2.2.10) is computed as shown for both muscles.

2.2.3. Musculoskeletal Mathematical Model

The general governing equation of motion of the musculoskeletal model can be expressed through the direct application of Lagrange-Euler formulation. Consider the general form of Lagrange-Euler equation as

$$\frac{d}{dt}\left(\frac{\partial T}{\partial \dot{q}_i}\right) - \frac{\partial T}{\partial q_i} + \frac{\partial V}{\partial q_i} = \tau_i \tag{2.2.12}$$

where q_i represents the i^{th} generalized coordinate. In systems that consist of articulated rigid bodies, the human structure as an example, q_i may represent either the segmental or joint translational and/or rotational degrees of freedom. In the context of the present study, it is appropriate to choose those degrees of freedom when modeling the open loop system that were the subject of measurements during the process of the closed loop system identification. Appearing on the right hand side of Equation (2.2.12) is the segmental or the joint applied moments, see Equation (2.2.4) for details.

Body segmental inertial parameters are essential in the formulation of the kinetic (T) and potential (V) energies expressed in Equation (2.2.12). Segmental masses and the locations of the center of masses, are usually estimated based on either cadavers studies or using geometrical and material approximations (Hanavan, 1964; Clauser *et al.*, 1969; Seirge and Arvikar, 1989).

The derived differential equation of motion can be represented in a matrix form as follows

$$J(q) \cdot \ddot{q} = H(q, \dot{q}) + C(q) + T(q, p) \tag{2.2.13}$$

where q are the generalized coordinates (outputs) $q \in R^r$, $H(q, \dot{q})$ are the nonlinear

Coriolis and Centripetal force vector, $H(q, \dot{q}) \in R^r$, $C(q)$ is the gravity loading force vector, $C(q) \in R^r$, $T(q, p)$ is the generalized force and/or torque vector, $T(q, p) \in R^r$, $J(q)$ is the system inertia matrix, and p is the muscle forces vector (input), $p \in R^m$. The acceleration vector $\ddot{q}$ of Equation (2.2.13), can be expressed as

$$\ddot{q} = f(q, \dot{q}, p) \tag{2.2.14}$$

where

$$f(q, \dot{q}, p) = J^{-1}(q) \cdot (H(q, \dot{q}) + C(q) + T(q, p)) \tag{2.2.15}$$

provided that $J^{-1}(q)$ exist. The output feedback estimation procedure proposed here is based on a family of linearized perturbation equations of Equation (2.2.14). The family of linearized equations are parameterized by a set of nominal (operating) points that define the nominal generalized coordinates q_{in}, velocities $\dot{q}_{in}$ and forces p_{in}. Using Taylor series expansion of Equation (2.2.14) about the nominal points and neglecting the higher order terms of the expansion, the associated linearized perturbation acceleration of the model is

$$\delta\ddot{q} = \nabla_{\dot{q}} f \,|_n \cdot \delta\dot{q} + \nabla_q f \,|_n \cdot \delta q + \nabla_p f \,|_n \cdot \delta l \tag{2.2.16}$$

where $\nabla_{\dot{q}} f \,|_n$, $\nabla_q f \,|_n$, and $\nabla_p f \,|_n$ are the Jacobian matrices evaluated at the nominal generalized velocities, coordinates, and muscle forces, respectively, $\delta\dot{q} = \dot{q} - \dot{q}_n$, $\delta q = q - q_n$, and $\delta p = p - p_n$. The smoothness of $f(q, \dot{q}, p)$ and the assumption that $\delta q_j^i \ll \delta q_j$, $\delta \dot{q}_j^i \ll \delta \dot{q}_j$, and $\delta p_j^i \ll \delta p_j$ for $\forall\ t \geq 0$ and $i = 2, 3, \ldots$, provides the

necessary conditions to neglect the higher order terms in the Taylor expansion. Thus, the linearization procedure can be used in human activities, such as walking, squatting, etc., that do not violate the necessary conditions for the approximation Equation (2.2.16).

The nominal generalized coordinates vector, q_n, is obtained experimentally by using either electrogoniometric systems (Finley and Karpovich, 1964) or photogrammetric means (Abdel-Aziz and Karara, 1971). Nominal velocities, $\dot{q}_n$, are computed from measured generalized coordinates trajectories.

The nominal muscle force vector, p_n, can be computed using the linearized muscle contraction dynamics Equation (2.2.10). The activation input, *a(t)*, is computed from the electromyosignal, measured experimentally, after using the equivalent to activation dynamics procedure explained in Section 2.1. However, initial muscle forces are essential to the computation of the nominal forces when using Equation (2.2.10). Thus, a nonlinear quasi-static optimization procedure is used to solve for the initial, or time zero, values of muscle forces. Two functional quantities need to be specified in order to perform the optimization, namely the objective function and the constraints equations. For the redundant musculoskeletal system, Crownishield (1978) hypothesized that the redundancy in the muscle forces spanning a joint is such that the muscles will distribute forces to minimize muscle energy. In later work, Pandy *et al.* (1990) proposed a mathematical model to define the minimum muscle energy hypothesized by Crownishield in the following form

$$\Phi = \sum_{i=1}^{m} (p_i / p_{io})^2 \qquad (2.2.17)$$

where p_i is the i^{th} muscle force and p_{io} is the i^{th} maximum isometric muscle force. Static

equilibrium of a joint may be chosen to be the set of equality constraints by which the objective function provided in Equation (2.2.17) is minimized. Hence, the form of the constraints that define static equilibrium can be easily obtained by setting both the generalized coordinate velocities and accelerations equal to zero in Equation (2.2.13) leading to the following general form

$$C(q_n(t=0)) + T(q_n(t=0), p_n(t=0)) = 0 \tag{2.2.18}$$

It should be clear when using Equation (2.2.18) that the initial system configuration is known from experimental data, and the goal of the optimization is to seek the values of $p_n(t=0)$ which minimizes Φ.

To implement the position feedback estimation procedure defined in the next section, Equation (2.2.16) is discretized by using the Laplace-transform and the bilinear transform (see Lewis, 1987). Then, Equation (2.2.16) can be expressed in terms of the backward delay operator q, (see Section 2.1) as follows

$$A^o(q) \cdot q(q) = B^o(q) \cdot p(q) \tag{2.2.19}$$

where

$$A^o(q) = A_2^o \cdot q^{-2} + A_1^o \cdot q^{-1} + I_r \tag{2.2.20}$$

$$B^o(q) = B_2^o \cdot q^{-2} + B_1^o \cdot q^{-1} + B_0^o \tag{2.2.21}$$

and

$$B_i^o = (A_0^*)^{-1} \cdot B_i^* \qquad i = 0, 1, 2 \tag{2.2.22}$$

$$A_i^o = (A_0^*)^{-1} \cdot A_i^* \qquad i = 1, 2 \tag{2.2.23}$$

In Equations (2.2.22 and 2.2.23) the matrices are related to the system Jacobians as

follows

$$A_0^* = \nabla_q f \Big|_n + (2/t_s) \cdot \nabla_{\dot{q}} f \Big|_n + (2/t_s)^2 \cdot I_r \tag{2.2.24}$$

$$A_1^* = 2 \cdot \nabla_q f \Big|_n - 2 \cdot (2/t_s)^2 \cdot I_r \tag{2.2.25}$$

$$A_2^* = \nabla_q f \Big|_n - (2/t_s) \cdot \nabla_{\dot{q}} f \Big|_n + (2/t_s)^2 \cdot I_r \tag{2.2.26}$$

$$B_0^* = B_2^* = B_1^*/2 = \nabla_p f \Big|_n \tag{2.2.27}$$

where t_s is the sampling interval, I_r is an $(r \times r)$ identity matrix, and (r) is the number of outputs.

The order of the open loop difference equation given in Equation (2.2.19) is clearly of a second order. Since the constant output feedback does not change the order of the open loop difference equations (Fallside, 1974; Lewis, 1987), the order of the closed loop system (n) to be identified is thus chosen to be 2. Both the closed and open loop systems should not only have the same order, n, but also should be modeled using the same I/O structure, ARX model for example. These two conditions are fundamental in the conceptual implementation of the position feedback estimation procedure.

2.3 Estimation of the Position Feedback Structure

An alternative to using the state feedback and the optimal control methods in the study of the feedback control problem in humans involves the estimation of the feedback structure. This method is based on the identification of the closed loop system from measured nominal trajectories of both the input and output data and on the linearized perturbation equations of a proposed open loop structure.

The block diagram shown in Figure 2.3.1 illustrates the general concept of the feed-

back structure estimation proposed here. The matrix [K], shown in Figure 2.3.1, defines the feedback structure gain matrix that relates the system outputs with the system inputs. Since we measured only position data in the identification process presented in Section 2.1, the feedback structure will represent only the position feedback control of the open loop system. However, if both the position and velocity data are available for measurements, the gain matrix [K] can represent the general state (positions and velocities) feedback matrix.

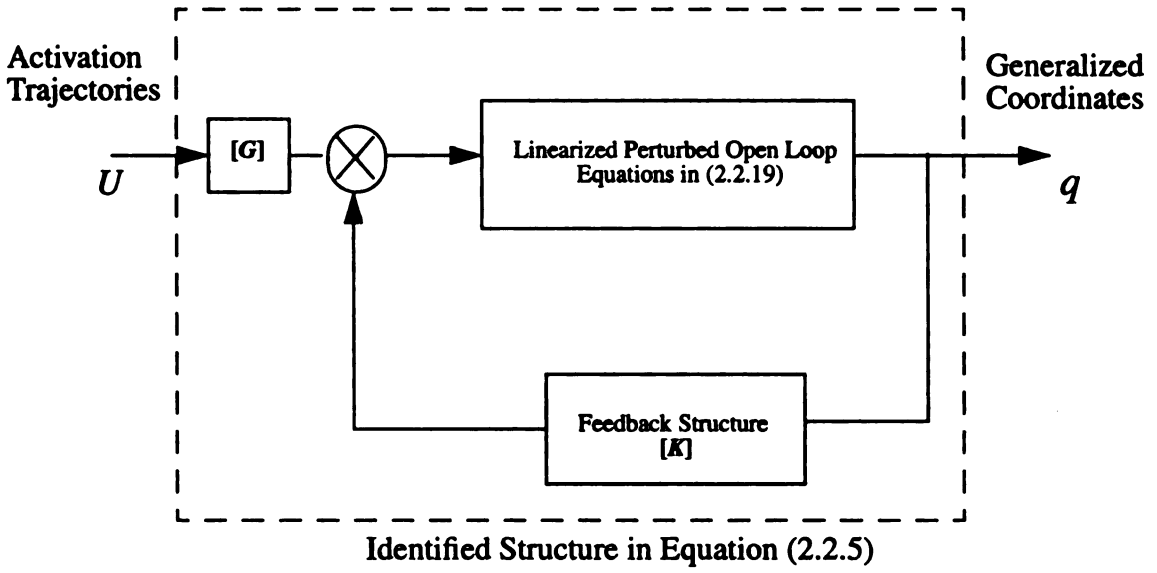

Figure 2.3.1. Schematic illustration of the output feedback estimation procedure developed in this study

The first step in the development of the output feedback estimation procedure is to construct a state space realization of both the open loop, Equation (2.2.18), and the closed loop, Equation (2.2.5), systems. Regardless of the form of the realization chosen, both systems should be represented using the same state space structure. Utilizing the block observer form, see Appendix (B), Equation (2.2.5) is written as

$$X(k+1) = A^c \cdot X(k) + B^c \cdot U(k) \tag{2.3.1}$$

$$q(k) = C^c \cdot X(k) + D^c \cdot U(k) \tag{2.3.2}$$

Similarly, the linearized perturbation equations of the open loop system of Equation (2.2.18) can be written in the block observer form as

$$X(k+1) = A^o \cdot X(k) + B^o \cdot P(k) \tag{2.3.3}$$

$$q(k) = C^o \cdot X(k) + D^o \cdot P(k) \tag{2.3.4}$$

where $X(k)$ is the state vector, $X(k) \in R^{nr}$, $q(k)$ is the output generalized coordinates, $q(k) \in R^r$, $P(k)$ and $U(k)$ are the force and activation input vectors, respectively, and $P(k) \in R^m$; $U(k) \in R^m$. The matrices given in the open loop state space model are dependent on both the operating points, through the extended linearization, and the model static and dynamic parameters.

The output feedback law can then be written as follows:

$$P(k) = G \cdot U(k) - K \cdot q(k) \tag{2.3.5}$$

Substituting Equation (2.3.5) into the output Equation (2.3.4), leads to

$$P(k) = [I_m + K \cdot D^o]^{-1} \cdot \{G \cdot U(k) - K \cdot C^o \cdot X(k)\} \tag{2.3.6}$$

where I_m is an (m x m) identity matrix. Equation (2.3.6) applies only if the inverse of $[I_m + K \cdot D^o]$ matrix exists, in other words the determinant of $[I_m + K \cdot D^o] \neq 0$. This condition is defined in Chen (1970) as the well-posedness of the output feedback problem. As will be seen later and for all practical reasons, this condition is satisfied in the present study.

Substituting both Equations (2.3.5 and 2.3.6) in the state Equations (2.3.3) yields

$$X(k+1) = \left\{A^o - B^o \cdot [I_m + K \cdot D^o]^{-1} \cdot K \cdot C^o\right\} \cdot X(k) +$$

$$\left\{B^o \cdot [I_m + K \cdot D^o]^{-1} \cdot G\right\} \cdot U(k) \qquad (2.3.7)$$

By direct comparison of Equations (2.3.7) and Equations (2.3.1), a closed form solution of the [K] and [G] matrices can be determined as follows (Munro, 1974; Fallside, 1974)

$$B^o \cdot [I_m + K \cdot D^o]^{-1} \cdot K = (A^o - A^c) \cdot C^{oT} \cdot (C^o \cdot C^{oT})^{-1} \qquad (2.3.8)$$

and

$$B^o \cdot [I_m + K \cdot D^o]^{-1} \cdot G = B^c \qquad (2.3.9)$$

A detailed discussion on the existence of the inverse of $C^o \cdot C^{oT}$ appears in Appendix (C). The necessary and sufficient conditions of the solution of Equation (2.3.8) for [K] are found in Munro (1974), and Fallside (1974). The solution is also extensively discussed in Vardulakis (1973). A unique explicit solution of Equation (2.3.8) for the matrix [K] depends on the existence of the $(B^{oT} B^o)^{-1}$ matrix, see the proof given at the end of this section. Since the B^o matrix is an operating point dependent matrix, or, in other words, an activity dependent matrix, the $(B^{oT} B^o)^{-1}$ may or may not exist for a particular activity (see later sections). Thus, an approximate least squares based method is considered in the present study. Hence, a minimum norm 2 solution of Equation (2.3.8) is given as

$$K = I_m \cdot \hat{B} \cdot [I_r - D^o \cdot \hat{B}]^{-1} \tag{2.3.10}$$

where

$$\hat{B} = B^{o*} \cdot \left\{ (A^o - A^c) \cdot C^{oT} \cdot (C^o \cdot C^{oT})^{-1} \right\} \tag{2.3.11}$$

and B^{o*} is the generalized inverse of B^o. It is well known in linear algebra (Ortega, 1987) that if B^o is a real (nr x m) matrix, then there exist orthogonal matrices $M = [m_1, m_2, \ldots, m_{nr}] \in R^{nr \times nr}$, $N = [n_1, n_2, \ldots, n_m] \in R^{m \times m}$ such that

$$B^o = M \cdot \Lambda \cdot N^T \tag{2.3.12}$$

$$\Lambda = \left[[diag(\sigma_1, \sigma_2, \ldots, \sigma_{nr_1}, 0, 0\ldots)] \; 0 \right] \in R^{nr \times m}; l_1 \leq nr \tag{2.3.13}$$

where l_1 is the rank of B^o and $\sigma_1 > \sigma_2 > \ldots > \sigma_{nr_1} > 0$ are the singular values of the matrix. Thus the generalized inverse of B^o can be represented in terms of M, Λ, and N as follows

$$B^{o*} = N \cdot \Lambda^* \cdot M^T \tag{2.3.14}$$

$$\Lambda^* = \begin{bmatrix} [diag(1/\sigma_1, 1/\sigma_2, \ldots, 1/\sigma_{nr_1}, 0, 0\ldots)] \\ 0 \end{bmatrix} \in R^{m \times nr}; l_1 \leq nr \tag{2.3.15}$$

It is important to note that the desired closed loop matrix A^c can only be fully attained if the row rank of B^o is full (i.e $raw\ rank(B^o) = l_1$, where $l_1 = nr$). For simplicity, consider the case where $D^o = 0$. Also let $\hat{A}$ be defined as follows

$$\hat{A} = A^o - B^o \cdot K \cdot C^o \tag{2.3.16}$$

where $\hat{A}$ represent the closed loop matrix to be attained, and [K] is the minimum norm 2 based output feedback solution given in Equation (2.3.10) provided that D^o is a zero matrix. Thus, the term $[I_m + K \cdot D^o]^{-1}$ in Equations (2.3.9 and 2.3.10) is only an (m x m) identity matrix. Hence, using the result in Equation (2.3.10) for K and the definition in Equations (2.3.12 and 2.3.14) for B^o and B^{o*}, respectively, in Equation (2.3.16) yields

$$\hat{A} = A^o - M \cdot \Lambda \cdot N^T \cdot \left\{ N \cdot \Lambda^* \cdot M^T \cdot (A^o - A^c) \cdot C^{oT} \cdot (C^o \cdot C^{oT})^{-1} \right\} \cdot C^o \tag{2.3.17}$$

In addition to N and M being orthogonal matrices, for the block observer realization chosen in this study, see Appendix C, the following is true

$$(C^o \cdot C^{oT})^{-1} = \left(\left[[I_r] \; [0] \right] \cdot \begin{bmatrix} [I_r] \\ [0] \end{bmatrix} \right)^{-1} = I_r \tag{2.3.18}$$

and

$$A^o - A^c = \begin{bmatrix} [\Delta_1]_{r \times r} & [0] \\ [\Delta_2]_{r \times r} & [0] \\ \cdots & \cdots \; \cdots \\ [\Delta_n]_{r \times r} & [0] \end{bmatrix}_{nr \times nr} \tag{2.3.19}$$

where

$$\Delta_i = A^c_{i1} - A^o_{i1} \qquad i = 1, 2, \ldots, n \tag{2.3.20}$$

Note that n in the above equations represents the order of the difference equations and r is the number of outputs. Using the results in Equations (2.3.18-20), the orthogonality of V matrix, and the definitions in Equations (2.3.13 and 2.3.15), Equation (2.3.17) reduces to

$$\hat{A} = A^o - M \cdot \begin{bmatrix} [I_{l_1 \times l_1}] & [0] \\ [0] & [0_{l_2 \times l_2}] \end{bmatrix}_{nr \times nr} \cdot M^T \cdot \begin{bmatrix} [\Delta_1]_{r \times r} & [0] \\ [\Delta_2]_{r \times r} & [0] \\ \cdots & \cdots \ \cdots \\ [\Delta_n]_{r \times r} & [0] \end{bmatrix}_{nr \times nr} \cdot C^{oT} \cdot C^o \quad (2.3.21)$$

where

$$C^{oT} \cdot C^o = = \begin{bmatrix} [I_r] \\ [0] \end{bmatrix} \cdot \begin{bmatrix} [I_r] & [0] \end{bmatrix} = \begin{bmatrix} [I_r] & [0] \\ [0] & [0] \end{bmatrix}_{nr \times nr} \quad (2.3.22)$$

and l_1 is the row rank of B^o or the number of the non-zero singular values of B^o with $l_2 = nr - l_1 \geq 0$. Now in the case where $l_1 = nr$, i.e B^o is of a full raw rank, together with the orthogonality of the M matrix and the result of Equation (2.3.22), Equation (2.3.21) reduces to

$$\hat{A} = A^o - \begin{bmatrix} [\Delta_1]_{r \times r} & [0] \\ [\Delta_2]_{r \times r} & [0] \\ \cdots & \cdots \ \cdots \\ [\Delta_n]_{r \times r} & [0] \end{bmatrix}_{nr \times nr} \quad (2.3.23)$$

It can be easily shown by using the definition of A^o from Appendix (C) and Equation (2.3.19), that $\hat{A} = A^c$. Therefore, the closed loop matrix A^c can be fully attained only

if B^o matrix is of a full rank. It is also obvious from Equation (2.3.21) that in the case where $l_1 < nr$ the minimum norm 2 solution will only affect and change the $l_1 \times l_1$ sub-matrix of A^o matrix, i.e incomplete attainability of the closed loop matrix.

It was shown from the previous discussion that the row rank of B^o matrix plays a major roll on the accuracy of estimating the feedback gains. Physically, the number of independent rows of B^o depends on the type of activity under study. Consider the general form of B^o matrix, in terms of system inertia, Coriolis, and gravitational matrices, given as follows

$$B^o = \begin{bmatrix} \overline{B_1} \\ \overline{B_2} \end{bmatrix} \tag{2.3.24}$$

where

$$\overline{B_1} = -(A_o^*/2) \cdot \left(\left(\nabla_\Theta f \Big|_n - (2/t_s)^2 \cdot I_r \right) \cdot B_o^* + B_o^* \right) \tag{2.3.25}$$

$$\overline{B_2} = -(A_o^*) \cdot \left(\left(\nabla_\Theta f \Big|_n - (2/t_s) \cdot \nabla_{\dot{\Theta}} f \Big|_n + (2/t_s)^2 \cdot I_r \right) \cdot B_o^* + B_o^* \right) \tag{2.3.26}$$

where A_o^*, *and*, B_o^* are given in Equations (2.2.24 and 2.2.27). The Jacobian matrices $\nabla_\Theta f$, *and*, $\nabla_{\dot{\Theta}} f$ are given in terms of system positional and velocity data in C.13 and C.14. Since $\nabla_{\dot{\Theta}} f$ is a velocity dependent matrix (see Appendix C for details), it is clear that it has more effect on the raw rank of B^o in activities that exhibit higher velocity

values, i.e ballistic.

Similar argument can also be made for the solution of Equation (2.3.9). Given that the output feedback problem is well-posed, the solution of Equation (2.3.9) can be expressed explicitly as follows

$$G = [I_m + K \cdot D^o] \cdot B^{o*} \cdot B^c \tag{2.3.27}$$

Recall from Section 2.2 that B^o and A^o are functions of the operating point matrices. Consequently, the feedback matrix [K], found from Equation (2.3.10), is also a function of the system operating points, hence the feedback structure is said to be adaptive. Thus, it is now possible to trace the feedback structure matrix as a function of the operating point. Because of the large number of the coefficients (elements), $r \cdot m$, the synthesis of these coefficients in relation to the inner-connections of the system should be carefully examined. Several possibilities of input/output connections, (see Equation (2.3.7)), will be discussed in the next Chapter.

CHAPTER THREE

AN ILLUSTRATIVE EXAMPLE

In this chapter, the proposed position feedback estimation procedure is applied to a selected human activity, squatting. A detailed discussion of the modeling aspects of the open loop system (skeletal system) is presented in Section 3.1. Issues concerning both the selection of the skeletal parameters, masses and moments of inertia, the muscle parameters, muscle static parameters and origin and insertion data are also addressed in this section. The modeling of the closed loop system is given in Section 3.2. In this section, the experimental setup together with the results of input (muscle activation, EMG) and output (segmental motion) data for the squatting test are shown. Results of the identification procedure are also given in this section. Lastly, the position feedback estimated data are shown in Section 3.3. Also given in Section 3.3 are interpretations of the data obtained from the solution of the position feedback problem. Finally, a discussion of the modeling concerns in the estimation of the output feedback matrix are presented.

3.1 Anthropomorphic Musculoskeletal Model "Open Loop"

A four segment model representing the squatting activity consists of the upper body, the thigh, the shank, and the foot. Since squatting is predominantly a sagittal plane motion, each body segment was assumed to have a single degree of freedom. Hence, the joints, ankle, knee, and hip, were modeled as single frictionless hinge joints. The anatomical locations of the joint centers were selected using the same definitions given by

Brand *et al.* (1982) and Hoy *et al.* (1990). The upper body joint location (the hip joint in the present study) was located at the center of the acetabulum. The knee joint was located at the midpoint between the medial and lateral femoral epicondyles. Finally, the ankle joint was considered to be at the midpoint between the medial and lateral malleoli. All anthropometric measurements of muscle origins and insertions given in Brand *et al.* (1982) and Hoy *et al.* (1990) are with respect to coordinate systems located at the joints' centers. Their data were directly used here without any modifications.

The planar linkage proposed assumes a left to right symmetry and is constrained by a joint located at the toes. Figure 3.1 provides a schematic stick figure of the proposed model.

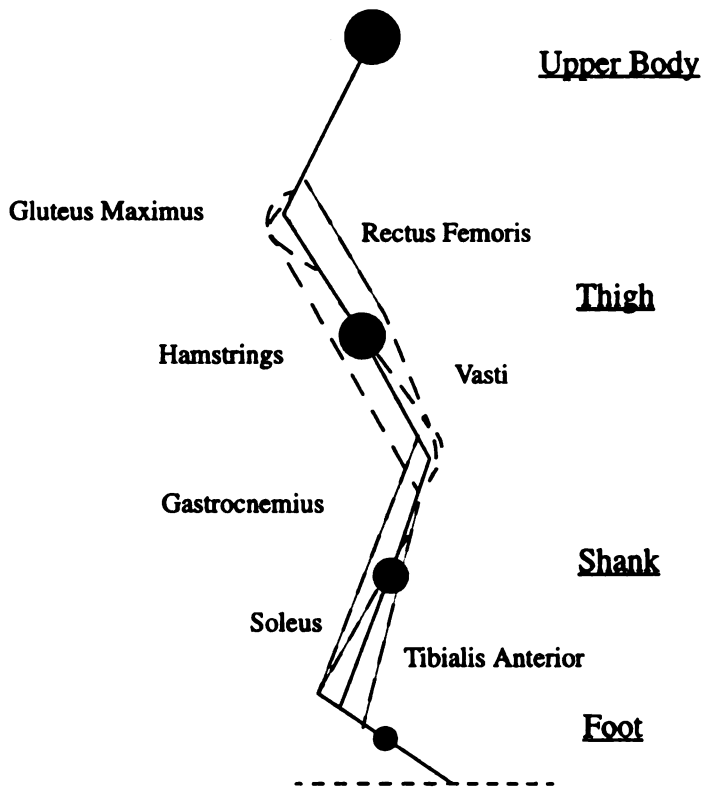

Figure 3.1.1 The sagittal plane linkage model including a set of muscles and muscle groups representing the squat activity under study

In this study, muscles with the same sagittal plane torque function, and which could not be lumped together, were considered as separate muscle groups. Since surface electromyography (SEMG) was used to measure the myosignals, we were limited to including only superficial muscles in the model. Hence, the total number of muscles and muscle groups that are the dominant muscles to control the sagittal squat model as well as being superficial was seven, see Figure 3.1.1. The muscle groups were, from proximal to distal, gluteus maximus, hamstrings, rectus femoris, vasti muscles, gastrocnemius, soleus, and tibialis anterior. Similar models were considered in the study of the postural and the vertical jump control problems by Gordon (1991), Anderson (1992) and others. To deal with muscles that have more than one insertion or origin point such as the Tibialis Anterior muscle, effective origins or insertion points were introduced to best represent the musculotendon path. That is, a curved musculotendon geometry was approximated by a set of straight line elements connecting the effective origins and effective insertions. Values of effective origins and insertions are also provided in Hoy *et al.* (1990).

The muscle static parameters were modified from those in the literature by comparing the net muscle isometric moments about a joint with experimental moment data. The outcome of such analysis affects the simulation results of Equation (2.2.9) for the evaluation of the rate of muscle force build up (c) appearing in Equation (2.2.10). Equation (2.2.10) was used to evaluate the nominal muscle force data, thus it is very important to choose the appropriate muscle static parameters to obtain an accurate nominal muscle force.

After the muscles' attachment coordinates are found, the computation of moment and moment arm values can be found using the method defined in Section 2.2. For the muscle groups shown in Figure 3.1.1, the origin insertion data are not presented here, but plots of

the isometric moments versus the joint angles will be presented later in this section. By definition, the isometric muscle moment is equal to the product of the muscle moment arm and the isometric muscle force. As an example of the moment arm calculation, consider the gastrocnemius muscle of the ankle joint. The insertion point of the gastrocnemius muscle is at the foot or in the (X_1, Y_1) coordinate system, see Figure 3.1.2. Also, its origin is at the femur or the (X_3, Y_3) coordinate system. As shown in Figure 3.1.2., the muscle spans two joints, the knee and the ankle joints, hence the (m) appearing in Equation (2.2.3) is equal to two in this case. The transformation matrix T_1 is by definition, the transformation of the (X_2, Y_2) with respect to the (X_1, Y_1) coordinate system, thus representing the ankle joint degree of freedom. Let the ankle joint angle be θ_a, then for the 2-D model shown in Figure 3.1.2, the (X_2, Y_2) to (X_1, Y_1) coordinate system transformation matrix T_1 takes the form

$$T_1 = \begin{bmatrix} \cos\theta_a & \sin\theta_a \\ -\sin\theta_a & \cos\theta_a \end{bmatrix} \tag{3.1.1}$$

Similarly, the transformation matrix of the (X_3, Y_3) to (X_2, Y_2) coordinate system is defined as T_2 which represents the knee rotational degree of freedom. For the proposed model this matrix takes the form

$$T_2 = \begin{bmatrix} \cos\theta_k & \sin\theta_k \\ -\sin\theta_k & \cos\theta_k \end{bmatrix} \tag{3.1.2}$$

The joint angles appearing in Equations (3.1.2 and 3.1.3) are related to the segmental angles shown in Figure 3.1.2 as follows

$$\theta_a = (\theta_2 - \theta_1) - \pi/2 \tag{3.1.3}$$

$$\theta_k = (\theta_2 - \theta_3) \tag{3.1.4}$$

The vector P_1 in Equation (2.2.3) is defined as the origin to origin distance from the (X_1, Y_1) to the (X_2, Y_2) coordinate systems. It is clear from the sketch in Figure 3.1.2. that $P_1 = 0$ because both origins are modeled to be located at the same point. The distance from the (X_2, Y_2) and (X_3, Y_3) origins, P_2, is equal to the shank length. The $\vec{r}_o$ and $\vec{r}_I$ vectors are the origin and insertion position vectors defined from the origins of the (X_1, Y_1) and the (X_3, Y_3) coordinate systems, respectively. Both vectors were found from the anthropometric data provided by Brand *et al.* (1981) or Hoy *et al.* (1990).

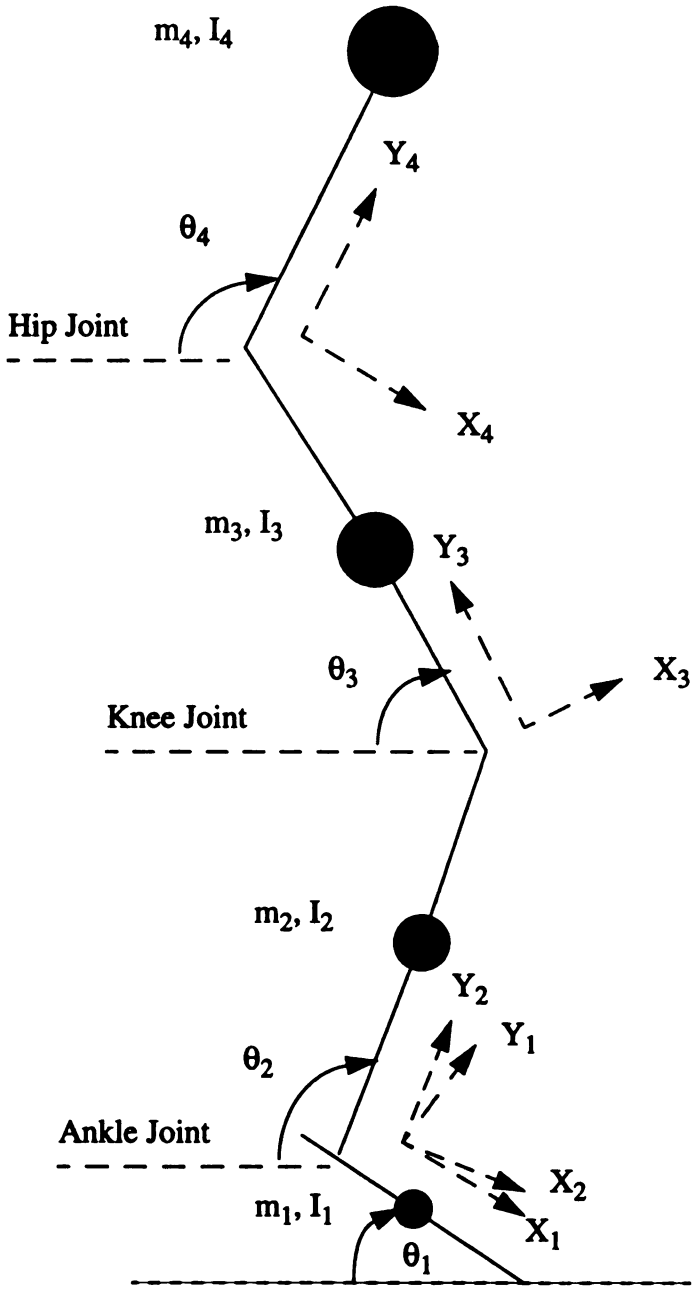

Figure 3.1.2 The sagittal plane linkage model showing the segmental coordinate systems

Hoy *et al.* (1990), developed a procedure by which the muscle isometric force can be obtained. This method reduces to a solution of a first order nonlinear algebraic equation. When the musculotendon length, L_{mt}, muscle static parameters, and muscle architecture are known, the only unknown is the internal variable defined as the muscle fiber length, L_m, see Figure 2.2.2. Since the goal of the analysis is to compute the isometric muscle force, the muscle activation is considered at its maximum, i.e $a(t) = 1$, see Section 2.1. In comparing the tendon force, p, computed first from a tendon model and then computed from the architectural configuration of the muscle, the muscle fiber length can be obtained. A linear model of the tendon was used when the muscle is in isometric contraction and is given as

$$\hat{p} = \hat{K} \cdot (\hat{L}_t - \hat{L}_s) \tag{3.1.5}$$

where $\hat{p} = p/p_o$ is the normalized tendon force, $\hat{L}_t = L_t/L_o$ is the normalized tendon length, $\hat{L}_s = L_s/L_o$ is the normalized tendon slack length and, p_o and L_o are the muscle optimal force and length given in Table 1, respectively. The non-dimensional tendon stiffness, $\hat{K}$, was assumed by Zajac (1989) and Hoy *et al.* (1990) to take the form

$$\hat{K} = 37.5/\hat{L}_s \tag{3.1.6}$$

The constant appearing in Equation (3.1.6) is related to the tendon elasticity and its peak isometric stress. More details of the variables shown in Equation (3.1.5) are in Section 2.2 and Appendix A. Using the expressions in A.1 and A.3 together with Equation (3.1.5), the normalized tendon force reduces to

$$\hat{p} = 37.5/\hat{L}_s \cdot \left(\hat{L}_{mt} - \hat{L}_s - \hat{L}_m \cdot \sqrt{1 - \left(\frac{\sin \alpha_o}{\hat{L}_m} \right)^2} \right) \tag{3.1.7}$$

where α_o is the resting muscle pennation angle given in Table 1, $\hat{L}_m = L_m/L_o$ is the unknown normalized muscle fiber length, and $\hat{L}_{mt} = L_{mt}/L_o$ is the normalized musculotendon length as defined in Equation (2.2.11). The tendon force can be computed by imposing force equilibrium on the muscle architecture shown in Figure 2.2.2. Thus, the tendon force can be also expressed as follows

$$\hat{p} = (\hat{p}_{iso}(\hat{L}_m) + \hat{p}_{pe}(\hat{L}_m)) \cdot \sqrt{1 - \left(\frac{\sin \alpha_o}{\hat{L}_m} \right)^2} \tag{3.1.8}$$

where $\hat{p}_{iso}(\hat{L}_m)$ and $\hat{p}_{pe}(\hat{L}_m)$ are the muscle stretch/isometric force relation given in Equation (2.2.8) and the muscle parallel element constitutive relation given in Equation (2.2.5), respectively. Due to the fact that, during squatting, the strain in the muscle and tendon can be large, the muscle passive (parallel) element was included in this analysis. Hoy *et al.* (1990) chose not to include the parallel elements.

The isometric tendon force was computed iteratively for every $\hat{L}_{mt}$ by finding the $\hat{L}_m$ that satisfies both Equation (3.1.8) and Equation (3.1.7). After the isometric muscle force is computed, by substituting the value of $\hat{L}_m$ in Equation (3.1.8), the muscle isometric moment can be evaluated for each positional data point by multiplying the moment arm by the isometric force. Instead of presenting the data for muscle's origins and insertions and isometric forces, plots of muscle isometric moments as a function of joint angles are presented. These plots were compared against experimental and analytical data provided in the literature (Inman *et al.*, 1980; Marsh *et al.*, 1981; Lindahl *et al* 1981; Sale *et al.*,

1982; Nemeth, 1983; Hoy *et al* 1990) to verify the use of both the muscle static parameters given in Table 1 and the muscle attachment coordinates.

Muscle Name	Optimal Force, p_o (N)	Optimal Length, L_o (m)	Pennation Angle, α_o (degrees)	Tendon Slack Length, L_s (m)
Tibialis Anterior	1500	0.070	5.00	0.1455
Soleus	3599	0.034	20.0	0.2376
Gastrocnemius	2372	0.072	12.0	0.4180
Vasti	7020	0.090	10.0	0.1264
Rectus Femoris	1344	0.082	5.00	0.3400
Hamstrings	3055	0.220	9.00	0.2100
Gluteus Maximus	1798	0.180	3.40	0.0090

Table 1: Musculotendon static properties of the muscles used in the analysis

Although measured muscle static parameters, muscle maximum isometric force, muscle fiber optimal length, tendon slack length, and muscle resting pennation angle, are available in the literature (Brand *et al.*, 1982; Hoy *et al.*, 1990; Yamagutchi *et al.* 1990; and others), the parameters of some of the muscles used in the present study were modified. The adjustments were made such that the sum of the computed isometric muscle forces at a joint are within 10% of the reported experimental isometric joint's moments (Inman *et al.*, 1980; Marsh *et al.*, 1981; Lindahl *et al* 1981; Sale *et al.*, 1982; Nemeth, 1983; Hoy *et al* 1990). An exact match between the reported experimental data and the simulation results obtained in this study is impossible due to discrepancies in both the

angle definitions and joint locations between both studies. For example, the ankle plantar flexion moments given in Figure 3.1.3. show that data points measured by Sale *et al.* (1982) are in a agreement with the computed moments in plantar and low dorsi flexion ankle angles. However, differences were seen at high dorsi flexion angles. This may be attributed to the location of the joint center definition which was not explicitly defined in the work of Sale *et al.* (1982). Similar observations had been reported in Yamaguchi (1989) and Hoy *et al.* (1990). Differences between experimental and simulated data may also be attributed to the fact that the present study includes only the superficial muscles where the electrical activity is experimentally easy to obtain. However, experimental data of joint moments include all muscles contributing to the isometric moments at the joint. Figure 3.1.4 illustrates the ankle doris flexion moment reported by Marsh *et al.* (1981) compared to the simulated Tibialis Anterior muscle's isometric moment about the ankle joint. Figure 3.1.4, the largest differential between experimental and analytical data occurs when the ankle is plantar flexed. In this study, the simulated data of the Tibialis Anterior muscle will represent the action of all the ankle dorsi flexors.

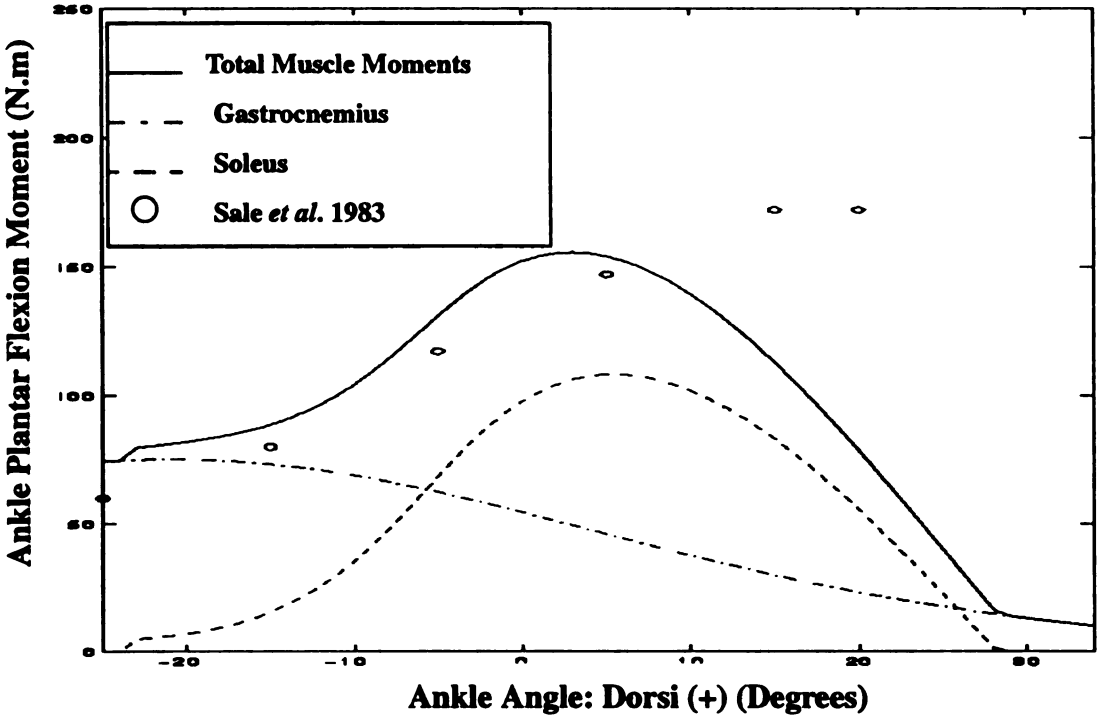

Figure 3.1.3. Maximum isometric ankle plantar flexion moments, with knee in full extension.

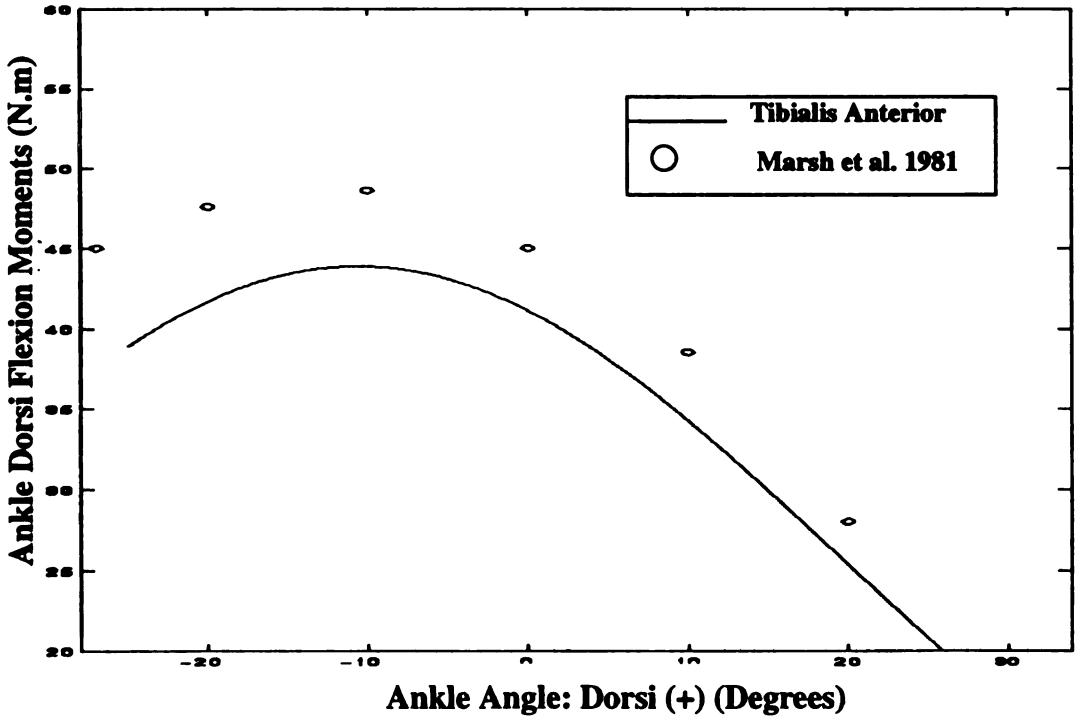

Figure 3.1.4. Maximum isometric ankle dorsi flexion moments

The contribution of the individual muscles to the summed muscle isometric extensor moments at the knee is shown in Figure 3.1.5. As shown in the figure the simulated total extensor moments were very similar to the experimental data reported by Lindahle *et al.* (1981). At knee flexion angle of about 60 degrees the rectus femoris isometric moment is about 20% of the vasti isometric moment, which is consistent with data reported by Hoy *et al.* (1990). Experimental data of the knee isometric flexion moments reported in Inman *et al.* (1980) together with the summed muscle isometric flexion moments are shown in Figure 3.1.6.

Experimentally, Inman *et al.* (1980) measured the resisting moments of the hamstring muscles by applying an external load on the shank. Thus, the gastrocnemius muscle was not included or loaded during the experiment, and the experimental data is only comparable to the simulated hamstrings moments as shown in Figure 3.1.6.

Isometric hip extensor moments together with the experimental data reported by Nemath *et al* 1983 are plotted in Figure 3.1.7. It is important to note that in the work of Nemeth *et al.* (1983), the hip joint angles were not defined with respect to anatomical bony landmarks, hence it is the range not the trend of the hip moments, shown in Figure 3.1.7 that is the subject of comparison between the experiments of Nemeth *et al.* (1983) and analytical data obtained in the this study. The rectus femoris muscle was considered as the hip flexor muscle because the other hip flexors' electrical activity was hard to obtain using surface EMG. The simulated rectus femoris isometric hip moment computed here is compared to the Rectus hip moment modeled in Hoy *et al.* (1990) as shown in Figure 3.1.8.

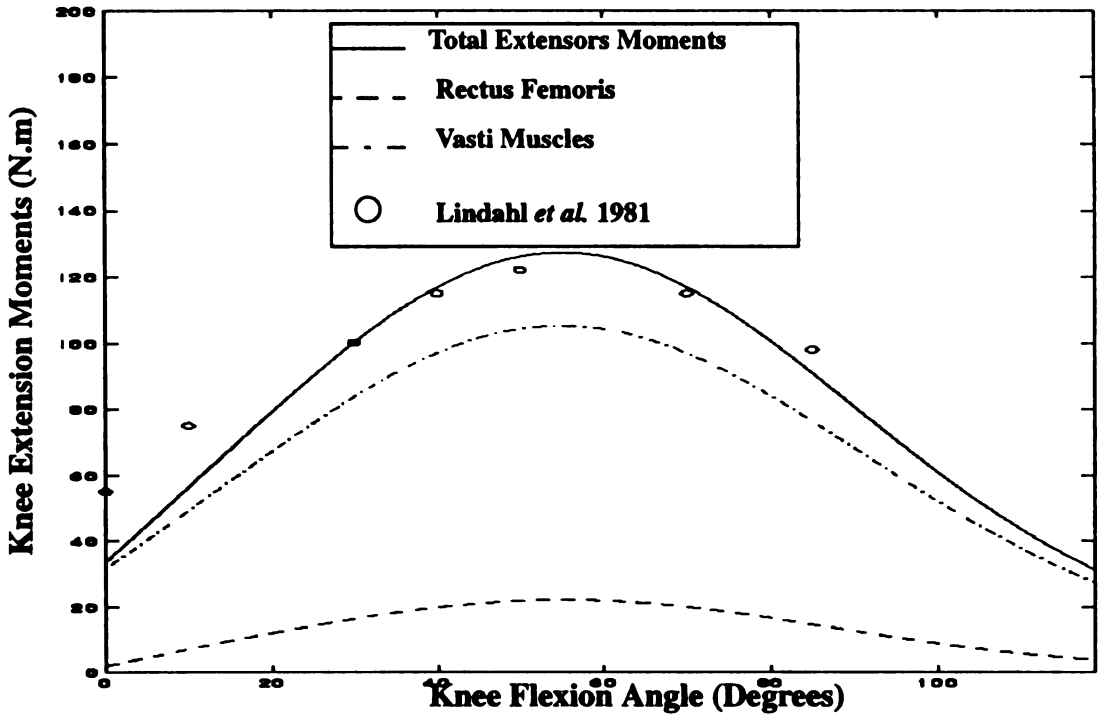

Figure 3.1.5. Maximum isometric knee extension moments, with hip in full extension.

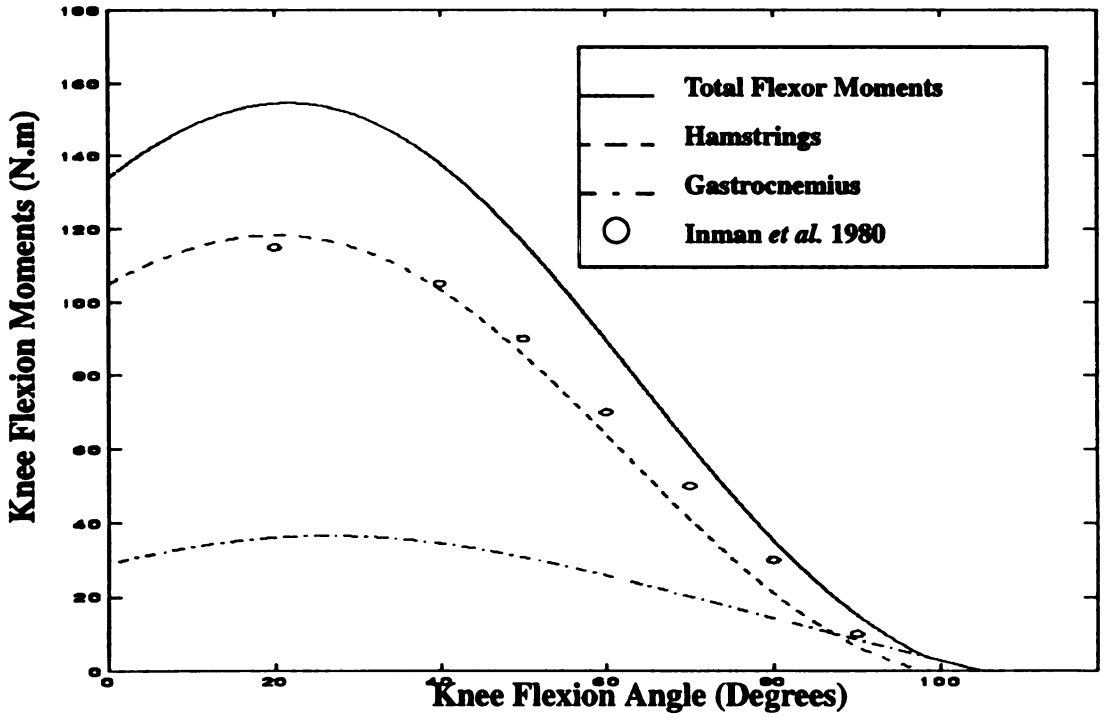

Figure 3.1.6. Maximum isometric knee flexion moments, with hip in full extension.

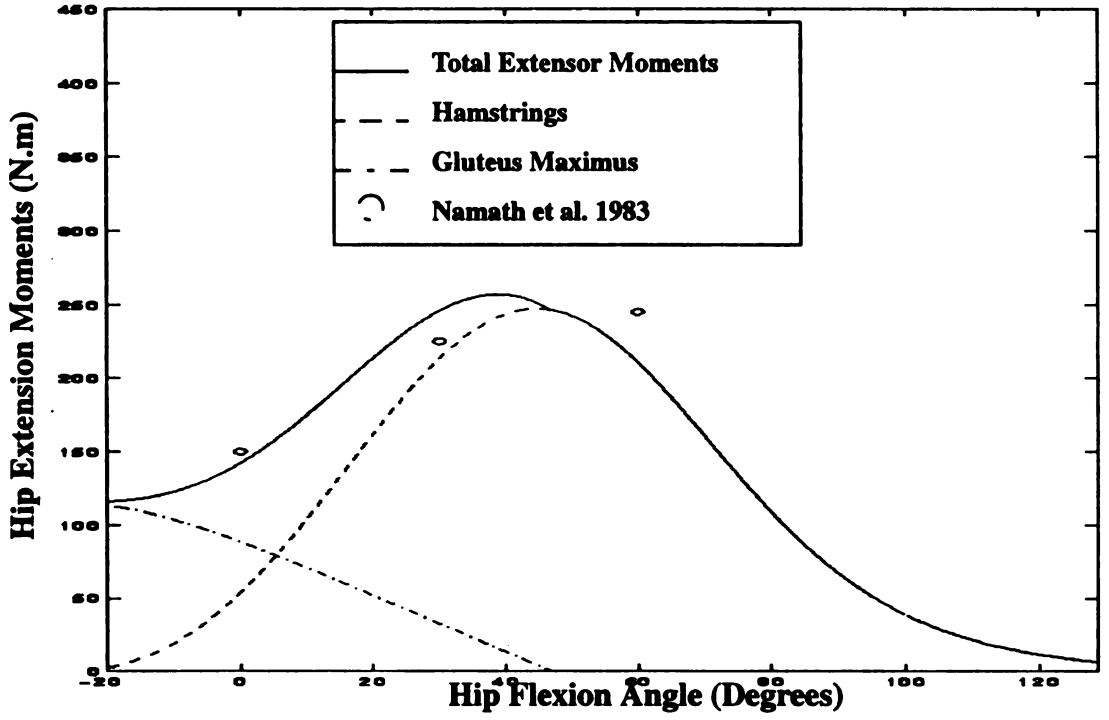

Figure 3.1.7. Maximum isometric hip extension moments, with knee in full extension.

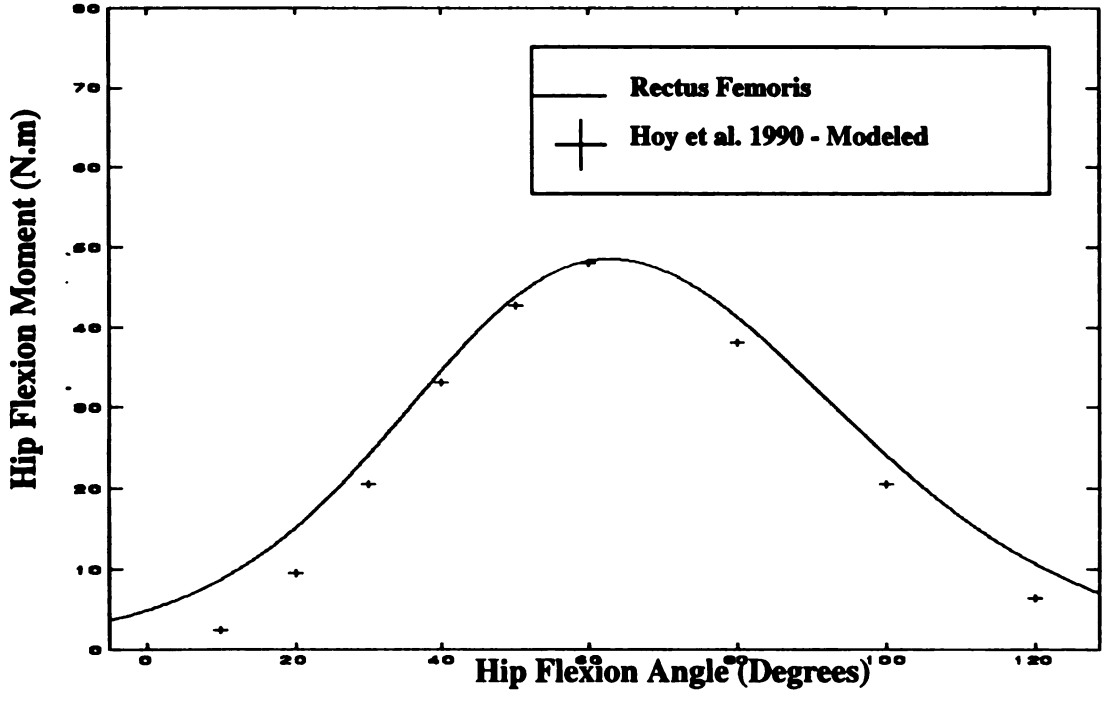

Figure 3.1.8. Maximum isometric flexor moment of the rectus femoris muscle about the hip joint, with knee in full extension.

The dynamic equations of motion for the model shown in Figure 3.1.3 were derived using the Lagrangian formulation discussed in Section 2.2.3. Following the notation given in Equation (2.2.13), the matrix form of the equations of motion is

$$J(\Theta) \cdot \ddot{\Theta} = B(\Theta) \cdot \dot{\Theta}^2 + C(\Theta) + D \cdot M(\Theta_J) \cdot P \qquad (3.1.9)$$

where Θ is the vector of segmental angles (output), $\Theta \in R^4$, Θ_J is the vector of joint angles (inter-segmental angles), $\Theta_J \in R^3$, P is the vector of muscle forces listed in the same sequence as they appear in Table 1, $P \in R^7$, $J(\Theta)$ is the inertia matrix, $B(\Theta)\,\Theta^2$ is a vector describing both Coriolis and centripetal effects with $\dot{\Theta}^T = \left[\dot{\theta}_1\ \dot{\theta}_2\ \dot{\theta}_3\ \dot{\theta}_4\right]^T$, D is a (4×7) matrix that transforms the joint moments into segmental moments, and $M(\Theta_J)$ is the moment arm matrix computed using Equation (2.2.3). Details of Equation (3.1.9) are given in Appendix (C). Also appearing in the appendix are explicit representations of the Jacobian matrices, defined in Equation (2.2.16), for the system equation of motion, Equation (3.1.9). Finally, the open loop input/output equation is obtained by substituting Equations (C.7), (C.15), and (C.16) in Equations (2.2.14-16).

3.2 Closed Loop Model

3.2.1 Experimental Setup

In this section, a detailed discussion is presented of the experimental setup to measure segmental angles (system outputs) and to measure muscular activity (system input) on a human subject performing a squat activity. After completion of informed consent (IRB 93 - 580), a healthy 23 years old female subject was asked to perform at least two squat cycles per trial. While performing the squat activity, the arms were crossed in front of the

upper body and were not considered as separate linkages. Given the subject's height and mass, every body segment mass and center of gravity location was computed based on anthropometric ratios given in Seireg and Arviker (1989). Moments of inertia were computed based on the data provided by Dempster (1955). Table 2 lists the body-segments parameters for the subject performing the squat activity. The parameters appearing in Table 2 are defined in Appendix C at the end of this thesis.

Body Segment	m_i (kg)	L_{ci} (m)	L_i (m)	I_i (Kg m^2)
Foot	1.599	0.116	0.254	0.011
Shank	7.760	0.270	0.477	0.080
Thigh	13.340	0.232	0.410	0.118
Upper Body	49.616	0.392	0.392	7.779

Table 2: The body-segmental parameters used for the skeletal model

To measure segmental angles, three retro-reflective markers were placed on the foot, the shank, the thigh, and the thorax. Palpable landmarks on these segments were chosen as locations of the three markers and were attached to the skin with hypoallergenic double-sided tape. Two of the markers were placed such that an anatomical body axis can be mathematically constructed. The anatomical targets used to form the anatomical axis for each body segment were from proximal to distal, T_1 and T_{10} on the thorax, medial and lateral femoral epicondyles at the thigh, proximal and distal shank targets at the anterior crest of the tibial bone, and finally the medial and lateral rear foot on the foot. The third target was placed in the same anatomical plane non-collinear with the other two. Figure 3.2.1. illustrates the targeting scheme used on the shank body segment. Four 100 Hz infra-

red video cameras were placed such that a calibrated space of 170 cm high, 120 cm length, and 100 cm width was within the visual field of every camera. The definition of the laboratory coordinate system and the calibration space are shown in Figure 3.2.1. The data acquisition tracking of the targets was done using a Bioengineering Technology and System (BTS) Elite system. The trajectories were filtered using a third order Butterworth low-pass filter.

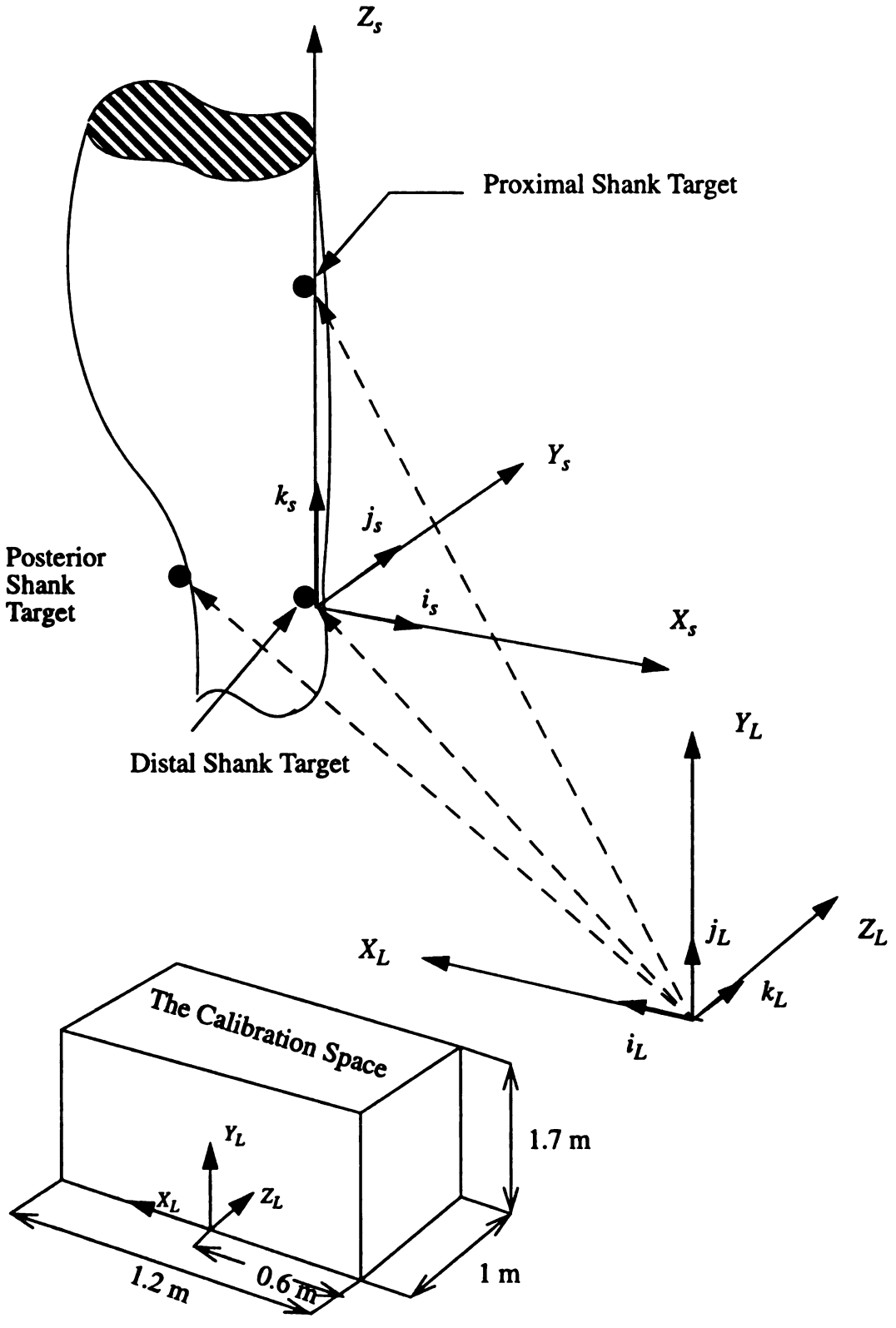

Figure 3.2.1. An illustrative sketch of the targeting scheme used in the present study on the shank and the location of the laboratory coordinate system in the calibration space

The muscle activity was measured using bipolar surface electrodes with on-site pre-amplification. To insure maximum detectability, the electrodes were located approximately at the muscle motor point. The motor points for the muscles used in this study were obtained from data provided in Griffin *et al.*, (1982, Appendix A and B), where the motor points were defined with respect to segmental dimensions. The 8 mm diameter silver electrodes were located on the approximate location of the muscle motor points with an inter-electrode fixed distance of 25 mm center to center. The distance chosen here was recommended in the work of Fuglevand et al. (1992), where both experimental and analytical models of bipolar electrode detectability was discussed as a function of both electrode size and inter-distance. A larger distance reduces the bipolar electrode detection strength, since, as discussed in Zipp (1978), the increase of the inter-electrode spacing distance reduces the band width of the electrode's transfer function affecting the rejection of important underlying electrical frequencies. For the agonist muscles, the rectus femoris and the vasti muscles, the distance between the electrodes was chosen to be greater than 80 mm to insure minimal cross-talk (see Winter et al., 1993).

After establishing the site of the electrode placement, the skin was shaved if necessary, prepared with alcohol, and dried. Double adhesive-backed tape was used to attach the electrodes to the skin. A small eight-channel junction box was strapped to the subject's back. A fiber optic wire was used to transmit the signal to a receiver with a sampling rate of 1000 Hz. The signal was then filtered using a band-pass Butterworth filter having a frequency band of 5-200 Hz.

3.2.2 Experimental Results

Using the measured targets' trajectories, segmental (fixed to segment) coordinate sys-

tems were computed for each sample time. As an illustration of the calculation, consider the shank segment shown in Figure 3.2.1. The segmental anatomical axis was chosen to be the axis running between the distal and proximal shank targets, Z_s. The unit vector corresponding to the anatomical axis is given as

$$\hat{k}_s = \frac{\overrightarrow{Proximal\ Shank} - \overrightarrow{Distal\ Shank}}{\left|\overrightarrow{Proximal\ Shank} - \overrightarrow{Distal\ Shank}\right|} \tag{3.2.16}$$

Let $\hat{i}_g$ be a unit vector in the segmental sagittal plane defined as

$$\hat{i}_g = \frac{\overrightarrow{Posterior\ Shank} - \overrightarrow{Distal\ Shank}}{\left|\overrightarrow{Posterior\ Shank} - \overrightarrow{Distal\ Shank}\right|} \tag{3.2.17}$$

Then the other unit vectors corresponding to the shank coordinate system (X_s, Y_s, Z_s) are computed from

$$\hat{j}_s = \frac{\hat{i}_g \times \hat{k}_s}{\left|\hat{i}_g \times \hat{k}_s\right|} \tag{3.2.18}$$

and

$$\hat{i}_s = \hat{j}_s \times \hat{k}_s \tag{3.2.19}$$

The location of each target used in the analysis is measured with respect to the laboratory coordinate system (X_L, Y_L, Z_L) see Figure 3.2.1 and the three unit vectors define the coordinate transformation from the laboratory to the shank coordinate systems. It should be noted that for all the body segments modeled in this study, the segmental coordinate system was chosen to be such that the *Z*-axis is superior, the *X*-axis is anterior and the *Y*-axis is taken to form a right handed coordinate system. The segmental angles θ_i were calculated using the joint coordinate method defined first by the work of Grood and Sun-

tag (1983). The construction of the joint coordinate system is based on the fact that the rotational kinematics of a body in a general three dimensional motion can be represented in terms of three consecutive rotations (Euler, 1748). As described in Grood and Suntag (1983), the key to the method is to choose one axis from one body segment and the other axis from the other segment (the laboratory in this case). The third axis is perpendicular to the other two axes, commonly known as the floating axis or the line of nodes. The segmental X-axis was chosen to be the first axis and the *Y*-axis of the laboratory as the second joint axis. For the shank segment, shown in Figure 3.2.1, the construction of the joint coordinate system is shown in Figure 3.2.2.

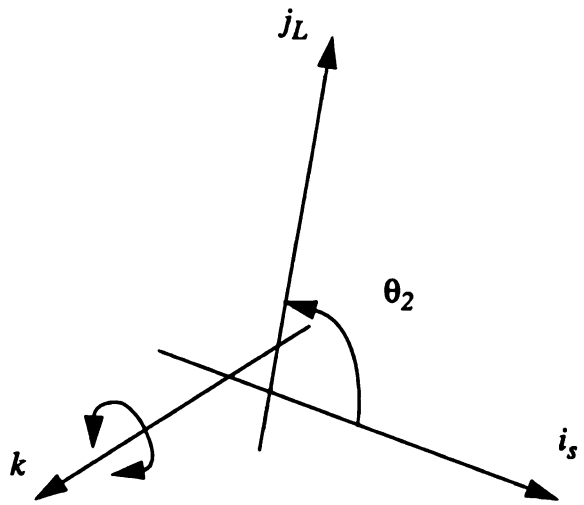

Figure 3.2.2. The joint coordinate system of the shank body segment

Where the $\hat{k}$-direction is commonly known as the floating axis and is computed as

$$\hat{k} = \frac{\hat{i}_s \times \hat{j}_L}{\left|\hat{i}_s \times \hat{j}_L\right|} \tag{3.2.20}$$

The rotation about the $\hat{k}$-axis defines the angle in the $(\hat{j}_L,\hat{i}_s)$ plane defined as the shank angle θ_2. The angle θ_2 is then computed from the following

$$\theta_2 = \pi/2 - \sin^{-1}(\hat{i}_s \bullet \hat{j}_L) \tag{3.2.21}$$

Similarly all the other angles were computed for more than two squat cycles and are shown in Figure 3.2.3. The angles plotted are the same angles defined in Figure 3.1.2, hence the thigh angle θ_3 at full extension takes a value of 90^o as shown in the figure.

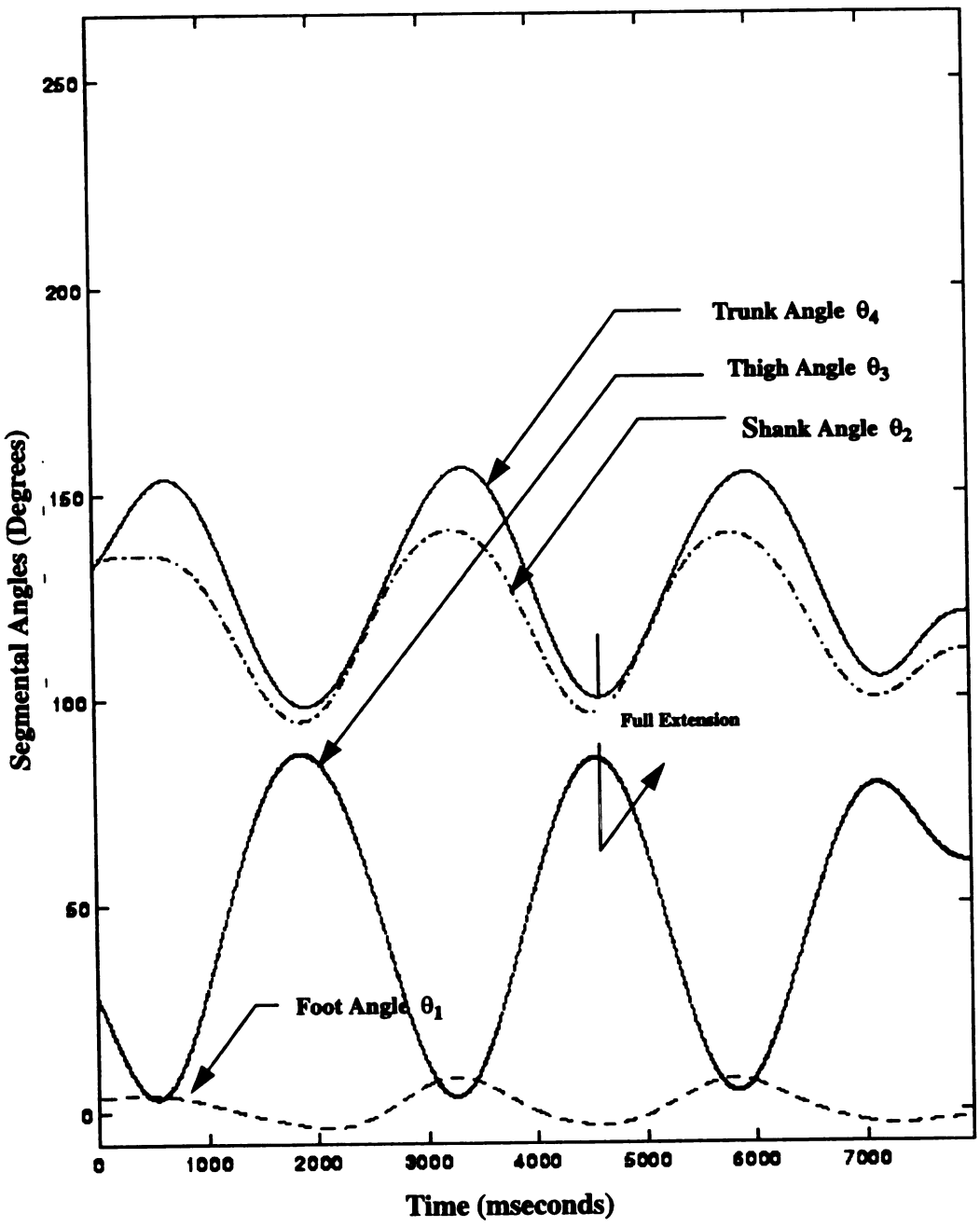

Figure 3.2.3. Segmental angles

The muscle activation curve (system input) was computed using the procedure discussed in Section 2.1. The measured electromyographic signal was rectified, modulated and then normalized to represent the muscle activation dynamics. Figures 3.2.4-7 show the processed experimental muscle activity for the group of muscles included in the present work, see Table 1.

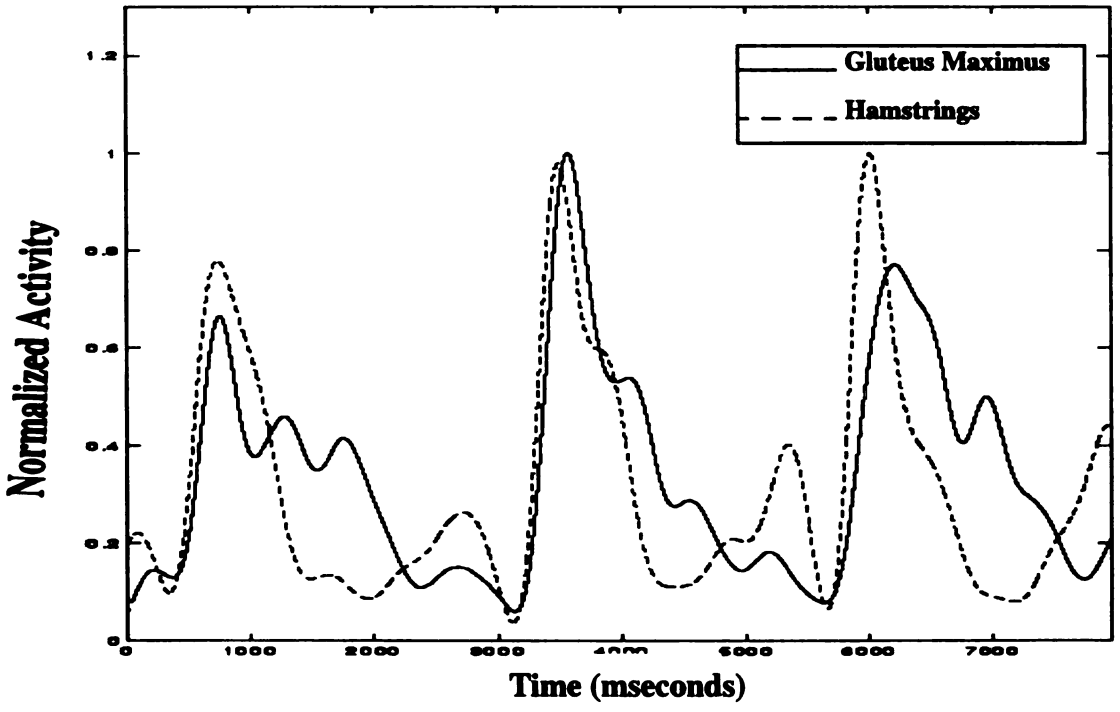

Figure 3.2.4. Muscle activity plots of hamstrings and gluteus maximus for three squat cycles

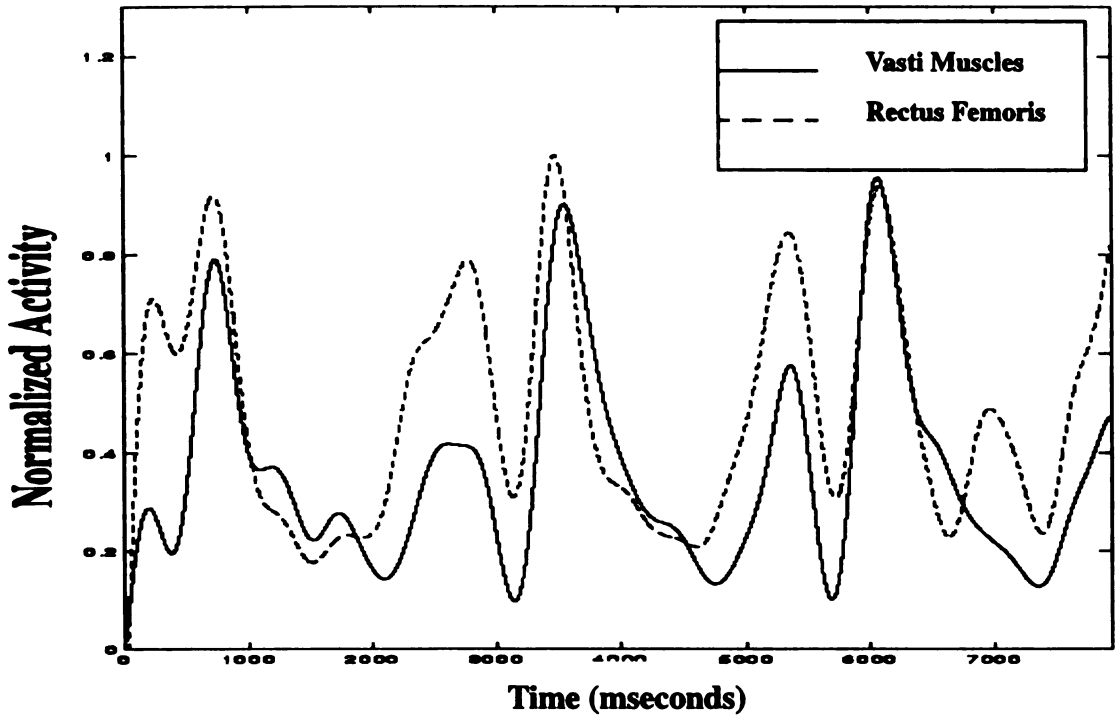

Figure 3.2.5 Muscle activity plots of rectus femoris and the vasti muscles for three squat cycles

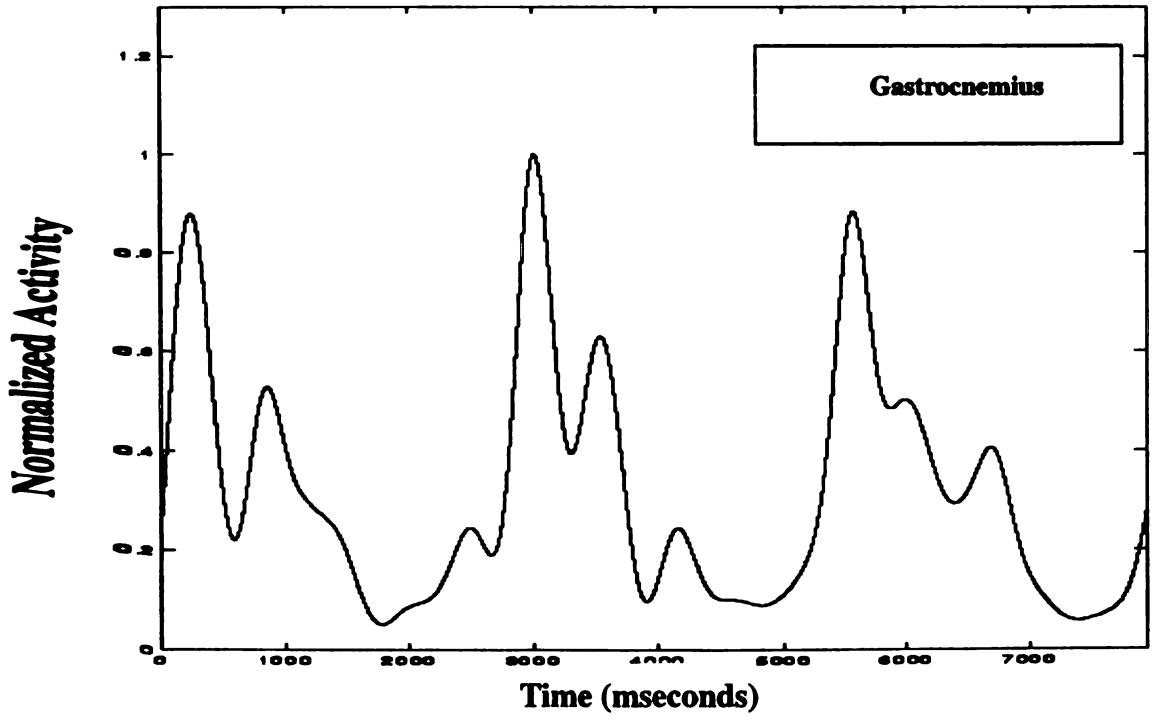

Figure 3.2.6. Muscle activity plots of the gastrocenimus muscle for three squat cycles

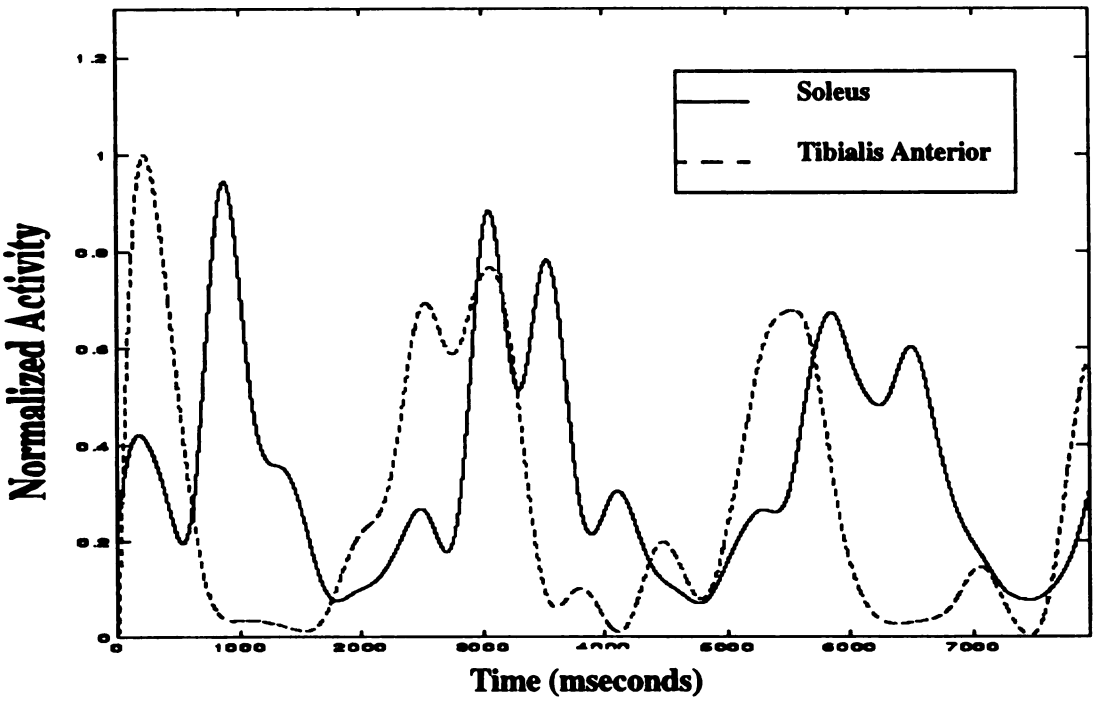

Figure 3.2.7. Muscle activity plots of the soleus and the tibialis anterior muscles for three squat cycles

3.2.3 Autoregressive Closed Loop Estimation

In this section the results of the identification of the closed loop system are given. Following the procedure discussed in Section 2.1, an Autoregressive (ARX) squatting model was constructed by utilizing the input/output data shown in Figures 3.2.4-7 and 3.2.3. To achieve a robust estimation, a static optimization procedure was constructed. The initial guesses of the parameters were chosen such that the closed loop state space model (Equations 2.3.1-2) is stable, i.e the eigenvalues lie in the unit circle (Strejc, 1981). This assumption is consistent with the fact that the observed experimental data represent a real subject. It should be clear that this static optimization procedure is independent of the physical system itself but is dependent on the state space model chosen to describe it.

Thus, the method proposed was used initially to get a stable starting point for the predictive error estimation procedure.

The estimated closed loop model, Equation (2.3.1), was then simulated using the measured muscle signals as inputs and the outputs of the simulation were compared to the measured segmental data as shown in Figure 3.2.8. A collective effect of all the estimated angles are also presented on the four degrees of freedom stick model shown in Figure 3.2.9. In both figures the solid lines represent the measured data while the dashed lines represent the simulated results. A small time shift between the measured and simulated data during the first squat cycle (compare the dashed and solid lines of the stick figures of Figure 3.2.9) is noted. This time shift did not occur during the second squat cycle. The variable time shift is attributed to the fact that the identification used in this study was of an off-line non-recursive nature. One approach to eliminate this problem is to use an on-line recursive identification procedure to estimate the system model. However, the availability of computer codes for on-line recursive identifier for a large MIMO ARX does not currently exist. Thus, the results of the identification procedure given in this section are considered sufficient in the sense of minimizing a robust estimated error criterion (Ljung, 1988).

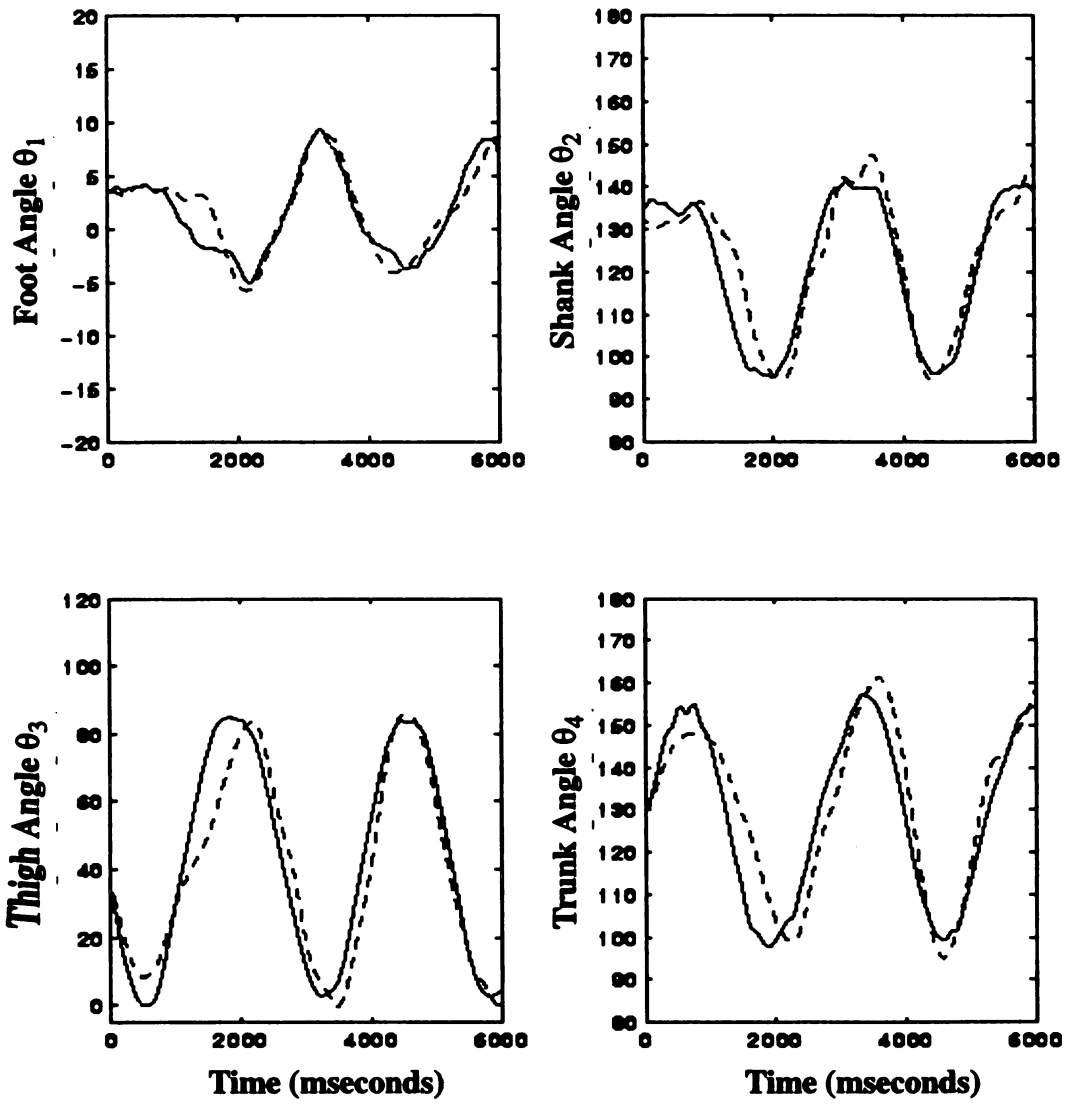

Figure 3.2.8. Measured segmental angles (solid lines) and simulated results according to the MIMO ARX model (dashed lines)

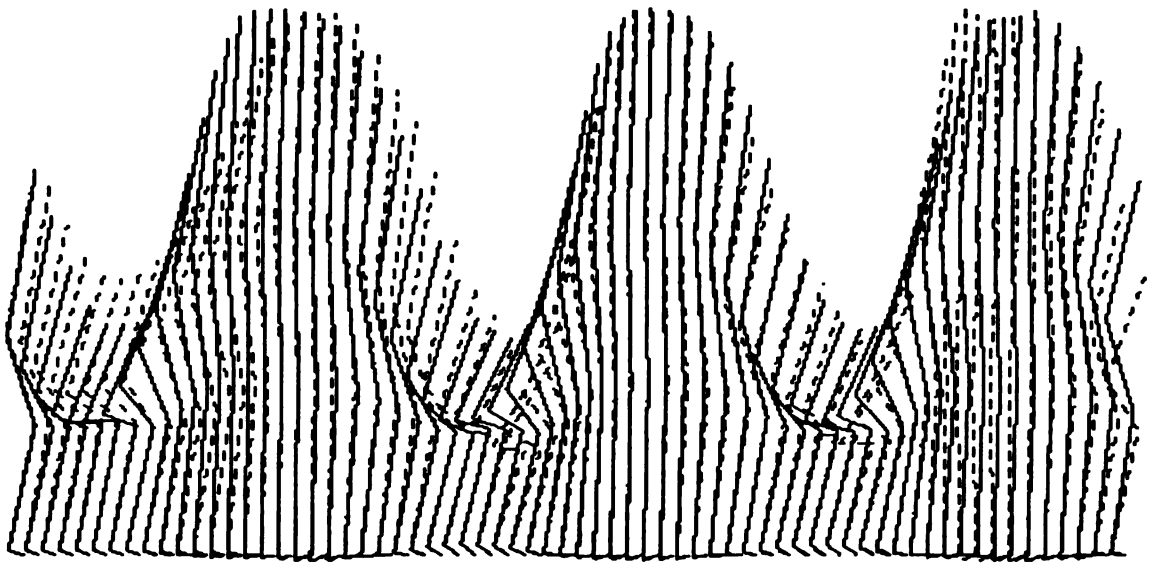

Figure 3.2.9. Stick figures of the four degrees of freedom rigid body segment in squat activity. The solid lines are the measured motion data, the dashed lines are simulated data.

3.3 Position Feedback Solution

3.3.1 Validity of the Solution of the Position Feedback Problem

Recall that the position feedback matrix [K] was computed based on a minimum norm 2 approximation criterion, see Equations (2.3.10 and 2.3.11). The approximate solution of the matrix [K] is found from the solution of Equation (2.3.10) as follows, see Section 2.3,

$$K = I_m \cdot \hat{B} \cdot [I_r - D^o \cdot \hat{B}]^{-1} \tag{2.3.10}$$

To test the validity of the above solution let us first reconstruct Equation (2.3.7) by substituting back the values of [K] computed above in Equation (2.3.7) as follows

$$\underline{X}(k+1) = \left\{A^o - B^o \cdot [I_m + K \cdot D^o]^{-1} \cdot K \cdot C^o\right\} \cdot \underline{X}(k) +$$

$$\left\{B^o \cdot [I_m + K \cdot D^o]^{-1} \cdot G\right\} \cdot U(k) \tag{3.3.1}$$

where $\underline{X}(k)$ is defined as the reconstructed state vector computed at a step k when using the solution of Equation(2.3.10) for the matrix [K]. Theoretically, for Equation (3.3.11) to represent the closed loop system defined in Equation (2.3.1), the terms $A^o - B^o \cdot [I_m + K \cdot D^o]^{-1} \cdot K \cdot C^o$ and $\left\{B^o \cdot [I_m + K \cdot D^o]^{-1} \cdot G\right\}$ should be equal to A^c and B^c, respectively. However, the above statement is only true when the B^o matrix is of a full raw rank, see Section 2.3 for details. The reconstructed state Equation (3.3.1) and the closed loop state Equation (2.3.1) were simulated using the same set of inputs and initial conditions and were compared as a validation of the estimation of the position feedback matrix [K]. The validation procedure is presented in Figure 3.3.1.

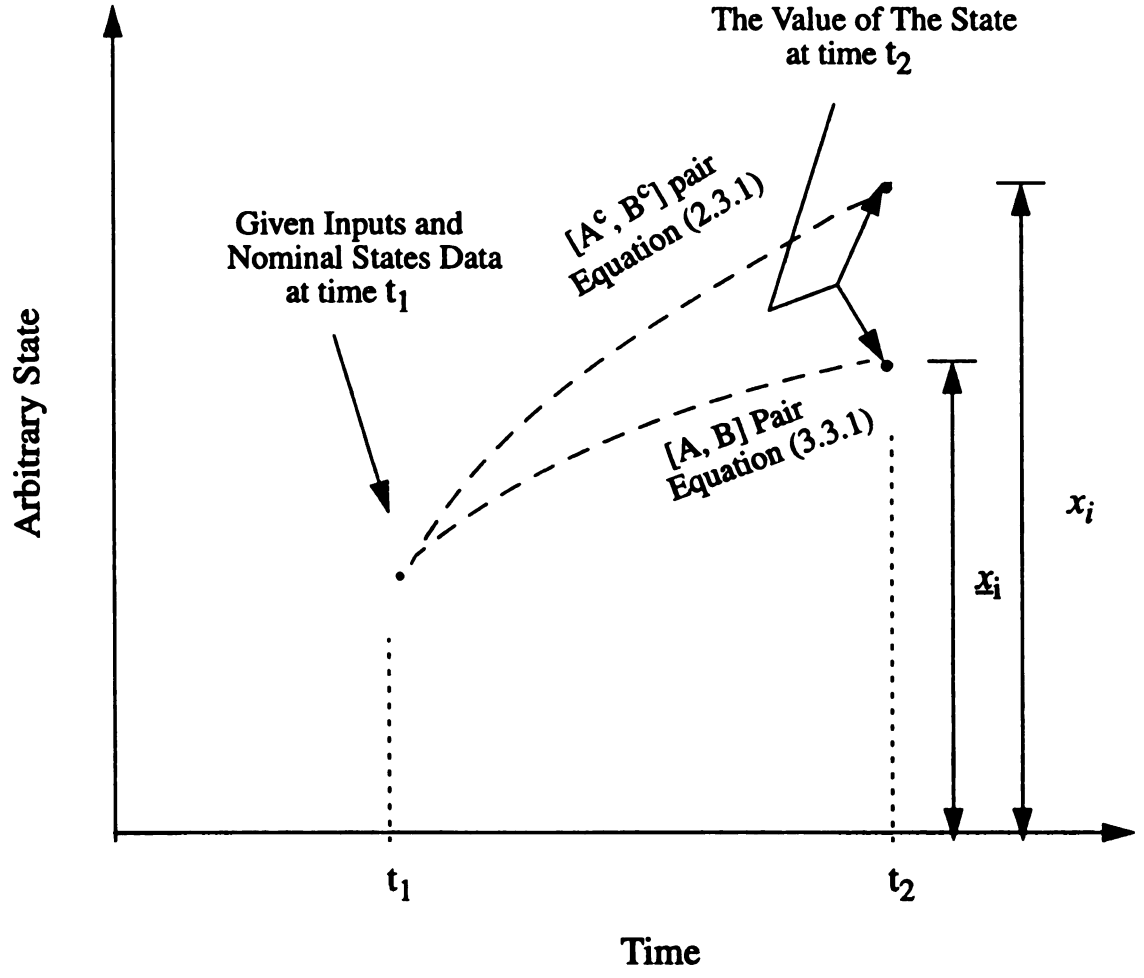

Figure 3.3.1. Schematic representation of the validation procedure

Let $\hat{x}_i(k)$ represent an arbitrary state computed from the simulation of Equation (3.3.1) and let $x_i(k)$ represent the corresponding state computed from the simulated closed loop system of Equation (2.3.1). The percentage relative error in computing the reconstructed state $\hat{x}_i(k)$ is defined as

$$Relative\ Percentage\ Error = \frac{\hat{x}_i(k) - x_i(k)}{x_i(k)} \times 100 \qquad (3.3.2)$$

Both $x_i(k)$ and $\underline{x}_i(k)$ are functions of operating points, thus the relative percentage error is also dependent on the operating point. As an example, the relative percentage error for two of the states, the trunk and shank angles, are plotted in Figures 3.3.2 and 3.3.3, respectively. From the figures, the percentage error in both the shank and trunk angle computations range from zero percent to less than 10%. The maximum error of about 9% in the shank angle simulation was observed to occur at 200 milliseconds, as shown in Figure 3.3.2. Small as it is, this maximum value occurs only for 50 milliseconds and the error then drops back to its lower value of about 2-3%. The 9% error corresponds to about 8 degrees error at a point where the actual shank angle is around 100 degrees, see Figure 3.2.3. This maximum range of error falls within the standard deviation across trails in a normal subject's squat activity (Bemis, 1992). The same conclusions can also be made for the trunk angle. As it was stated in section 2.3, the source of the error is the fact the for the simulated squat activity, the row rank of B^o was not full.

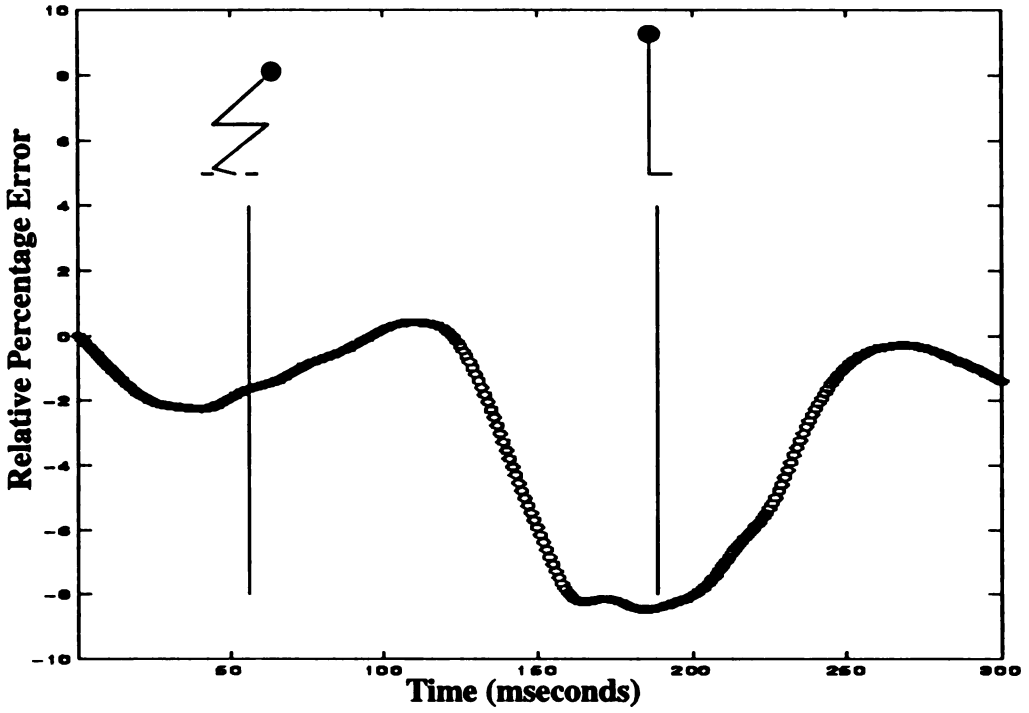

Figure 3.3.2. Relative percentage error plot for the computation of the shank angle.

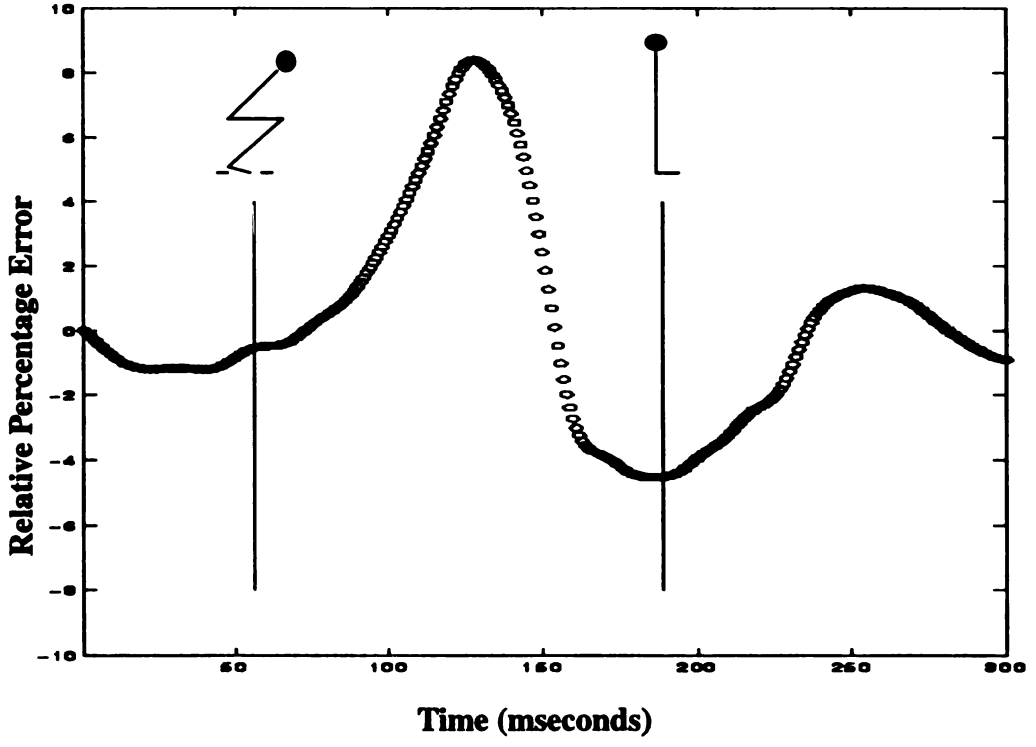

Figure 3.3.3. Relative percentage error plot for the computation of the trunk angle.

3.3.2. Interpretation of Some of the Position Feedback Elements

Since the $\hat{B}$ appearing on the right hand side of Equation (2.3.10) is a function of the system operating points, defined by a set of nominal muscle forces and motion trajectories, the matrix [K] computed using Equation (2.3.10) is also a function of the operating points. Thus for the present application, the *7 x 4* elements of matrix [*K*], *4*-outputs and *7*-inputs, are expected to change as the operating points change. The matrix [*K*] was defined in Equation (2.3.11)

$$P(k) = G \cdot U(k) - K \cdot q(k) \tag{2.3.11}$$

represents the contribution of the output vector $q(k)$ to the muscle force vector $P(k)$. In other words, the element $(-k_{ij})$, for the present example $i = 1, 2, \ldots, 7$ and $j = 1, \ldots, 4$, of the matrix [-*K*] represents the feedback gain relating the j^{th} output of the system, θ_j, to the i^{th} input, p_i. For example, the first row of the [-*K*] matrix, $(-k_{1j})$ $j = 1, \ldots, 4$, represents the feedback gains or components from the segmental angles $\theta_1, \theta_2, \theta_3, and\ \theta_4$ to the tibialis anterior muscle force. A positive value of the $(-k_{ij})$ element implies a positive contribution of the j^{th} motion on the force produced in the i^{th} muscle, see Equation (2.3.11). In other words, the joint motion is demanding more muscle force for the proposed open loop system behavior to track that of the identified closed loop structure. Conversely, a negative value of the $(-k_{ij})$ element indicates that a particular motion is requiring less force generation. These element can be represented in terms of feedback gains relating joint angles to muscle forces since joint and segmental angles are analytically related, see Appendix C.

To demonstrate the adaptability of the elements of the feedback matrix [K] to the changes in operating points, consider the one squat cycle shown in Figures 3.3.4a and 3.3.4b. The figures show the joint angles and the associated stick figure for one squat cycle. As an illustration only, consider the feedback coefficients mapping the three joint angles, ankle, knee, and hip, to the tibialis anterior muscle, as shown in Figure 3.3.5. It is clear that the feedback gains are not constant throughout the range of time considered. The values of the coefficients change depending on the configuration, the configurational speed, and the muscle nominal forces in the system. It is well known that structurally the tibialis anterior muscle is of no relation to either the knee or the hip joints, however Figure 3.3.5 clearly shows the motion of this joint is related to the force developed in the tibialis anterior muscle. This observation is consistent with the hypothesis that states that all the muscles involved in a particular activity are related somehow through a global feedback structure. This phenomenon is also clear when considering the feedback gain plots from the knee and hip joints to the soleus muscle and the ankle and hip joints to the vastus muscle as seen in Figures 3.3.6 and 3.3.7, respectively. The positive or negative contribution of these motions, positive and negative contribution is simply related to the sign of the $(-k_{ij})$ element, are dependent on the operating point.

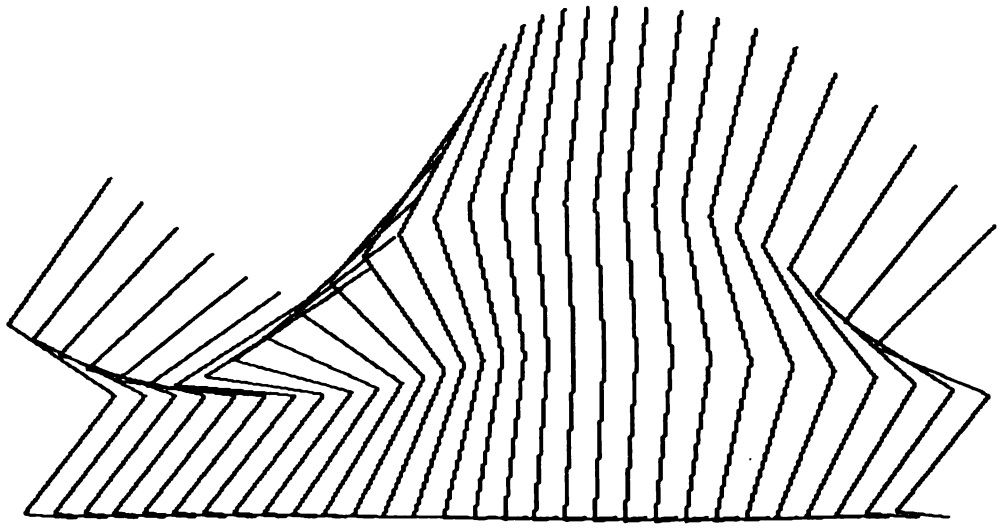

(b)

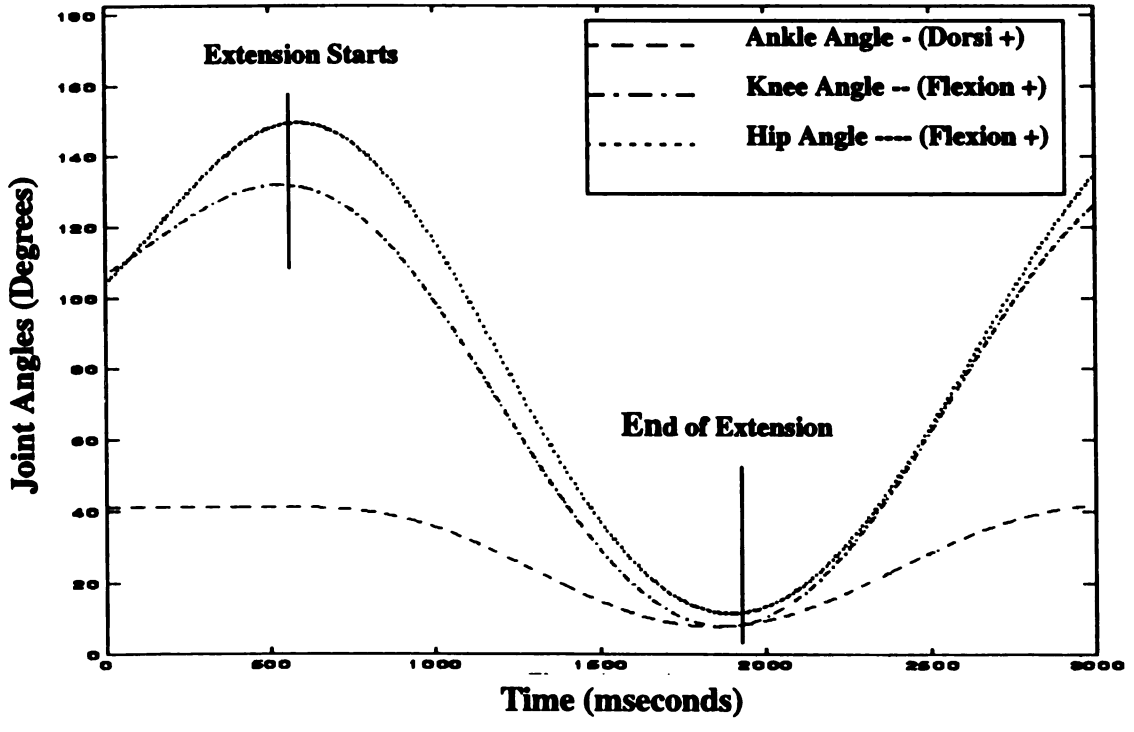

(a)

Figure 3.3.4. The stick figure and the associated joint motions for the one squat cycle.

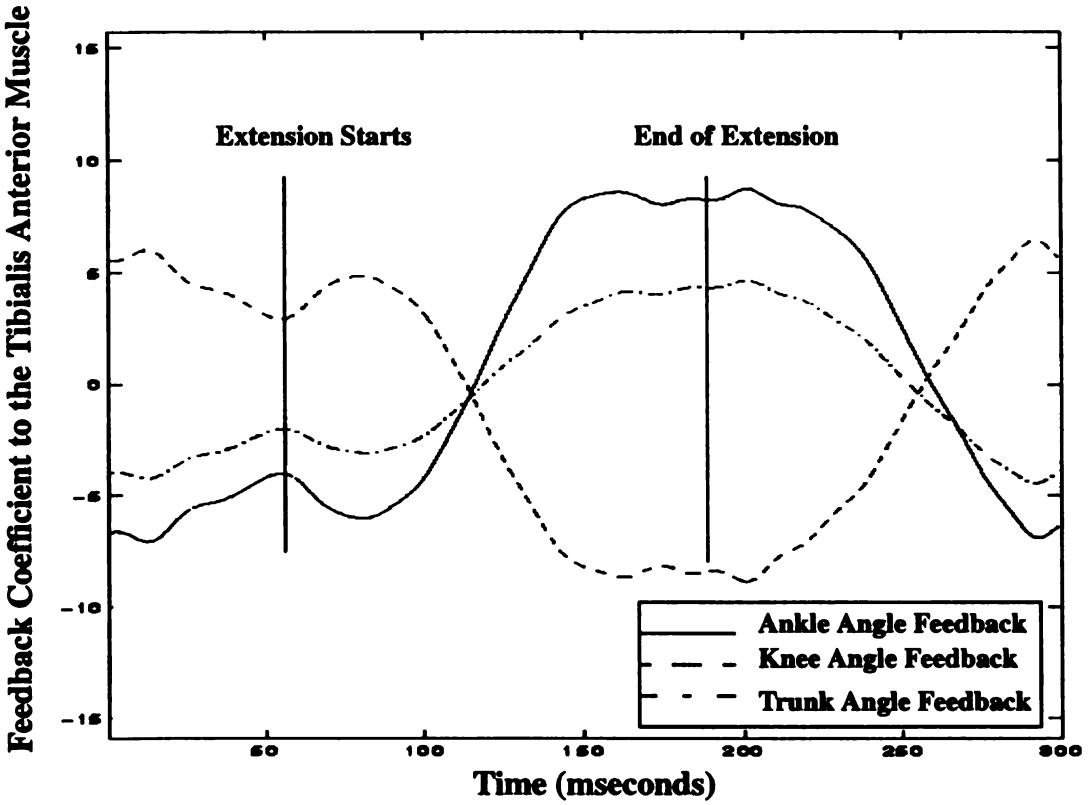

Figure 3.3.5 Feedback gain plot from the ankle, knee, and hip motions to the tibialis anterior muscle.

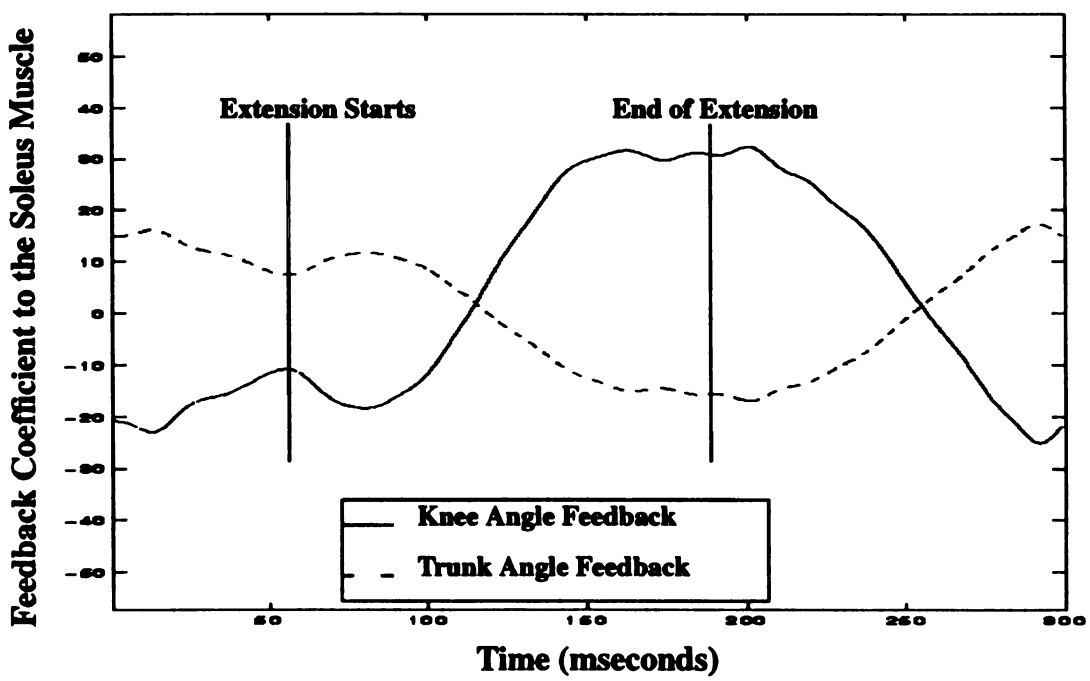

Figure 3.3.6 Feedback gain plot from the knee and the hip motions to the soleus muscle

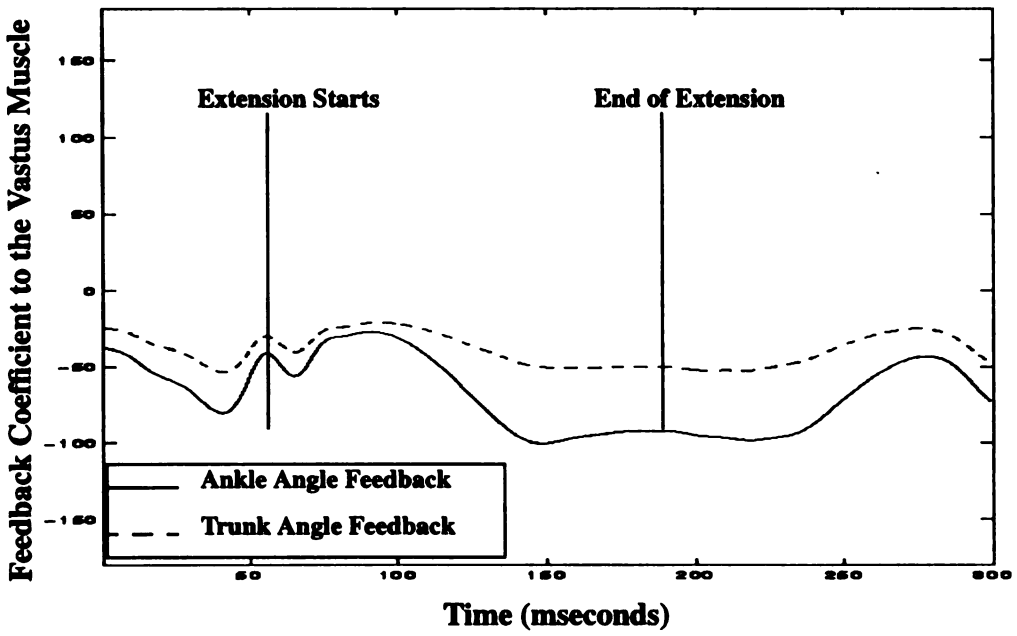

Figure 3.3.7 Feedback gain plot from the ankle and the hip motions to the vastus muscle.

Although the hypothesis of internal coordination has been proposed by different researchers in the fields of neurosciences and human dynamics, the characterization of such interaction has not been fully investigated. This is largely due to the fact that a general human activity exhibits nonlinear dynamics that are usually analytically complex. The use of extended linearization to address the nonlinearity of the system dynamics with algebraic control theory in the present work can be considered as a first step in the direction of the quantization of the feedback interaction (Dhaher, 1996).

Let us next examine the effect of the individual joint motion on the feedback gain of the muscle(s) spanning a particular joint. To demonstrate this concept, consider first the ankle joint. The graph shown in Figure 3.3.8 is a cross-plot of the ankle angle versus the

feedback gain associated with the soleus muscle for the squat cycle shown in Figure 3.3.4. As the ankle angle increases in the dorsal direction, the soleus muscle feedback gain increases towards the positive value but remains negative all the way up to an ankle angle of about 30^{o}. Since the soleus muscle is considered a plantar flexor at the ankle joint, the trend shown in Figure 3.3.8 indicates that the feedback structure is trying to give the soleus muscle the signal to facilitate the dorsi flexion process. However, as the dorsi flexion angle increases beyond the 30^{o} mark of ankle dorsi flexion, the feedback gain switches to a positive value to demand an increase of the muscle force to provide both the braking effect on the excessive dorsi flexion and maintain the dorsi angle ankle of the open loop model consistent with the measured ankle angle of the closed loop model. On the other hand, the Tibialis Anterior muscle is receiving more and more negative feedback gains in order to facilitate the counter action of the soleus muscle as discussed above, see Figure 3.3.9.

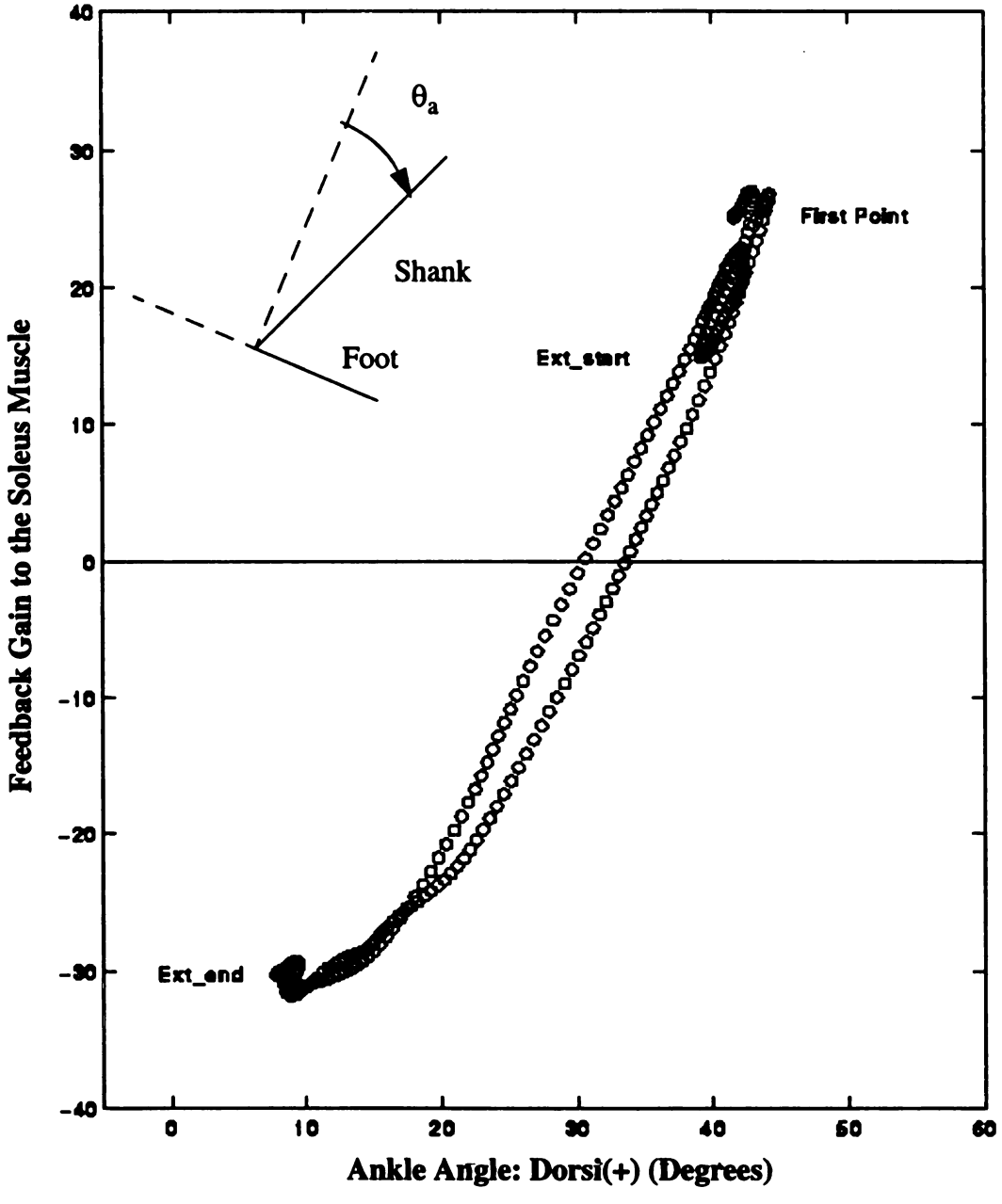

Figure 3.3.8 Ankle angle feedback gain plot to the soleus muscle for a squat activity

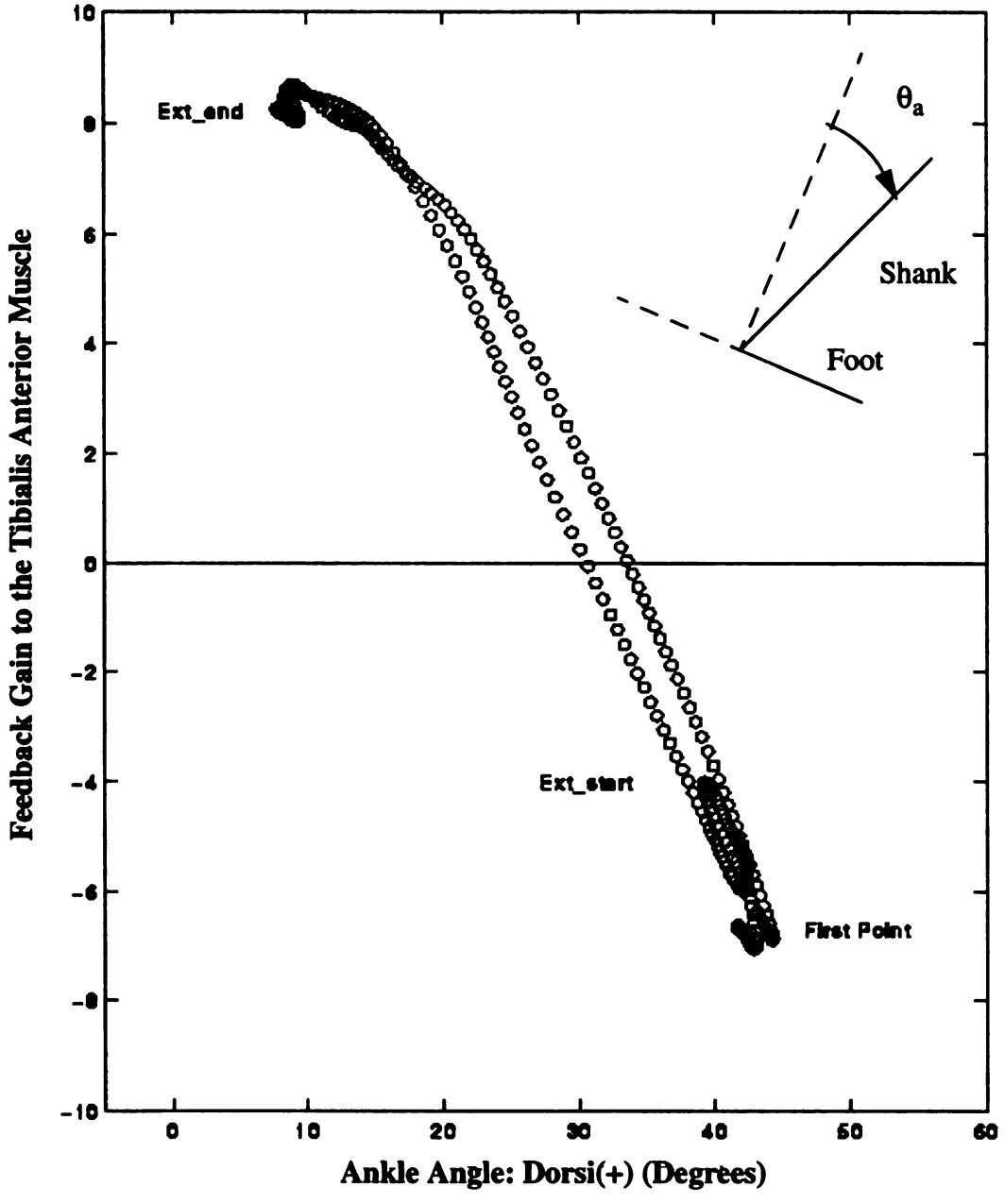

Figure 3.3.9 Ankle angle feedback gain plot to the tibialis anterior muscle for a squat activity

Similar trends were also observed at the knee joint. As the knee angle increased, the feedback gain to the Rectus muscle increases to maintain its negative value to facilitate more and more knee flexion as shown in Figure 3.3.10. However, as seen in Figure 3.3.10, this trend does not appear to continue throughout the range of knee flexion. At about a knee angle of approximately 50^{o} the rectus femoris starts receiving positive feedback gains to increase the muscle force to counteract the gravity and dynamic effects and avoid a total collapse at the knee joint. This is clear from the rapid increase of the feedback gain values at large knee angles around 120^{o}. Unlike the Rectus muscle, the hamstrings are acting in the same manner as the Tibialis Anterior muscle at the ankle joint. The only major difference is that the hamstrings muscle is required to reduce the amount of force buildup by getting large values of negative feedback gains at large knee flexion angles in order to reduce the counter action against the rectus femoris muscle, see Figure 3.3.11.

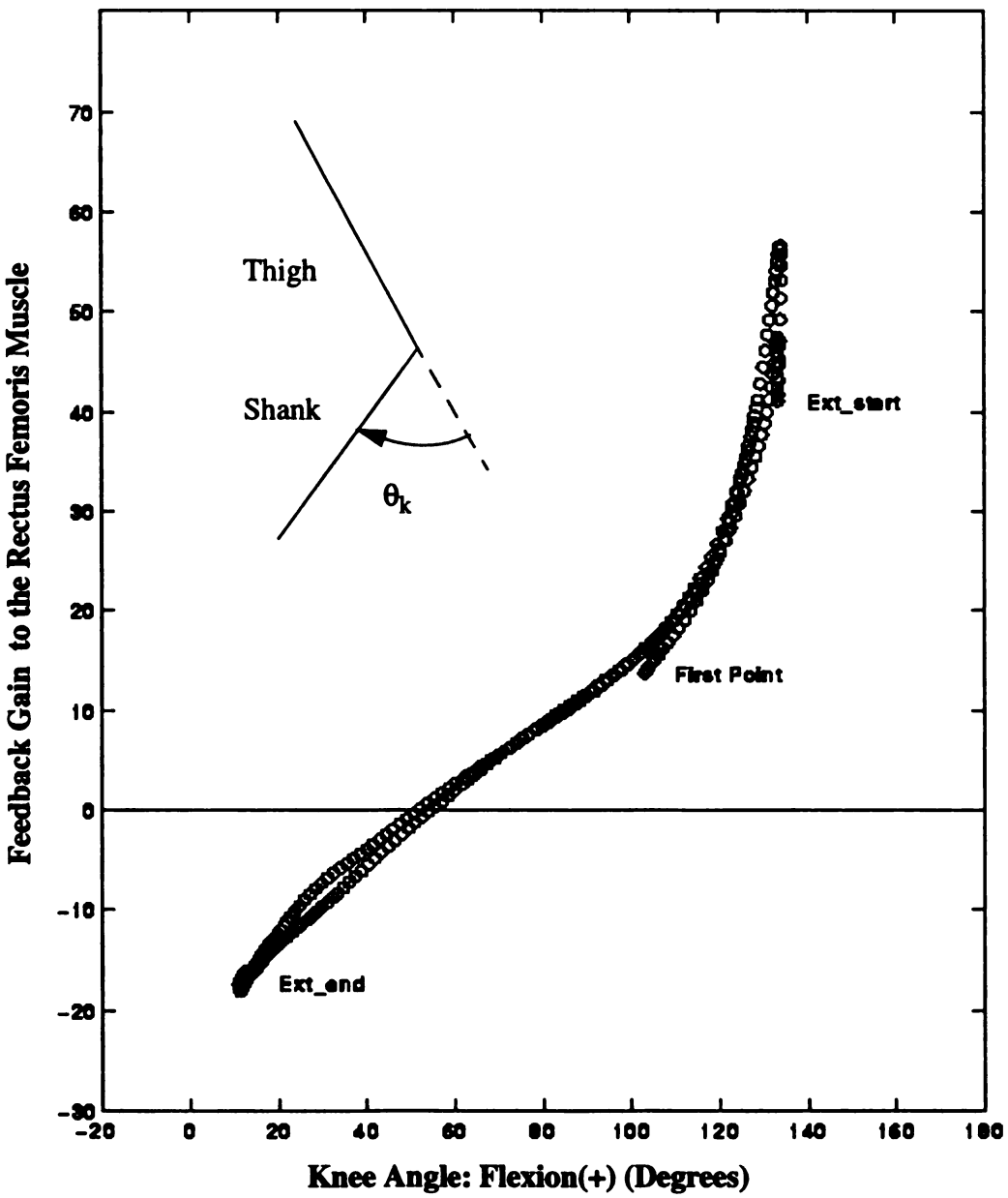

Figure 3.3.10 Knee angle feedback gain plot to the rectus femoris muscle for a squat activity

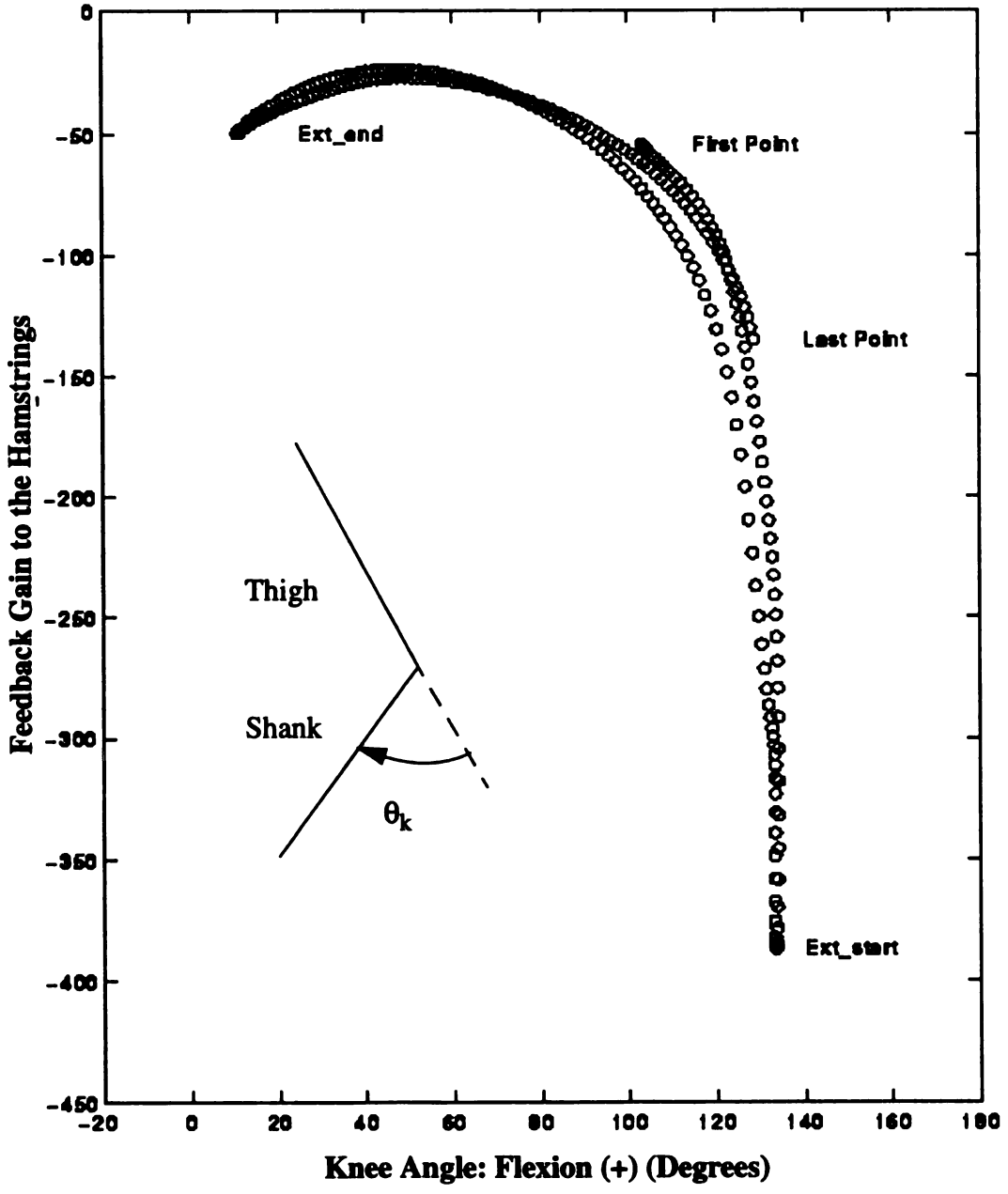

Figure 3.3.11 Knee angle feedback gain plot to the hamstrings muscle for a squat activity

The last joint to examine is the hip/trunk joint. As shown in Figure 3.3.12, the feedback gain to the gluteus maximus muscle is negative for all hip angles less than 100^{o}. However, the feedback gain switches in sign after the angle that forces the gluteus maximus to produce more muscle force to control the large hip/trunk flexion angle. Although, both the hamstrings and the gluteus maximus muscles are considered to be hip extensors, the feedback gain plots does not show a similar positive/negative synergy. While the feedback gain from the hip joint motion to the gluteus maximus muscle switches in sign, the hamstring feedback gain remains positive throughout the squat cycle considered, see Figure 3.3.13. This may be attributed to the fact the hamstring muscle is considered the major hip extensor muscle and is considered to be active in a positive sense for the whole rang of hip flexion angles. Also, note the rapid increase of the positive feedback structure to the hamstrings muscle as the hip joint angle passes the 140^{o} mark. Finally, it is very important to not that although the hamstring muscle is getting negative feedback gain from the knee angle, it is receiving positive feedback from the hip angle, see Figures 3.3.11 and 3.3.12. This is attributed to the fact that the hamstrings acts as an action generator at the hip joint and a facilitator at the knee joint in the extension mode of the squat activity.

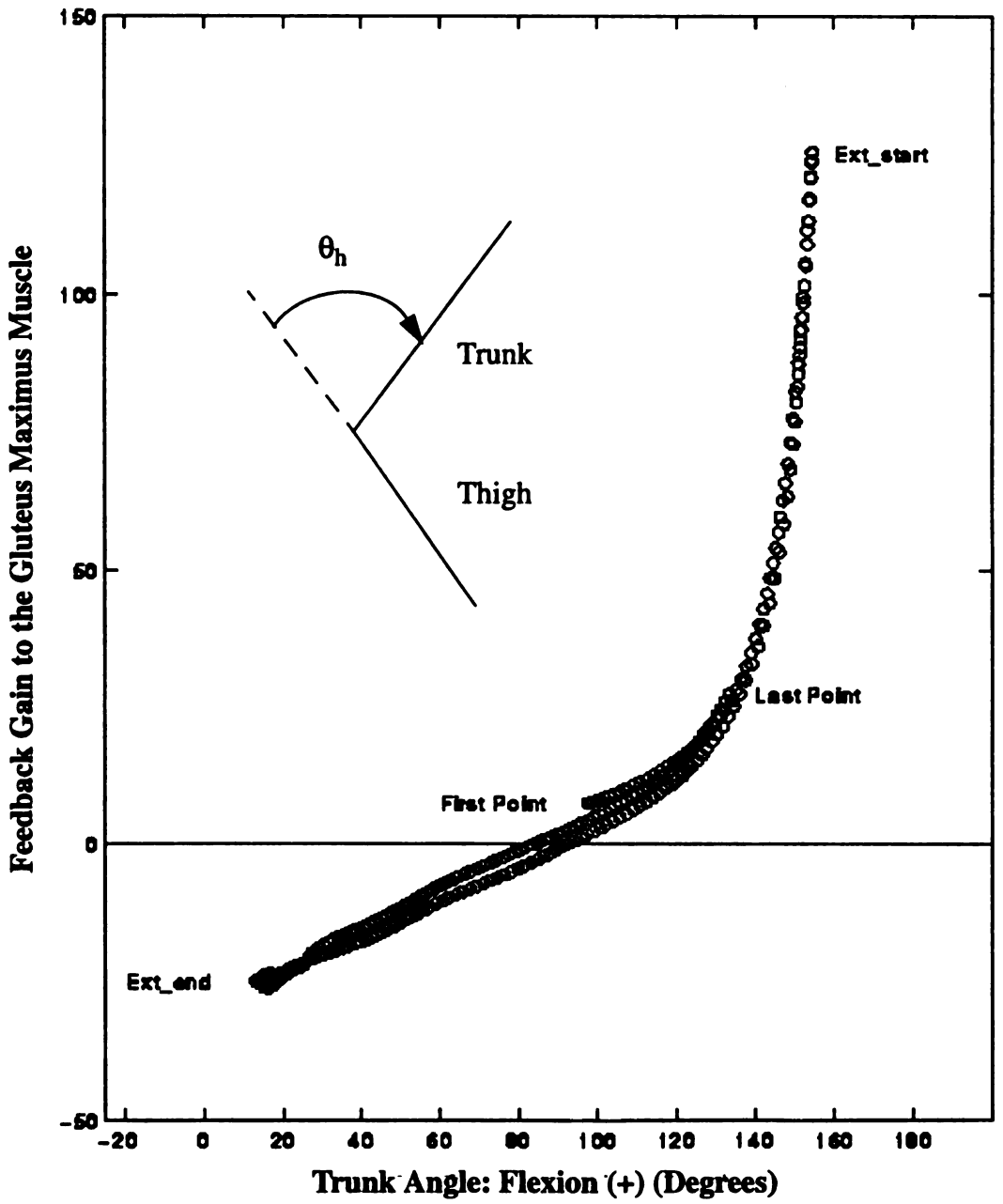

Figure 3.3.12 Hip angle feedback gain plot to the gluteus maximus muscle for a squat activity

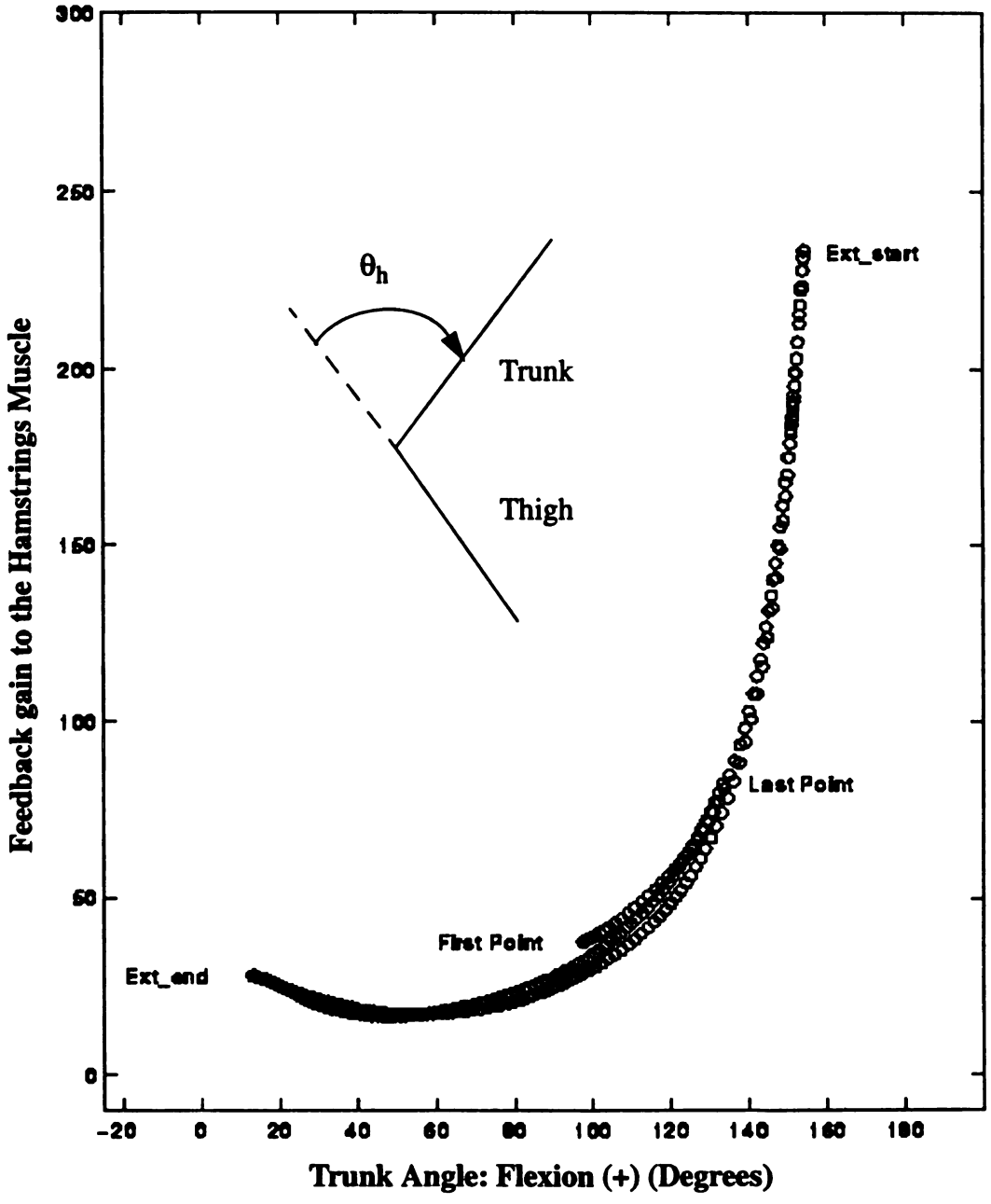

Figure 3.3.13 Hip angle feedback gain plot to the hamstrings muscle for a squat activity

To further analyze the position feedback synergy in the musculoskeletal in squat activity, let us consider the position feedback cross plots of the agonist and antagonist muscles included in the model. Structurally, muscles are classified as a uni-articular or a bi-articular, where the latter means that the muscle spans two joints at the same time. The rectus femoris muscle is an excellent example because it spans both the hip and the knee joints. A uni-articular muscle is a muscle that structurally spans a single joint, the soleus muscle. When comparing the feedback gains of two antagonistic uni-articular muscles that are associated with the joint angle both muscles span, a linear coupling was observed. This is clear in the cross plot of the gain associated with the ankle angle to the soleus and Tibialis Anterior muscles shown in Figure 3.3.14. Since negative and positive feedback gains are representations of demands by the system for less and more muscle force generation, respectively, the positive/negative synergy across the uni-articular antagonistic muscles in squat activity appears to be justifiable. If one of the antagonistic muscles is creating an action, braking or driving the opposite muscle should facilitate that action. This is generally true for the uni-articular antagonistic muscles, however, it appears that in the case of a bi-articular antagonistic muscles the positive/negative synergy does not necessary hold. As an example, consider the cross plot given in Figure 3.3.15, where the hamstring feedback gains associated with the knee joint are plotted against the rectus femoris position feedback gains. It is obvious that the bi-articular nature of both muscles not only produces a nonlinear form of coupling, but also loses the positive/negative synergy observed in the uni-articular case. Although the feedback gain to the rectus femoris muscle has switched in sign during the squat cycle, the corresponding hamstring feedback gain maintained the same sign. This trend may be attributed to the fact that unlike the uni-

articular antagonistic muscles, the bi-articular muscles are supposed to accommodate the motion of the other joint hence the feedback structure is more complex.

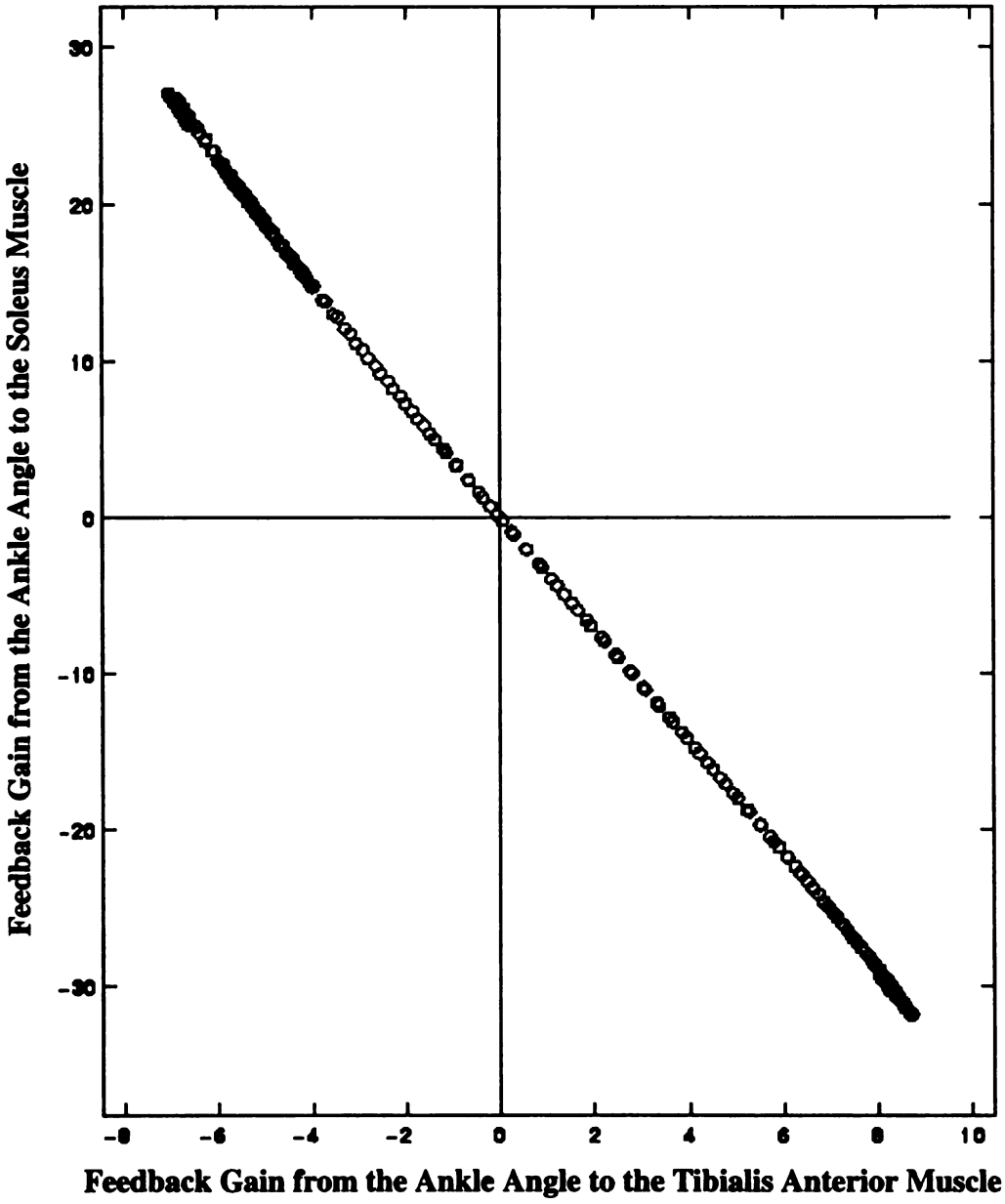

Figure 3.3.14 Position feedback gain associated with the ankle angle cross plot of the soleus and tibialis anterior muscles for a squat activity

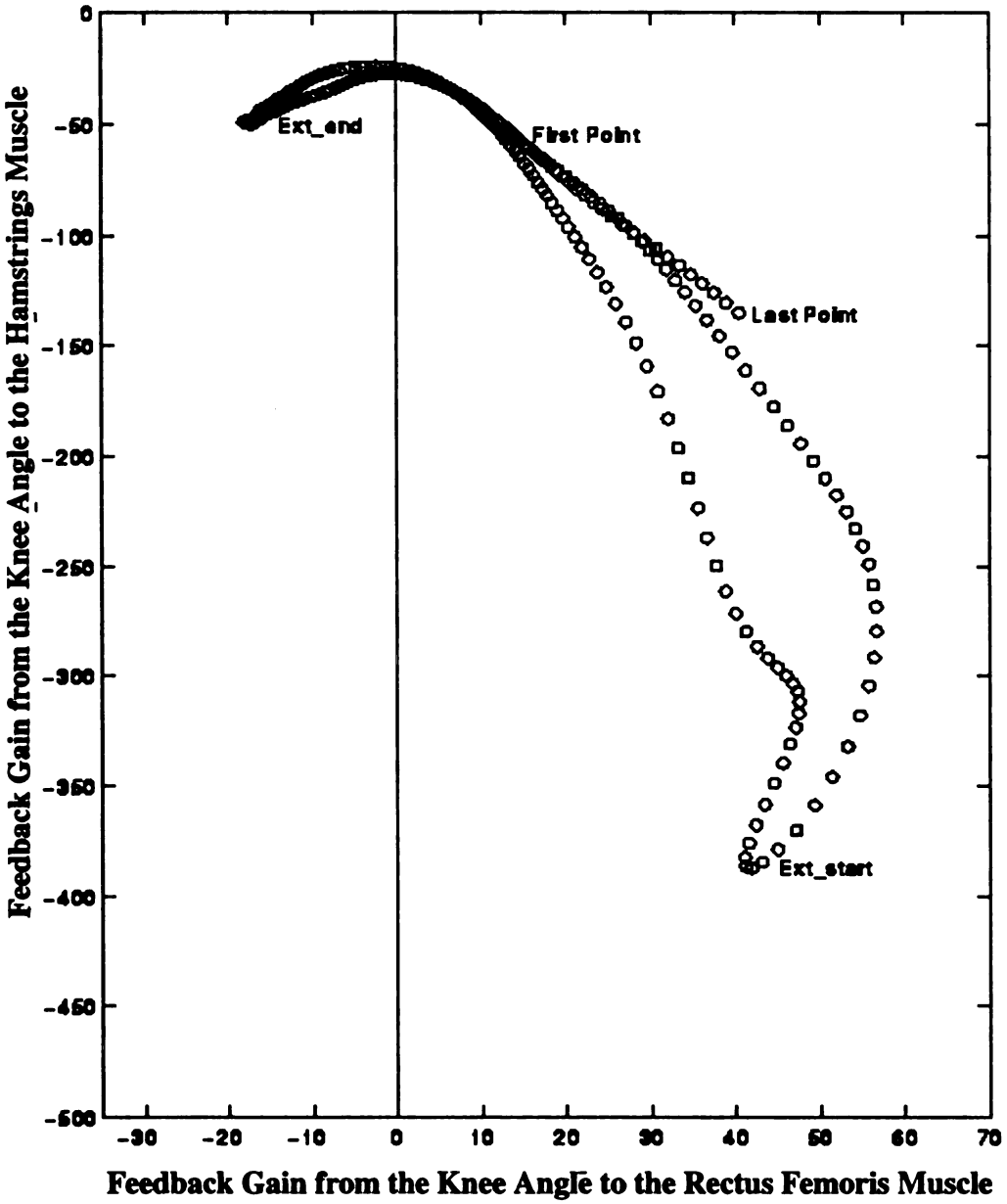

Figure 3.3.15 Position feedback gain associated with the knee angle cross plot of the hamstring and rectus femoris muscles for a squat activity

The next set of muscles is the group of muscles that are agonistic, i.e muscles that have similar actions at a joint, for example, the hamstrings and the gluteus maximus muscle at the hip joint. Since a uni-articular group of agonist muscles does not exist in the model proposed here, we will only consider the case of agonist muscles regardless of their structural relation to the joints. The nonlinear coupling observed in the case of the bi-articular antagonistic muscle is also present in the case of the feedback gain cross plots of the agonist muscles when at least one of the muscles is a bi-articular muscle, see Figure 3.3.16. This nonlinearity is attributed to the fact that one of the agonist muscles is bi-articular, the hamstrings. While the uni-articular muscle feedback gain changes sign, see Figure 3.3.16, the hamstring antagonistic muscle maintained the same feedback gain sign throughout the squat cycle. This trend was also observed in Figure 3.3.15. However, unlike the antagonistic case, the agonist muscles act together to generate an action, ecentric or concentric. The cross plot given in Figure 3.3.16 supports that definition where it can be observed that the position feedback synergy of the gluteus maximus and the hamstring muscle appears to exhibit a positive/positive feedback synergy through the extension phase of the squat cycle.

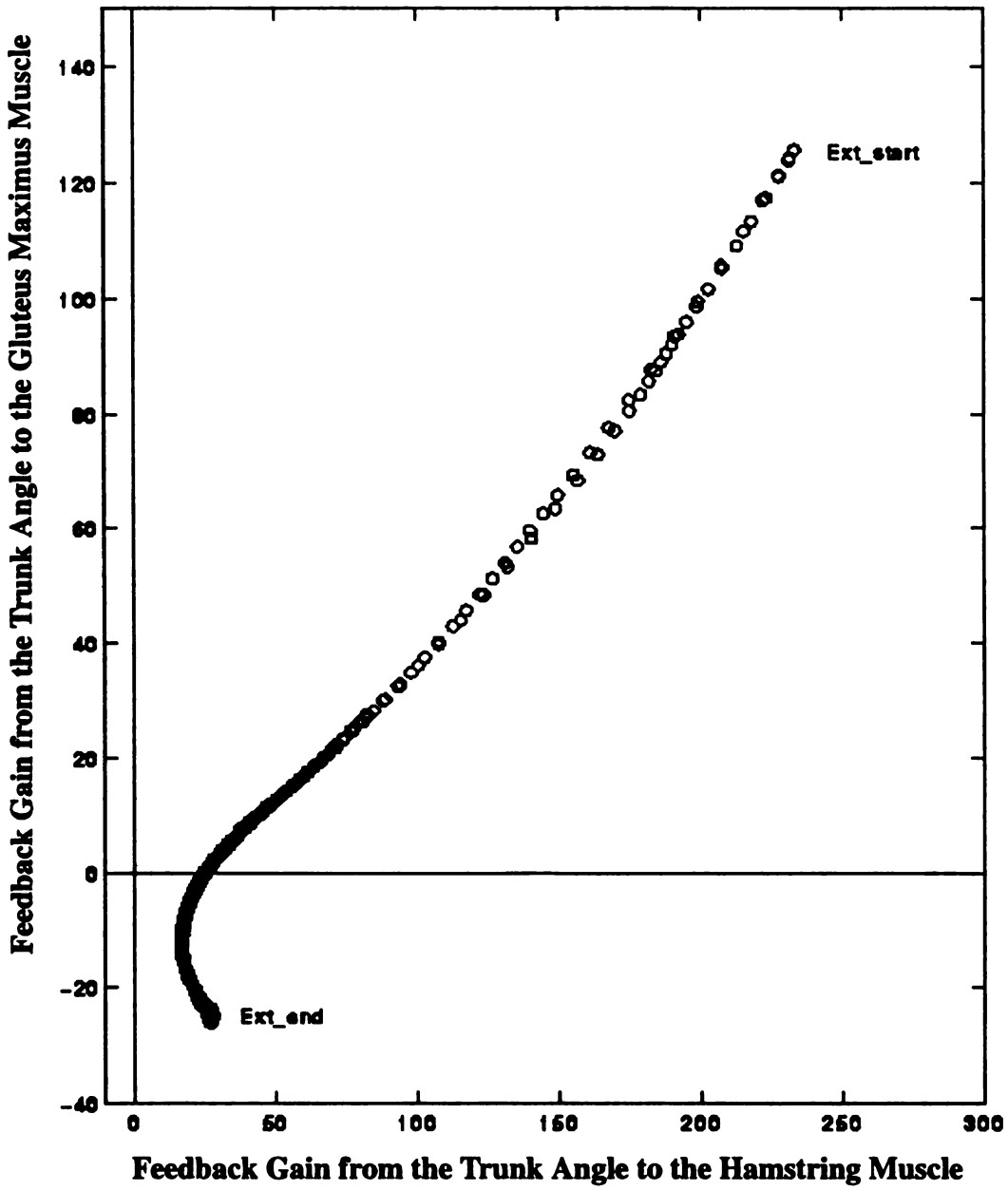

Figure 3.3.16 Position feedback gain associated with the hip angle cross plot of the gluteus maximus and the hamstring muscles for a squat activity

CHAPTER FOUR

CONCLUSIONS

This study described an alternate yet physically justifiable approach to computing the feedback gains. This method is based on the idea that any human activity can be characterized by an input/output mathematical model. The model inputs and outputs signify measured muscular activity and nominal motion trajectories. This model becomes the structure that includes both human dynamics and control, and is a physical representation of closed loop system dynamics. To obtain such a mathematical model, a detailed discussion of the parametric identification method was developed. The development was restricted to a general input/output human dynamic model.

The development of an open loop system is a major component in the study concerning the feedback problem. An anthropomorphic musculoskeletal model (open loop), where muscles are considered as moment generators, was developed. Since the open loop model that was developed is nonlinear, an extended linearization method was used to overcome nonlinearity. The Jacobian-based linearization procedure reduces the nonlinear model to a family of linearized systems, parameterized by the same set of measured nominal operating points. Also the generalized forms relating Jacobian matrices with open loop system inertia, Coriolis, and gravitational matrices are derived.

A key step in the procedure is to represent both the estimated closed loop system and

the proposed open loop models in the same state space structure representation. The block observer form was used as a standard state space realization of closed and open loop systems. A detailed development of an explicit solution of the feedback gain matrix was presented. Also the conditions for good feedback estimations were addressed. The utility of the proposed method was demonstrated by applying it to the squat activity. Quantitative results of the positional feedback gains were presented.

The accuracy in estimating the position feedback matrix is dependent on the type of activity under study. For more ballistic movements a more accurate estimation is expected. Since the squat activity is slow, its estimation of position feedback was not perfect in the sense that all the closed loop model matrices were not fully attained by the proposed output feedback law. To test how accurate the estimation was, the open loop system combined with estimated position feedback was first simulated. Then, the result of the simulation was compared with nominal motion trajectories obtained from the estimated closed loop model. Although the squat activity studied was slow, the error in the feedback gain estimation was low.

Compensatory functions of muscles were characterized by observing the adaptability of the feedback gain values relating a specific joint motion to the force generation in different muscles in the structure. Results showed that activity of a muscle is affected by feedback from angular motions of all the joints in the structure. When comparing feedback coefficients of two antagonistic uni-articular muscles, the coupling was approximately linear. Positive feedback to the driving muscle was accompanied by a negative feedback to the antagonistic muscles. For bi-articular antagonistic muscles, the feedback coupling was more complex. The results also showed that a positive feedback

to the driving muscle at a joint may or may not be accompanied by a negative feedback of the antagonistic muscle. Positive/positive or positive/negative feedback synergy in antagonistic bi-articular muscles was shown to depend on many parameters that include the motions of one or more joints.

Using the proposed method, the feedback structure can be estimated for a general nonlinear dynamic structure. It can compute the feedback gains without resorting to any assumptions over the dynamic behavior of the closed loop system. In addition, the method provided quantifiable data that is valuable information concerning feedback synergy in human structure. Improvements on this method may include incorporating recursive (on-line) methods in estimating the closed loop model.

An area of future research may be to investigate the potential use of this method in solving the complex orthopaedic problems of predictive surgeries. Such problems involve the prediction of the motion of a human structure after undergoing a muscle transfer surgery. It is well known (Vukobratrovic *et al.*, 1990) that the open loop human structure is inherently unstable in the absence of any feedback control. It has been shown in this study that the estimated feedback gain, together with the open loop system, results in a collective system that simulates the real activity, the closed loop stable system. Therefore, surgery can now be simulated on a stable system that consists of the open loop model and the estimated feedback gain structure. Questions pertaining to the effect of surgeries on muscle activation and position feedback gains should be addressed. Studies appearing in the literature showed that muscle activation does not vary with the transfer surgery (Waters *et al.*, 1982, as an example). Another issue of concern is the sensitivity of the pre-surgery estimated feedback structure to system

parameters (muscle origin and insertion coordinates). Analytical sensitivity studies can be constructed using the explicit form of the feedback gain solution provided in this study.

Another area of future work is to simulate muscular neurological deficiencies and their effect on the human motion. Muscle spasticity is considered to be one of the common neurological deficiencies in which the muscle's activation curves show constant distribution (Bowsher *et. al.*, 1992). There are two means to carry out such research. The first approach involves the testing of subjects with pre-existing neurological deficiencies. The results can then be used to establish general trends of gain values associated with each deficiency. A second, more analytical approach, involves the parameterization of the muscle's activation curves in terms of a set of nodal points. These nodal points can be altered to simulate different neurological deficiencies. A numerical sensitivity study can then be developed to examine the effect of changing nodal points on the estimated feedback gains.

Appendices

APPENDIX A

MUSCLE CONTRACTION DYNAMICS

The contraction dynamics of the muscle model proposed in Gordon *et al.* (1986) and shown in Figure 2.2.2 is derived in this appendix. Since the volume of the muscle is assumed to be constant, the muscle pennation angle at any muscle fiber length is related to the pennation angle measured at muscle optimal length as follows

$$L_o \cdot \sin\alpha_o = L_m \cdot \sin\alpha = w = constatnt \tag{A.1}$$

Differentiating Equation (A.1) with respect to time gives

$$\dot{\alpha} = (-\dot{L_m}/L_m) \cdot \tan\alpha \tag{A.2}$$

From geometry, the musculotendon length is related to the muscle fiber length at any time as follows (see Figure 2.2.2.)

$$L_{mt} = L_t + L_m \cdot \cos\alpha \tag{A.3}$$

where L_t is the tendon length. After differentiating Equation (A.3) and then combining it with Equation (A.2), the musculotendon velocity V_{mt} is related to the muscle fiber velocity as follow

$$V_{mt} = V_t + V_m/\cos\alpha \tag{A.4}$$

where V_t and V_m are the tendon and muscle fiber velocities, respectively. Similarly

$$V_m = V_{se} + V_{ce} \tag{A.5}$$

where V_{se} and V_{ce} are the series element and contractile element velocities, respectively.

By inspection of Figure 2.2.2, the force in the tendon p is related to the muscle fiber

force, p_m as follows

$$p = p_m \cdot \cos(\alpha) \tag{A.6}$$

Note that p is the force passing through the muscle tendon. Since experimental data of the tendon are given in terms of its stiffness K which is defined mathematically as

$$K = \frac{dp}{dt} / V_t \tag{A.7}$$

the differentiation of Equation (A.6) with respect to time yields

$$\frac{dp}{dt} = \frac{dp_m}{dt} \cdot \cos(\alpha) - p_m \cdot \dot{\alpha} \cdot \sin(\alpha) \tag{A.8}$$

Substitute from Equation (A.2) for $\dot{\alpha}$ in the above equation yields

$$\frac{dp}{dt} = \frac{dp_m}{dt} \cdot \cos(\alpha) + p_m \cdot \frac{V_m}{L_m} \cdot \tan(\alpha) \cdot \sin(\alpha) \tag{A.9}$$

But from the equilibrium condition on the model, the following relation can be easily verified

$$\frac{dp_m}{dt} = \frac{dp_{se}}{dt} + \frac{dp_{pe}}{dt} \tag{A.10}$$

Using the same stiffness to rate of force relation given in Equation (A.7), Equation (A.10) can be expressed as

$$\frac{dp_m}{dt} = K_{se} \cdot V_{se} + K_{pe} \cdot V_{pe} \tag{A.11}$$

From the geometry of the muscle model shown in Figure (2.2.2), it is easy to note that $L_{pe} = L_m$, hence the velocities are equal. Using the previous statement and Equation (A.4), Equation (A.11) reduces to

$$\frac{dp_m}{dt} = (K_{se} + K_{pe}) \cdot V_m - K_{se} \cdot V_{ce} \tag{A.12}$$

Substituting Equation (A.6) and Equation (A.12) in Equation (A.9) yields

$$\frac{dp}{dt} = (K_{se} + K_{pe}) \cdot V_m \cdot \cos(\alpha) - K_{se} \cdot V_{ce} \cdot \cos(\alpha) + \left(\frac{p}{L_m}\right) \cdot V_m \cdot (\tan(\alpha))^2 \tag{A.13}$$

By letting $K_m = K_{se} + K_{pe}$ and using Equations (A.4 and A.7), and with some algebraic manipulations, Equation (A.13) takes the form

$$\frac{dp}{dt} = \frac{K \cdot K_{m\alpha} \cdot \cos\alpha}{K + K_{m\alpha} \cdot \cos\alpha} \cdot \left\{ V_{mt} - \frac{K_{se}}{K_{m\alpha}} \cdot V_{ce} \right\} \tag{A.14}$$

where

$$K_{m\alpha} = K_m \cdot \cos(\alpha) + \frac{p}{L_m} \cdot (\tan(\alpha))^2 \tag{A.15}$$

In Equation (A.14), the musculotendon K_{se}, K_{pe}, $\cos(\alpha)$, L_m, and V_{ce} can be evaluated using the constitutive equations given in Section 2.2.2. All terms are then expressed in terms of L_{mt}, p, and $a(t)$, as in the case of V_{ce}, by using the geometric relations in this appendix. Thus the general form of Equation (A.14), which represents the muscle contraction dynamics, can be expressed as

$$\frac{dp}{dt} = f(L_{mt}, V_{mt}, p, a(t)) \tag{A.16}$$

APPENDIX B

BLOCK OBSREVER STATE SPACE REALIZATION

Kailath (1980) gives a detailed account of various state space realization of multi-input multi-output (MIMO) systems. In this appendix we shall introduce only one of the MIMO state spaces, the Block Observer form of an Autoregressive (ARX) input/output discreet model.

Consider the following general second order ARX input/output model. This equivalent to $n = 2$ in Equations (2.1.5; 2.3.3),

$$(I_r + \overline{A_1} \cdot q^{-1} + \overline{A_2} \cdot q^{-2}) \cdot \zeta(q) = (\overline{B_2} \cdot q^{-2} + \overline{B_1} \cdot q^{-1} + \overline{B_o}) \cdot \xi(q) \qquad \text{(B.1)}$$

where $\zeta(q)$ is the output vector, $\zeta(q) \in R^r$, $\xi(q)$ is the input vector, $\xi(q) \in R^m$, and $\overline{A_1}, \overline{A_2}, \overline{B_1}, and, \overline{B_2}$ are constant coefficient matrices. It can easily be shown that the Block Observer state space representation of the system in Equation (B.1) takes the form (Strejc, 1981)

$$X(k+1) = A \cdot X(k) + B \cdot \xi(k) \qquad \text{(B.2)}$$

$$\zeta(k) = C \cdot X(k) + D \cdot \xi(k) \qquad \text{(B.3)}$$

where

$$A = \begin{bmatrix} -\overline{A_1} & I \\ -\overline{A_2} & [0] \end{bmatrix}_{2r \times 2r}$$

$$B = \begin{bmatrix} \overline{B_1}^* \\ \overline{B_2}^* \end{bmatrix}_{2r \times m}$$

$$C = \left[I_r \; [0] \right]_{r \times 2r},$$

$$D = \overline{B_o}$$

and

$$\overline{B_i}^* = -\overline{A_i} \cdot \overline{B_o} + \overline{B_i} \qquad i = 1, 2$$

APPENDIX C

EQUATIONS OF MOTION

The dynamic equations of motion of the 4 DOF skeletal model shown in Figure 3.1.2 are given in a vector matrix form in Equation (3.1.9) of Section 3.1

$$J(\Theta)\cdot\ddot{\Theta} = B(\Theta)\cdot\dot{\Theta}^2 + C(\Theta) + D\cdot M(\Theta_J)\cdot P \tag{3.1.9}$$

Where

$$J(\Theta) = \begin{bmatrix} a_{11} & -a_{12}\cos(\theta_1-\theta_2) & a_{13}\cos(\theta_1-\theta_3) & -a_{14}\cos(\theta_1-\theta_4) \\ -a_{12}\cos(\theta_1-\theta_2) & a_{22} & -a_{23}\cos(\theta_3-\theta_2) & a_{24}\cos(\theta_4-\theta_2) \\ a_{13}\cos(\theta_1-\theta_3) & -a_{23}\cos(\theta_3-\theta_2) & a_{33} & -a_{34}\cos(\theta_3-\theta_4) \\ -a_{14}\cos(\theta_1-\theta_4) & a_{24}\cos(\theta_4-\theta_2) & -a_{34}\cos(\theta_3-\theta_4) & a_{44} \end{bmatrix} \tag{C.1}$$

$$B(\Theta) = \begin{bmatrix} 0 & -a_{12}\sin(\theta_1-\theta_2) & -a_{13}\sin(\theta_1-\theta_3) & -a_{14}\sin(\theta_1-\theta_4) \\ -a_{12}\sin(\theta_1-\theta_2) & 0 & -a_{23}\sin(\theta_3-\theta_2) & a_{24}\sin(\theta_2-\theta_4) \\ a_{13}\sin(\theta_1-\theta_3) & -a_{23}\sin(\theta_3-\theta_2) & 0 & -a_{34}\sin(\theta_3-\theta_4) \\ -a_{14}\sin(\theta_1-\theta_4) & -a_{24}\sin(\theta_2-\theta_4) & -a_{34}\sin(\theta_3-\theta_4) & 0 \end{bmatrix} \tag{C.2}$$

$$C(\Theta) = \begin{bmatrix} -c_1 g\cos\theta_1 \\ c_2 g\cos\theta_2 \\ -c_3 g\cos\theta_3 \\ c_4 g\cos\theta_4 \end{bmatrix} \tag{C.3}$$

$$D = \begin{bmatrix} 2 & 0 & 0 \\ -2 & -2 & 0 \\ 0 & 2 & 2 \\ 0 & 0 & -2 \end{bmatrix} \tag{C.4}$$

and

$$a_{11} = I_1 + m_1 \cdot {l_{c1}}^2 + (m_1 + m_2 + m_3) \cdot {l^2}_1$$

$$a_{12} = c_2 \cdot l_1$$

$$a_{13} = c_3 \cdot l_1$$

$$a_{14} = c_4 \cdot l_1$$

$$a_{22} = I_2 + m_2 \cdot {l_{c2}}^2 + (m_3 + m_4) \cdot {l^2}_2$$

$$a_{23} = c_3 \cdot l_2$$

$$a_{24} = c_4 \cdot l_2$$

$$a_{33} = I_3 + m_3 \cdot {l_{c3}}^2 + m_4 \cdot {l^2}_3$$

$$a_{34} = c_4 \cdot l_3$$

$$a_{44} = I_4 + m_4 \cdot {l_{c4}}^2$$

$$c_1 = m_1 \cdot l_{c1} + (m_2 + m_3 + m_4) \cdot l_1$$

$$c_2 = m_2 \cdot l_{c2} + (m_3 + m_4) \cdot l_2$$

$$c_3 = m_3 \cdot l_{c3} + m_4 \cdot l_3$$

$$c_4 = m_4 \cdot l_{c4}$$

The parameters given in the above equations are defined as follows

I_i = moment of inertia of segment i about its center of mass.

l_i = length of segment i.

l_{ci} = distance of body segment center of mass from distal end.

m_i= mass of segment i.

θ_i = the angle that segment i makes with the horizontal.

θ_a, θ_k, and θ_h are the ankle, knee, and hip joint angles, respectively.

$\Theta_J^T = [\theta_a, \theta_k, \theta_h]^T$; joint angles vector.

$\Theta^T = [\theta_1, \theta_2, \theta_3, \theta_4]^T$; system output vector.

The linearization of Equation (3.1.9) is tacking place around the operating points (nominal data) obtained and used in the identification of the closed loop system. The method of linearization defined in Section 2.2.3 is dependent on the evaluation of the Jacobian matrices in terms of the system states (positions, velocities) and system inputs. Let us rewrite Equation (3.1.9) in the following form

$$\ddot{\Theta} = f(\Theta, \dot{\Theta}, P) \tag{C.5}$$

where

$$f(\Theta, \dot{\Theta}, P) = J^{-1}(\Theta) \cdot (B(\Theta) \cdot \dot{\Theta}^2 + C(\Theta) + D \cdot M(\Theta_J) \cdot P) \tag{C.6}$$

The function $f(\Theta, \dot{\Theta}, P) \in R^4$, is a nonlinear function of system states. The gradient of f with respect to $\theta_i \in \Theta$ is defined as the differentiation of the function with respect to θ_i, or

$$\nabla_{\theta_i} f = \frac{\partial J^{-1}}{\partial \theta_i}(\Theta) \cdot (B(\Theta) \cdot \dot{\Theta}^2 + C(\Theta) + D \cdot M(\Theta_J) \cdot P)$$

$$+ J^{-1}(\Theta) \cdot \left(\frac{\partial B}{\partial \theta_i}(\Theta) \cdot \dot{\Theta}^2 + \frac{\partial C}{\partial \theta_i}(\Theta) + D \cdot \frac{\partial M}{\partial \theta_i}(\Theta_J) \cdot P \right) \qquad \text{(C.7)}$$

Note that if $J^{-1}(\Theta)$ exists then $\frac{\partial J^{-1}}{\partial \theta_i}(\Theta)$ can be computed from the following formula

$$\frac{\partial J^{-1}}{\partial \theta_i}(\Theta) = J^{-1}(\Theta) \cdot \frac{\partial J}{\partial \theta_i}(\Theta) \cdot J^{-1}(\Theta) \qquad \text{(C.8)}$$

Thus the computational difficulty of finding $\frac{\partial J^{-1}}{\partial \theta_i}(\Theta)$ is avoided by using Equation (C.8). On the right hand side of Equation (C.7), the moment arm matrix is not explicitly defined in terms of segmental angles but is computed by using inter-segmental angles, joint angles, as shown in Section 2.2.1. Hence, the term $\frac{\partial M}{\partial \theta_i}(\Theta_J)$ is computed from

$$\frac{\partial M}{\partial \theta_i}(\Theta_J) = \frac{\partial M}{\partial \theta_a}(\Theta_J) \cdot \frac{\partial \theta_a}{\partial \theta_i} + \frac{\partial M}{\partial \theta_k}(\Theta_J) \cdot \frac{\partial \theta_k}{\partial \theta_i} + \frac{\partial M}{\partial \theta_h}(\Theta_J) \cdot \frac{\partial \theta_h}{\partial \theta_i} \qquad \text{(C.9)}$$

where

$$\theta_a = (\theta_2 - \theta_1) - \pi/2 \qquad \text{(C.10)}$$

$$\theta_k = \theta_2 - \theta_3 \qquad \text{(C.11)}$$

$$\theta_h = \theta_4 - \theta_3 \qquad \text{(C.12)}$$

The terms $\frac{\partial \theta_a}{\partial \theta_i}, \frac{\partial \theta_k}{\partial \theta_i}, and, \frac{\partial \theta_h}{\partial \theta_i}$ in Equation (C.9) takes one of the values (1, 0, -1)

depending on which segmental angle is used in the differentiation. The Jacobian matrix evaluated with respect to the vector Θ is then expressed as

$$\nabla_{\Theta} f = \left[\nabla_{\theta_1} f \; \nabla_{\theta_2} f \; \nabla_{\theta_3} f \; \nabla_{\theta_4} f\right] \tag{C.13}$$

Similarly, the Jacobian matrix of f with respect to $\dot{\theta}_i$ is evaluated from Equation (C.6) as follows

$$\nabla_{\dot{\theta}_i} f = J^{-1}(\Theta) \cdot B(\Theta) \cdot \frac{\partial \dot{\Theta}^2}{\partial \dot{\theta}_i} \tag{C.14}$$

Therefore the whole Jacobian matrix $\nabla_{\dot{\Theta}} f$ reduces to

$$\nabla_{\dot{\Theta}} f = 2 \cdot J^{-1}(\Theta) \cdot B(\Theta) \cdot diag(\dot{\theta}_i) \tag{C.15}$$

Finally, $\nabla_P f$ matrix is evaluated following the same procedure used to obtain Equation (C.15) and can be expressed as follows (C.16)

$$\nabla_P f = J^{-1}(\Theta) \cdot D \cdot M(\Theta_J) \cdot I_7 \tag{C.17}$$

and I_7 is a (7×7) identity matrix.

References

REFERENCES

1 Abdel-Aziz Y.I. and Karara H.M.: Direct Linear Transformation from Comparator Coordinates into Object Space Coordinates in Close-Range Photogrammetry, *Proceedings of the Symposium on Close-Range Photogrammetry*, January 26-29, 1971.

2 Alexander R.McN., and Vernon A.: The Dimensions of Knee and Ankle Muscles and the Force they Exert, *J. Human Movement Studies*, 1, pp 115, 1975.

3 Altringham J.D. and Johunson I.A.: The pCa-tension and velocity characteristics of skinned fibers isolated from fish fast and slow muscle, *J. Physiol.(Lond)*, 333, p 42, 1982.

4 Agarwal G.C., Berman B.M. and Stark L.: Studies in Postural Control Systems I. Torque disturbance input, *IEEE Trans. Syst. Soci. Cybern. SSC-6*, 2, pp 116, 1970.

5 Anderson III B.A.: Storage and Utilization of Elastic Strain Energy During Human Jumping: An Analysis based on Predictions of an Experimentally Verified Optimal Control Model, Masters Thesis, University of Texas at Austin, 1992.

6 Bahler A.S.: Series Elastic Component of Mammalian Skeletal Muscle, Amer., *J. Physiol.*, 213, pp 1550, 1967.

7 Bahler A.S., Fales, J.T. and Zieler K.L.: Dynamic Properties of Mammalian Skeletal Muscle, *Gen. Physiol.*, 51, pp369, 1968.

8 Barker R.A.: *Neuroscience an illustrated guide*, Ellis Horwood, N.Y., 1991.

9 Baumann W.T. and Rugh W.J.: Feedback Control of Nonlinear Systems by Extended Linearization, *IEEE Trans. on Automatic Control AC-31*, 1, pp 40, January 1986.

10 Becket R. and Chang K.: An evaluation of the Kinematics of Gait by Minimum Energy, *J. Biomechanics*, 1, pp 147, 1968.

11 Belanger A.Y., McComas A.J. and Elder G.B.C: Physiological Properties of Two Antagonistic Human Muscle Groups, *Eur. T. Appl., Physiol.* (51), p. 381, 1983.

12 Bemis T.A. : The parallel squat exercise: A Biomechanical comparison between normal and anterior cruciate ligament deficient knees, Ph.D. Thesis, Department of Biomechanics, Michigan State University, 1992.

13 Bernstein N.A.: On The Motion Synthesis, Medgiz, Moscow, 1947.

14 Bowsher K.A., Damiano D.L. and Vaughan C.L.: Joint Torques and Co-Contarctions During Gait for Normal and Cereberal Palsy Children, *Proceeding of NACOB II, The Second North American Congress on Biomechanics*, Chicago, August 24th-28th, 1992.

15 Boyed I.A.: The isolated mammalian muscle spindle, *Trends Nuerosci.*, 3, pp 258, 1980.

16 Boyed I.A. and Roberts T.D.M.: Proprioceptive discharges from stretch receptors in knee joint of the cat, *J. Physil.*, 122, pp 38, 1953.

17 Brain K.: Evaluation of Generalized Model of Human Postural Dynamics and Control in Sagittal Plane, *Biol. Cybern.*, 61, pp 37, 1989.

18 Brand R.A., Crowninshield R.D., Wittstock C.E., Pedersen D.R., Clark C.R. and Van Kricken F.M.: A Model of Lower Extremity Muscular Anatomy, *J. Biomed. Eng.*, 104, pp 304, 1982.

19 Brooks V.B.: *The Neural Basis of Motor Control*, Oxford University Press, N.Y. 1986.

20 Bruker R.E., Levine D.N., Tsains P. and Zajac R.E.: Physiological types and histochemical profiles in motor unit of cat gastrocnemius, *J. Physiol.*, 234, p 273, 1973.

21 Camana P.C., Hemami, H. and Stockwell C.W.: Determination of Feedback for human: An Optimal Control Model for Analyzing Human Postural Balance, *J. Cybern.*, 7, pp 199, 1977.

22 Carlson F.D.: Kinematic Studies on the Mechanical Properties of Muscle, In Tissue Elasticity, Remington, J.W. Washington, *Amer. Physiol. Soc.*, 1957.

23 Chance M.A. and Bayazitolque V.O.: Development and Application of Generalized d-Embark Force for Multi-Freedom Mechanical Systems, *ASME Trans., J. Eng. Ind.*, 93, pp 317, 1971.

24 Chao E. Y. and Rim K.: Application of Optimization Principle in Determining the Applied Moments, *J. Biomechanics*, 6, pp 497, 1973.

25 Chen C.T.: *Introduction to Linear Control Theory*, Holt Rinehart and Winston, N.Y., 1970.

26 Chow C.K. and Jacobson D.H.: Studies of Human Locomotion Via Optimal Programing, *Math. Biosci.*, 10, pp 239, 1971.

27 Clauser C.E., McConville J.T. and Young J.W.: Weight, Volume, and Center of mass of segments of human body, Aerospace Medical Research Laboratory, AMRL-TR-69-70, 1969.

28 Close R.I.: Dynamic Properties of Mammalian Skeletal Muscle, *Physiol. Rev.*, 52, pp129, 1972.

29 Collins E.G., Phillips D.J. and Hyland D.C.: Robust Decentralized Control Laws for ACES Structure, *IEEE Control System Magazine,* pp. 62, April 1991.

30 Crago P.E., Chizeck H.J., and Hambrecht F.T.: Sensors for use with functional neuromuscular stimulation, *IEEE Trans. Biomed. Eng.*, Vol. 33, p. 256, 1986.

31 Crowe A.: Mechanical Model of Muscle and its Application to the intrafusal Fibers of the mammalian Muscle Spindle, J. *Biomechanics*, 3, pp 538, 1970.

32 Crowninshield R.D.: Use of Optimization Techniques to Predict Muscle Forces, *ASME Trans. J. Biomed. Eng.*, 100, pp 88, 1978.

33 Crowninshield R.D. and Brand R.A.: A Physiological Based Criterion of muscle force Prediction in locomotion, *J. Biomechanics*, 14, 11, pp 793, 1981.

34 Dempster W.T.: Space Requirements of the Seated Operator, WADC Tech. Rept. p. 55, Wright. Patterson Air Force Base, Ohio, 1955.

35 Dhaher Y.Y.: Characterization of the position feedback synergy in uni- and bi- articular mucsle in the skeletomotor, *First Annual Conference of The International FES Society (IFESS' 96),* Cleveland FES Center, Cleveland OH, May 14-16, 1996.

36 Dhaher Y.Y. and Soutas-Little R.W.: Postural Balance Modeled as a Double Inverted Pendulum, *First Annual North American Clinical Gait Laboratory Conf.*, Portland, Oregon, April (7-9), 1994.

37 Diener H.C. and Dichgans J.: On the role of Vestibular, Visual and Somatosensory information for Dynamic Postural Control, *Progress in Brain Research*, (Pompeiano O. and Allum J.H.J., Ed), Elsevier, Amesterdam, 76, pp 253, 1988.

38 Ebashi S. and Endo M.: Calcium Ion and Muscle Contraction, *Prog. Biophy.*, 18, pp. 123, 1968.

39 Ettmema G.J.C. and Huijing P.A.: Architecture and elastic properties of the series elastic element of muscle - tendon complex, In Multiple Muscle Systems: *Biomechanics and Movement Organization*, (Winters J.M. and Woo S.L-Y., Ed), Springer-Verlage, New York, 1990.

40 Fallside F.: *Control System Design by Pole-Zero Assignment,* Academic Press, September 1974.

41 Finley F.R. and Karpovich P.V.: Electrogoniometric analysis of normal and pathological gaits, *Res-Quart,* 35, p 379, 1964.

42 Fisher, O.: Theoretische Grundlayen Fureine Mechanik der Lebenden Korper, pp 52, Teubner, Berlin, 1906.

43 Franklen H.M., Veltink P.H., Baardman G., Redmeijer R.A. and Boom A.B.K.: Cycle-to-Cycle control of the swing phase of paraplegic gait induced by functional electrical stimulation, *Med. Biol. Eng. Comput.* in press.

44 Franklen H.M., Veltink P.H., Tijsmans R., Nijmeijer H. and Boom A.B.K.: Identification of the Quadriceps-Shank dynamics using Randomized Interpulse internal Simulation, *IEEE Trans. Rehab. Eng.*, 3, 2, June 1995.

45 Fuglevand A.J., Winter, D.A., Patla A.E., and Stashuk D.: Detection of Motor Unit action potentials with Surface electrodes: influence of electrode size and spacing, *Biol. Cybern.* (67), p. 143, 1992.

46 Fung Y.C.B.: Elasticity of Soft Tissues in Simple Elongation, *Am. J. Physiol.*, 213, pp 1532, 1967.

47 Gill P.E. and Murray W.H.: *Practical Optimization,* Academic Press, London, 1981.

48 Gordon M.E.: An anlaysis of the bimechanics and muscular synergeies of human standing, Ph.D. thesis, Department of Mechanical Engineering, Stanford University, September 1990.

49 Goh C.J. and Teo K.L.: Control Parametrization: A unified approach to optimal control problems with general constraints, *Automatica*, 24, pp 3, 1988.

50 Goldstein H.: *Classical Mechanics*, Addison-Wesley, Mass., 1959.

51 Golliday G.L.Jr. and Hemami, H.: Postural Stability of the tow degree of freedom Biped by general linear feedback, *IEEE Trans. on Automatic Control*, February, pp 74, 1976.

52 Gordon M.E., Hoy M.G., Zajac F.E., and Maclean K.E.: The Musculoskeletal Model of Human Lower Extremity, *RESNA 9th Annual Conference*, Minneapolis, Minnesota, pp 448, 1986.

53 Gordon A.M., Huxley A.F. and Julian F.I.: Variation in the Isometric Tension with Sarcomere length in vertebrate muscle fibers, J. *Physiol.*, 184, p 170, 1966.

54 Green D.G.: A Note on the Modeling Muscle Physiological Regulator, *Med. Biol. Eng.*, 7, pp 41, 1969.

55 Griffin J.E., Karselis T.C. and Currier D.P: *Physical Agents for Physical Therapists*, Charles C Thomas Publisher, 1982.

56 Grigg P. and Greenspan B.J.: Response of Primate Joint Affernet Neurons to Mechanical Stimulation of Knee Joint, *J. Neurophysiol.* 4, 1, 1977.

57 Hagedorn P.: On The Stability of Steady Motions in Free and Restrained Dynamical Systems, *J. App. Mech.*, 46, pp 427, 1979.

58 Hanavan E.P.: A mathematical model of human body, Aerospace Medical Research Laboratories, AMRL-TR-64-102, 1964.

59 Hasan Z.: A Model of Spindle Affernet Response to Muscle Stretch, *J. Neurophysiology*, 49, 4, April 1983.

60 Hatze H.: Theory of Contraction and Mathematical Model of Striated Muscle, *J. Theory. Biol.*, 40, p 219, 1973.

61 Hatze H.: Biodynamic Models and Their Applications, *J. Acoust. Soc. Am.*, 50, pp 1397, 1971.

62 Hatze H.: The Complete Optimization of Human Motion, *Math. Biosci,* 28, pp 99, 1976.

63 Hatze H.: A Control Model of Skeletal Muscle, Ph.D Thesis, University of South Africa, January 1975.

64 Hatze H.: Zum Thema: Eine Mechanik der Leibesubungon, Leibesub. - Leibeserz., 6, pp 6, 1965.

65 Hatze H.: Die Biophoronome Erfassung der Menschlichen Bewegung in Einem System Particular Differentialgleichunger, Leibesub. - Leibeserz., 7, pp 3, 1967.

66 Hatze H.: A myocybernetic control model of skeletal muscle, *Biol. Cybern.*, 25, pp. 103, 1977.

67 Hatze H.: The Change - Transfer Model of Myofilaments Interaction: prediction of Forces Enhancement and Related Myodynamic Phenomenon, In Multiple Muscle Systems: *Biomechanics and Movement Organization*, (Winters J.M. and Woo S.L-Y., Ed), Springer-Verlage, New York, 1990.

68 He J., Levine, and Loed G.E.: Feedback gains for correcting small perturbations to statnding posture, *IEEE Trans. on Automatic Control*, Vol. 36, p. 322, 1991.

69 Helal J-N. and Bouissou P.: The Spacial Integration effect of Surface Electrode Detecting Myoelectric Signal, *IEEE Trans. on Biomed. Eng.* (39), (11), p. 1161, November 1992.

70 Hemami H.: Modeling, Control, and Stimulation of Human Movement, *CRC Critical Reviews in Biomedical Engineering,* 13, 1, 1985.

71 Hemami, H. and Camana P.C.: Nonlinear Feedback in Simple Locomotion Systems, *IEEE Trans. Automatic Control AC-21*, 6, pp 855, 1976.

72 Hemami, H. and Cvetkovic V.S.: Postural Stability of Biped Models via Lyapunove's Second Method, *IEEE Trans. Automatic Control AC-22*, 1, pp 66, 1977.

73 Hemami, H. and Golliday G.L.Jr.: The Inverted Pendulum and Biped Stability, *Math. Biosc.*, 34, pp 95, 1977.

74 Herman R.N., Grillber S., Stein P.S.G. and Stuart D.S.: *Neural Control of Locomotion*, Plenum Press, N.Y., 1976.

75 Hemami H. and Jaswa V.C.: On a Three - Link Model of the Dynamics of Standing up and Setting down, *IEEE, Trans. System, Man, Cybern, SMC-8*, pp 115, 1978.

76 Hill A.V.: The Heat of Shortening and the Dynamic Constants of Muscle, *Proc. Roy. Soci. B. (Lond),* 126, pp 136, 1938.

77 Hill A.V.: The Series Elastic Element Component of Muscles, *Proc. Roy. Soci. B. (Lond)*,137, pp 273, 1950.

78 Hill A.V.: The Mechanics of Active Muscle, *Proc. Roy. Soci. B. (Lond),* 141, pp 104, 1953.

79 Hill D.K.: Tension Due to Interaction Between the Sliding Filaments in Resting Striad Muscle, *J. Physiology,* 199, pp 637, 1968.

80 Horak F.B., Nashner L.M. and Diener H.C.: Postural Strategies associated with the Somatosensory and Vestibular Loss, *Exp. Brain Res.*, 82, pp 167, 1990.

81 Houk J.C., Singer J.J. and Goldman M.R.: An evaluation of length and force feedback to soleus muscles of decerebrated cats, *J. Neurophysiol.,* 33, pp 784, 1970.

82 Hout R.C. and Little R.W.: A Constitutive Equation for Collagen Fibers, *J. Biomechanics*, 5, pp423, 1972.

83 Hoy G.M., Zajac F.E. and Gordon M.E.: A Musculoskeletal Model of human Lower Extremity: The effect of muscle, tendon and moment arm on the moment-angle relationship of the Musclotendon actuators at the hip, Knee, and Ankle, *J. Biomechanics*, 23, 2, p 157, 1990.

84 Huston R.L. and Passarello, C.E.: *The Mechanics of Human Motion, In Human Body Dynamics Impact, Occupational and Athletic Aspects* (Ghista D.N., Ed), Oxford University Press, London, pp203, 1982.

85 Inman V.T. Ralston H.J. and Todd F.: *Human Walking* (Lieberman J.C., Ed), Wiliams and Wilkins, Baltimore, MD, 1981.

86 Iqbal K. and Hemami, H.: Stability and Control of frontal Four Link Biped System, *IEEE Trans. on Biomed. Eng.*, 40, 1, October 1993.

87 Isermann R.: *Digital Control Systems Volume II*, Springer-Verlag, 1989.

88 Ishida A. and Miyazaki S.: Maximum Likelihood Identification of Postural Control System, *IEEE Trans. on Biomedical Engineering BME-34*, 1, pp 1, January 1987.

89 Jenkins G.M., and Watts D.G.: *Spectral Analysis and its Applications*, San Francisco, Ca, Holden - Day, 1969.

90 Jhonson G.A., Choi, N.Y., Tramaglini D.M., McMahon P.J. and Woo S. L-Y.: Viscoelastic Properties of Human Patellar Tendon: Age Related Changes, *Proceeding of NACOBII, the 2ed North American Congress on Biomechanics*, Chicago, August 24th - 28th, 1992.

91 Johansson R. and Magnussson M.: Human Postural Dynamics, *CRC Crit. Rev. in Biomed.*, 18, 6, 1991.

92 Kailath T.: *Linear Systems*, Prentice-Hall, Englewood Cliffs, N.J., 1980.

93 Kane T.R. and Scher M.R.: Human Self - Rotation by Means of Limb Movement, J. *Biomechanics*, 3, pp 39, 1970.

94 Khang G. and Zajac F.E.: Paraplegic Standing Controlled by Functional Neuromuscular Stimulation Part I - Computer Model and Control-System Design, *IEEE Trans. on Biomed. Eng.*, 36, 9, pp 873, September 1989.

95 Khang G. and Zajac F.E.: Paraplegic Standing Controlled by Functional Neuromuscular Stimulation Part II - Computer Model and Control-System Design, *IEEE Trans. on Biomed. Eng.*, 36, 9, pp 885, September 1989.

96 Koivo A.J. and Guo T.H.: Adaptive Linear Controller of Robotic Manipulators, *IEEE Trans. Automatic Control AC-28*, 1, p 162, 1983.

97 Komistek R.D., Soutas - Little R.W., Stich J.B., Dhaher Y.Y., and Paxson R.D.: Dynamic Model of Human Lower Extremity Joint Forces, *2ed World Congress of Biomechanics VRIJE UNIVERSITEIT*, Amesterdam, The Netherlands, pp 10, July 1994.

98 Kralj A., Bajd T., and Turk R.: Electrical stimulation providing functional use of paraplegic patient muscle, *Med. Prol. Technol.*, Vol. 7, p. 3, 1980.

99 Krogman W.M. and Johnston F.E.: Human Mechanics, Four monographs a bridged. Technology, Doc. Repot. No. AMRL - TOR - 63 - 123, Wright - Patterson Air Force Base Ohio.

100 Kuo A.: An Optimal Control Model for Analyzing Human Postural Balance, *IEEE Trans. Biomed. Eng.*, 42, 1, pp 87, 1995.

101 Lawson C.L. and Hanson R.J.: *Solving Least Squares Problems*, Prentice-Hall Inc., Englewood cliffs, New Jersey, 1974.

102 Lee C.S.G. and Chung M.L.: An adaptive control strategy for mechanical Manipulators, *IEEE Trans. Automatic Control AC-29*, 9, p 837, 1984.

103 Lee C.S.G. and Chung M.L.: Adaptive perturbation control with feed forward compensation for robot manipulators, *Simulation*, 44, 3, p 127, 1985.

104 Lehman S.L. and Stark L.W.: Perturbation analysis applied to eye, head, and arm movement models, *IEEE Trans. Syst. Man Cybern. SMC-13*, 5, pp 972, 1983.

105 Leu M.C. and Hemati N.: Automatic Symbolic Derivation of Dynamic Equations of Motion for Robotic Manipulators, *ASME J. Dynamics, System, Meas., and Cont.*, 108, pp172, Sept. 1986.

106 Lewis L.F.: *Applied Optimal Control and Estimation: Digital design and estimation*, Prentice Hall, Englewood Cliffs, NJ, 1992.

107 Levine W.S. and Zajac F.E.: Unpublished analysis, 1984.

108 Lieh J., Rodgers M.M., Tummarkota S. and Schrag D.R.: Multibody Dynamics for Biomechanical Systems, *ASME Advances in Bioengineering BED-22*, pp 597, 1992.

109 Ljung L.: *System Identification - Theory for Users*, Egelewood Cliffs, NJ, Prentice-Hall, 1986.

110 Magnus R.: Some Results of Studies in the Physiology of Posture, Cameron Prize Lecturers, Lancinate, 211, 2, pp 531, 1926.

111 Magnussson M.: On The OptoKinetic Mechanism, Ph.D. Thesis, Department of Oto-rhinolaryngology, University of Lund, 1986.

112 Markhede G. and Grimby G.: Measurements of strength of the hip joint muscles, *Scand. J. Rehab. Med.* (12), p. 169, 1980.

113 Maros D. and Orlanda N.: Contribution to the determination of the equations of motion for multi-degree of freedom Systems, *ASME Trans, J. Eng. Ind.*, 93, pp 191, 1971.

114 Nagurka M.L. and Yen V.: Fourier-Based Optimal Control of Nonlinear Dynamic Systems, *ASME Trans. J. Dyn. Syst., Meas. and Cont.*, 112, pp 17, 1990.

115 Nashner L.M.: A Model describing Vestibular detection of body Sway motion, *Octa Otolaryngology*, 72, pp 429, 1971.

116 Nashner L.M.: Vestibular Postural Control Model, *Kybernetik*, 10, pp 106, 1972.

117 Nashner L.M.: Vestibular and reflex Control of Normal Standing, *Advances in Behavioral Biology*, 7, (Stein R.B., Pearson K.G., Smith R.S. and Redford J.B., Ed), Plenum Press, N.Y., 1973.

118 Needham D.M.: *Macina Carnits*, Cambridge University Press, 1971.

119 Nubar V. and Contini R.: A minimal principle in biomechanics, *Bull. Math. Biophys.* 23, pp 337, 1961.

120 Ortega J.M.: *Matrix Theory - A second course*, Plenum Press, 1987.

121 Owens D.H.: *Multivariable and Optimal Systems*, Academic Press, London, 1981.

122 Pandy M.G., Anderson F.G. and Hull D.G.: A Parameter Optimization Approach for the Optimal Control of A Large-Scale Musculoskeletal System, *ASME Trans. J. Biom. Eng.*, 114, pp 450, November 1992.

123 Pandy M.G., Garner B.A. and Anderson F.C.: Optimal Control of Non-ballistic Muscular movements: A Constraint-Based Performance Criterion for raising from Chair, *ASME Trans. J. Biom. Eng.*, 117, pp 15, February 1995.

124 Pandy M.G., Zajac F.E., Sim E. and Levine W.S.: An Optimal Control Model for Maximum-High Human Jumping, *J. Biomechanics*, 23, 12, pp 1185, 1990.

125 Pierrynowski M.R. and Morrison J.B.: A Physiological Model of the evaluation of Muscular Forces in Human Locomotion: Theoretical Aspect, *Math. Biosci.*, 75, pp 69, 1985.

126 Pringle J.W.S.: Models of Muscle, *Symposium Soci. Exper. Biol.*, 1, pp41, 1960.

127 Raibert M.H. and Graig J.J.: Hybrid Position/Force Control of Manipulators, *ASME Trans. J. Dyn. Syst. Meas. and Control*, 103, pp 126, 1981.

128 Reichardt W.: Analogy between noiogram information and computation of relative movement by visual system of the fly, *Naturwissenschaften*, 67, pp 8411, 1980.

129 Reichardt W. and Poggio T.: Figure ground discrimination by relative movement in visual system of the fly I. Experimental Result, *Biol. Cybern.* 35, pp 81, 1979.

130 Rugh W.J.: Design of nonlinear compensator for nonlinear systems by extended linearization technique, in *Proc. IEEE Conf. Decision Control*, Las Vegas, pp 69, NV, 1984.

131 Sale D., Quinlan J., Marsh E., McComas A.J. and Belanger A.Y.: Influence of Joint position on ankle plantar flexion in humans, *J. Appl. Physiol. Respirat. Environ. Exer. Physiol.* (52), p. 1636, 1982.

132 Seirge A. and Arvikar R.L.: A mathematical Model for the Evaluation of Forces in Lower Extremities of the Musculoskeletal System, *J. Biomechanics*, 6, pp 313, 1973.

133 Seirge A. and Arvikar R.L.: *Biomechanical Analysis of Musculoskeletal Structure for Medicine and Sports*, Hemisphere Publishing Corporation, New York, 1989.

134 Scudder G.N.: Torque curves produced at the knee during isometric and isokinetic exercises, *Arch. Physiol. Med. Rehab.* (61), p. 68, 1980.

135 Shiavi R.: Electromyographic patterns in adult locomotion: A Comprehensive Review, *J. Rehabilitation Research and Development*, 22, p 573, 1985.

136 Shiping Ma. and Zahalak G.I.: Activation dynamics for a distribution-moment model, *Math. Comput. Modelling*, 11, pp 778, 1988.

137 Sirisena H.R. and Tan K.S.: Computation of Constrained Optimal Controls Using Parametric Techniques, *IEEE Trans. J. Automatic Control AC-19*, pp 431, 1974.

138 Soderstrom T.: *Lecture Notes in Identification*, Control System Analysis Group, Uppsala University, Sweden, 1984.

139 Soderstrom T. and Stoica P.: System identification, Prentice-Hall International Series in Systems and Control Engineering, 1989.

140 Sonnenblick E.H.: Series Elastic and Contractile elements in Heart Muscle Changes in Length, *Annual Meeting of the American Physiol. Socie.*, 14th April 1964.

141 Soong T.T. and Huang W.N.: A Stochastic Model for Biological Tissue Elasticity in Simple elongation, *J. Biomechanics*, 6, pp451, 1973.

142 Stanic U. and Trnkoczy A.: Closed loop positioning of hemiplegic patient's joint by means of functional electrical stimulation, *IEEE Trans. Biomed. Eng. Vol. BME-21*, p. 365, 1974.

143 Strejc V.: *State Space Theory of Discrete Linear Control*, Prague, Czechoslovak, John Wiley & Sons, 1981.

144 Sugi H.: Tension Changes During and After Stretch in frog Muscle Fiber, *J. Physiol.*, 134, pp 237, 1972.

145 Takeyaki M. and Arimoto S.A.: A new feedback method for dynamic control of manipulators, *ASME Trans. J. Dyn. Syst. Meas. and Control,* 102, pp 119, 1981.

146 Tashman S., Zajac F.E., and Perkash I.: Modeling and Stimulation of Paraplegic Ambulation in Reciprocating Gait Orthosis, *ASME Trans. J. Biomed. Eng.,* 117, pp 300, August 1995.

147 Tewell B.R. and Wilkie D.R.: An Analysis of the Mechanical Components of frog's Striad Muscle, *J. Physiol.*, 143, pp 515, 1958.

148 Vane J.M. and Sitchin A.: Derivation of the first -order difference equations for dynamical systems by direct application of hamiltonian principle, *ASME Trans., J.Appl. Mech.,* 37, pp 276, 1970.

149 Von Gierke, H.E.: Biodynamic Models and Their Applications, *J. Acoust. Soc. Am.*, 50, pp 1397, 1971.

150 Vukobratrovic M., Borovac M., Surla D. and Stokic D.: *Scientific Fundamentals of Robotics 7: Biped Locomotion Dynamic, Stability, Control and Application*, Springer-Verlag, Berlin Heidelberg, 1990.

151 White S.C., Yack H.J., and Winter D.A.: A Three Dimensional Musculoskeletal Model for Gait Analysis Anatomical Variability Estimate, *J. Biomechanics*, 22, pp 885, 1989.

152 Walters R.L., Frazier J., Garland D.E., Jordan C., Perry J.: Electromyographic Gait Analysis befor and after Operative Treatment for Hemiplegic Equinus and Equino-varus Deformity, *J. Bone and Joint Surgery*, 64-A, 2, pp 284, 1982.

153 Whitney D.E.: Force Feedback Control of manipulators fine movement, *ASME Trans. J. Dyn. Syst. Meas. and Control,* 99, pp 91, 1977.

154 Wilkie D.R.: Measurement of the Series Elastic Component at Various times during a Single Muscle Twitch, *J. Physiol. (Lond)*, 134, pp 527, 1956.

155 Williams W.J.: A System-Oriented evaluation of the role of Joint receptors and other afferents in position and motion sensory, *CRC Crit. Rev. in Biomed. Eng.*, 7, 3, 1991.

156 Winter D.: *Biomechanics and Motor Control of Human Movements*, John Wiley &Sons, Inc., 1990.

157 Winter D., Rau G., Kadefors R., Broman H., and Deluca C.: Units, Terms, and Standards in the reporting EMG research, *Intern. Soci. of Electrophysiology and Kinesiology*, August, 1980.

158 Winters J.M. and Stark L.: Muscle Models: What is Gained and What is Lost by Varying Model Complexity, *Biol. Cybern.*, 55, pp 403, 1987.

159 Winters J.M., Fuglevand A.J., and Archer S.: Crosstalk in Surface electromyography in agonist Muscles, *8th annual East Coast Clinical Gait Laboratories Conference*, May 5-8, Mayo Clinic, Rochester, MN 1993.

160 Wittenburg J.: *Dynamics of Systems of Rigid Bodies*, B.G. Teubner, Stuttgart, 1977.

161 Yamaguchi G.T., Sawa A.G.W., Moran D.W., Fessler M.J. and Winters J.M.: A survey of human Musclotendon actuator parameters, In Multiple Muscle Systems: *Biomechanics and Movement Organization*, (Winters J.M. and Woo S.L-Y., Ed), Springer-Verlage, New York, 1990.

162 Young L.R.: A Control Model of Vestibular System, *International Federation of Automatic Control (IFAC), Technical and Biological Problems in Control, A Cybernetic View*, (Iberall S. and Reswick J.B., Ed), pp 543, Instrument Society of America, Pittsburgh, 1970.

163 Zajac F.E.: Muscle and Tendon: Properties, Models, Scaling, and Application to Biomechanics and Motor Control, *CRC Critical Reviews in Biomedical Engineering*, 17, 4, pp 349, 1989.

164 Zajac F.E., Topp E.L. and Stevenson P.J.: Musclotendon Actuator Models for Use in Compute Studies and Design of Neuromuscular Stimulation Systems, *RESNA 9th Annual Conference*, Minneapolis, Minnesota, 1986.

165 Zhang Li-Q., Shiavi R. and Wilkes M.: Modeling and identification of human musculoskeletal walking system, in *Proceeding of the 22ed Southeastern Symposium on System Theory*, Cookeville, TN, pp 150, March 11 - 13, 1990.

166 Zhang Y-F. and Hemami, H.: Impact effects of Biped Contact with environment, *IEEE Trans. Syst. Man Cybern. SMC-14*, 3, pp 437, 1984.

167 Ziegler J.M., Anderson F.C., Pandy M.G. and Whalen R.I.: Musculoskeletal Models Computational Algorithms Supercomputers, *ASME Advances in Biomedical Engineering BED-22*, pp 601, 1992.

168 Zipp P.: Effect of electrode parameters on the band width of the surface e.m.g. Power Spectrum, *Med. Biol. Eng. Comput.*, 16, p. 537, 1978.